ISAS - INTERNATIONAL SCHOOL FOR ADVANCED STUDIES

SPECTRAL ANALYSIS OF STELLAR POPULATIONS

Candidate:

Ravi Kumar Gulati

Supervisors:

Prof. Maria Lucia Malagnini

Thesis submitted for the degree of

"Magister Philosophiae"

Astrophysics Sector

Academic Year 1988-89

TRIESTE

SISSA - SCUOLA INTERNAZIONALE SUPERIORE DI STUDI AVANZATI

TRIESTE

Strada Costiera 11

ISAS - INTERNATIONAL SCHOOL FOR ADVANCED STUDIES

SPECTRAL ANALYSIS OF STELLAR POPULATIONS

Candidate:
Ravi Kumar Gulati

Supervisor:
Prof. Maria Lucia Malagnini

Thesis Submitted for the degree of
Magister Philosophiae

Academic Year 1988-1989

CONTENTS

4. Evolutionary Population Synthesis

5. Spectral Features Description

PART II: MODEL ATMOSPHERES

6. Stellar Atmosphere Models

7. Synthetic Spectrum Computation

INTRODUCTION

The understanding of fundamental physical processes such as the formation, internal organization and evolution of stellar systems ultimately relies on the study of the stellar components of the systems. More specifically, the concept of stellar population has been linked with different characteristics of a stellar sample, i.e., its metallicity, age, positional and dynamical properties. The light from a stellar system such as a galaxy can be considered as the superposition of light from stars and stellar clusters of various ages, which evolve in spectrum and in bolometric luminosity according to their age and mass.

With the exception of a few nearby stellar systems, the study of other systems is based on the information included in their integrated light. Therefore, we need some methods which will allow us to ascertain the nature of the underlying objects responsible for the integrated light.

Conceptually, in spectral synthesis techniques, a comparison is made between a combination of individual stellar spectra of given spectral types and the observed integrated spectral energy distribution (SED). First of all, this problem was faced by Whipple (1935), but only after the development of new instruments and of data processing facilities, the solution to this problem has begun to cast light on the populations of unresolved stellar systems.

Despite the fact that the methods of stellar population synthesis have been applied to stellar systems successfully, still there remains the problem of disentangling the interdependence of metallicity and age on the resulting

integrated spectral energy distribution, in the sense that the increasing of the metal abundance produces the same effect as a spectral energy distribution due to a lower temperature, which is the same effect one obtains by increasing the age of a more metal-poor population (O'Connell, 1980).

Therefore, even for a simple population characterised by a relatively small range of age and metallicity, broadband photometry is inadequate to disentangle the contributions due to these two fundamental parameters. However, the use of high S/N data and of sufficiently high resolution or alternatively careful selection of spectral features and bands can restrict the solution area. One of these bands, suggested by Faber (1977), is the so-called Mg-band centred at 5167$\AA$, which is a good indicator of metallicity and can be easily distinguished in the composite spectra. The empirical relationship between the line strength index Mg-b and metallicity for stellar systems is hampered due to lack of information regarding stars of nonsolar chemical composition, in particular super-metal rich stars. An alternative way to incorporate such kind of stars is to synthesize artificially the synthetic spectra of metal-rich model atmospheres.

Along this direction of work, we are preparing a grid of theoretical models for the synthetic indices, which would provide in principle a powerful tool to disentangle the effects of metallicity from those due to age, thus helping in clarifying the relationship between age and chemical evolution in stellar systems.

In the first part of this thesis, we will review the general properties of stellar systems; the stellar population concept; different methods adopted to analyse the composite spectra and, in particular, the evolutionary approach; and the spectral features that are important in terms of physical

parameters.

The second part of the thesis is devoted to the original work, which we are carrying out to set up a comprehensive library of synthetic spectra for stellar populations analysis. The description of stellar atmosphere models and the method to compute the model atmospheres and synthetic spectra are discussed here.

The main aim of this work will be the computation of a new grid of stellar atmosphere models, which is exhaustive in temperature, gravity and metallicity, and inclusive of molecular blanketing. Then synthetic spectra will provide the tool for comparing our own set of stellar spectroscopic observations at intermediate resolution with theoretical predictions in order to establish fiducial reference points. Eventually, the complete grid will permit us to generate composite template stellar populations for interpreting extensive observational data available for stellar clusters and galaxies, with the aim of understanding the nature of their integrated radiation in terms of evolutionary histories.

Part I

STARS AND STELLAR SYSTEMS

1 GENERAL PROPERTIES OF STELLAR SYSTEMS

Stellar systems are physical aggregates of stars which are bound together by their mutual gravitation. They are linked to the hierarchy of cosmological bodies, which may have condensed by similar physical processes. Thus starting from the smallest and less massive systems, we discuss here the following systems:

1) Associations and Open Clusters;
2) Globular Clusters;
3) Galaxies.

The general properties of stellar systems are revealed through study of photographic plates, and of photometric and spectrophotometric data. From these data, we can construct a reasonably detailed picture of stellar systems. It is not possible to perform star- by-star analysis at least with the present instruments for all stellar systems. We classify the stellar systems on the basis of their appearance on the photographic plates, and rely on the information contained in the integrated light based on our knowledge of solar neighbourhood stars and nearby stellar systems. The main characteristics of the systems, for which such kinds of analysis is feasible, can be sketched through their color-magnitude diagrams.

The most preferred color-magnitude diagram is a plot between V and (B-V), based on UBV photometry. It is highly advantageous to use this system because many stars of interest that are too faint for high dispersion spectroscopy can be observed with UBV photometry. For the last decade, CCD's have enabled observers to obtain higher precision color-magnitude

diagrams. Given an interstellar extinction, it is easy to transform apparent magnitude to absolute magnitude for stars in the cluster. As, in case of a cluster or a group of stars which occupy a small volume of space relative to their distance from the observer, stars are essentially at the same distance.

1.1 Associations and Open Clusters

Associations are extremely loose and irregular groups of stars. They have low space density and contain about 100 stars in a volume of 100 pc radius, are observed in our Galaxy and in general in the spiral arms of galaxies. They are made up of stars of the same or very close spectral types.

For example, I Ori, is an association rich in O stars; the other kind of association is the T- association, which is rich in T Tauri variables (for example, Per T2). About a hundred of such associations are known in our Galaxy. Sometimes O- and T-associations are found together, as in the Orion nebula. The space densities within associations are very low as they are unbound systems and are actually dissolving into the field on a relatively short time scale (a few million years), hence the stars seen in associations are very young; they often show definite expansional motions.

For example, O stars have a life time of about a million years, and T Tauri stars are still in a stage of contraction onto the main sequence. Evidence, that the T Tauri stars are young objects, results from their position on the H-R diagram (luminosity vs temperature plot) where stellar evolutionary theoretical tracks predict young objects. These young objects are either in phase of gravitational contraction or are new-born stars. Associations are very interesting stellar systems, which enable us to understand the evolution of pre-main sequence stars.

Open clusters usually contain tens to a few hundred stars. A typical open cluster is a rather irregular, loosely concentrated group of stars in a volume having a radius on the order of 10 pc (see Fig. 1.1).

Open clusters have a wide range of stellar densities extending from 0.25 stars pc^{-3} for the Hyades cluster to about 10^3 stars pc^{-3} at the centre of the richest clusters. The richest clusters can be detected at large distances provided there is low interstellar extinction, whereas the poorer clusters can be discriminated from the random fluctuations in the field only if they are nearby.

The integrated light from open clusters is mostly contributed from early type stars. Open clusters are found in the spiral arms of the spiral galaxies, where star formation is considered to be active.

In broad terms, the morphology of a typical CM diagram of open clusters is similar to that of field stars, showing the same kind of sequence. Virtually all open-cluster CM diagrams have a well defined main sequence, which extends to some specific upper limit of brightness. Comparison of the observational CM diagram of open clusters with theoretical evolutionary tracks, allows us to derive their age, because the upper end of the main sequence terminates where the more massive members start to evolve out of the main sequence. In fact, they spend on the ZAMS (zero-age main sequence) less time than stars located on the lower part of the main sequence.

As an illustration, in Fig 1.2, open clusters of various ages are put together on the same CM diagram. It is obvious that the very young cluster, NGC 2362 , can still contain O stars, while progressively older cluster will contain no stars earlier than type B, and A, F and so on. The CM diagrams of young clusters typically have a main sequence extending

to O or B, a sprinkling of supergiants across a wide Hertzsprung gap, and a concentration of few M supergiants.

The CM diagrams of intermediate-age clusters, such as M11 or M41, show a main sequence terminating at late B stars or A stars, a well- developed red-giant branch seperated from the main sequence by a narrower Hertzsprung gap, and no supergiants. The oldest clusters, such as M67, show a main sequence only up to F stars and then a continuous subgiant branch, without Hertzsprung gap, extending into a moderately luminous giant branch. Depending upon the initial mass of the stars, the ultimate fate of stars is white dwarfs, which are compact objects of low magnitude. White dwarfs can be observed in those clusters that are close enough for them to be detected (e.g. Hyades cluster).

1.2 Globular Clusters

Globular clusters are among the most versatile of astronomical objects. As compared to open clusters, globular clusters are very rich in stars, roughly spherically symmetric, and usually found both near the galactic center and in remote regions in the halo. These systems typically contain hundreds to thousands stars in volume equivalent to the radius of about 20 to 50 pc. They have very high star density which keeps them dynamically stable and long lived.

Their radial surface brightness distributions, are so similar to those of many elliptical galaxies that they are considered also as extremely low mass elliptical galaxies. On the basis of their radial star-density profile, they are classified, by H. Shapley and H.B.Sawyer, into concentration classes. They are subdivided into classes, I,.....,XII, where class I corresponds to the

highest degree of concentration, and class XII corresponds to the lowest.

Since globular clusters are very bright stellar systems, they can be seen at large distance. Hence, they can be used as a yard stick for extragalactic structure research, if we can assume that their absolute brightness is the same as that of the galactic globular clusters of the same concentration class. Globular clusters are also of profound importance because observations of these relatively nearby systems are used as a template for understanding elliptical galaxies, for which less detailed information can be achieved.

The integrated spectral energy distribution of these systems cover a wide range of spectral classes from F2 to G5. Spectroscopic analyses indicate that halo clusters have spectra analogous to subdwarf spectra, which suggests a large metal deficiency in the cluster stars. Clusters with later-type spectra are generally found near the galactic center, and their spectra are compatible with nearly normal metal abundances.

As it is difficult to interpret the composite spectra in detail, but in terms of metallic lines, these clusters have been differentiated into eight metallic line groups say, I to VIII. Here class I corresponds to an extremely weak-lined spectrum and very metal poor content, and class VIII corresponds to a strong-lined spectrum and essentially normal metal content.

Since the pioneering work of Shapley in 1917, it has been known that globular clusters have a very distinctive stellar content and their CM diagrams differ from those of early- and intermediate-age open clusters. As an illustration, in Fig 1.3b, we show an updated CM diagram of the cluster M3 (Buonanno *et al.* 1986), whose photograph is given in Fig. 1.3a. In this figure 10,637 stars are plotted: of these, 9,879 from a sample that is

complete down to V=21.5 mag, while the remaining 758 are taken from a sample that is complete down to V=18 mag. The color-magnitude diagram of M3 is particularly useful to test the evolutionary sequences predicted for stars later than the Sun, since it covers most of the range of evolutionary stages for low mass stars.

From this CM diagram we can draw the following salient features of globular clusters .

1) the upper end of the main sequence terminates at a late spectral type, this suggests that all globular clusters are old;

2) a subgiant branch joins continuously onto the main sequence at the turnoff point; there is no Hertzsprung gap;

3) a red-giant branch extends upward and to the right. The brightest stars are always red giants with absolute magnitude about $M_v = -2$ to -3 mag;

4) a horizontal branch near $M_v = +0.5$, which may contain a few hot blue stars, extends redward untill it rises in the asymptotic giant branch lying above the first giant branch;

5) within the horizontal branch there is an instability strip containing RR Lyrae variables;

6) a few blue stragglers are occasionally found lying along an extension of the main sequence above its turnoff point.

Not every cluster CM diagram shows all these features, and, as we shall see, there is considerable variation from cluster to cluster in the detailed morphology. Globular clusters are particularly useful to stellar evolution studies for three main reasons : (a) they have more stars in comparison to open clusters; (b) their stars are virtually coeval; and, (c) in most cases they are chemically homogeneous. In other words, globular clusters rep-

resent the purest and simplest stellar populations we can find in nature, in contrast to field populations, which result from admixtures of ages and compositions that make the intercomparison of theory and field star observation cumbersome and, to some extent, unavoidably ambiguous. They also present the ideal template stellar populations for testing and for the calibration of theoretical evolutionary population syntheses. Given their very old age, galactic globular clusters can be used only to check stellar models of somewhat smaller age than the Sun but for a variety of chemical compositions (Renzini and Fusi Pecci, 1988), while Magellanic globular clusters, which span the full range of ages, can be used to test evolutionary sequences for models up to $10M_{\odot}$.

1.3 Galaxies

Galaxies are composed of stars, interstellar matter and dust, with a variety of properties that correlate remarkably with their morphological classification (a photographic sample is illustrated in Fig. 1.4). Hubble, on the basis of their shapes, classified galaxies into three main types : spirals, elliptical, and irregulars. The Hubble Atlas of Galaxies (Sandage, 1961), and recent Atlas of Galaxies by Sandage and Bedke (1988) are essential sources of information for photographs and description of typical galaxies, while Arp's (1966) Atlas of Galaxies illustrates a great variety of peculiar galaxies.

Spirals have a high concentration of stars in the center known as nucleus, while spiral arms are prominent in the outer regions. The arms are sometimes attached to opposite sides of nucleus, and sometimes they are attached to opposite ends of a bar that passes through the nucleus. The

latter ones are known as barred galaxies. All spirals are very flat stellar systems, and large amounts of absorbing dust are often apparent in them. The spirals are classified from Sa type, with large nuclear bulges and tightly wound arms, to Sc types, with small bulges and extended arms. The nuclear bulges closely resemble to elliptical galaxies, while the spiral arms, or more often bits of spiral arcs, are traced by patchy blue stars and gas and dark dust lanes, superimposed on an underlying smoother disk of redder stars.

The galaxies classified as S0 have disks but lack of spiral structure and its associated young stars and gas; Hubble put them between type E and Sa, but van den Berg (1976) pictures them as a sequence parallel to the spirals, ordered by bulge to disk ratio. Similarly there are barred spirals of types SBa, with tight arms through, SBc, with loosely wound arms. The Hubble sequence illustrated in Fig. 1.5 has been elaborated by de Vaucouleurs (1959) (Fig. 1.6) into a more detailed system indicating intermediate and additional structural features.

Elliptical galaxies show little or no structure of any kind. As the name suggests, the shape is elliptical. Elliptical galaxies occur with varying degrees of flatness, and little interstellar matter is present in them. They are the earliest galaxies, with no indication of recent star formation. They have an apparently smooth distribution of yellow-red stars and seldom any sign of internal structure.

Irregular galaxies are those which do not fit into the categories of elliptical and spiral galaxies. They have no obvious symmetry in their appearance, and have large amounts of interstellar matter.

Although the sequence E-S0-Sa-Sb-Sc-Irr I was based purely on the

shapes of galaxies, it is strongly related to stellar populations. The earliest galaxies show no signs of hot young stars and undetectably little gas or dust, while the latest galaxies are experiencing active star formation and have significant amount of interstellar matter.

The Yerkes classification system of galaxies (Morgan and Mayall, 1957; Morgan, 1958,1959; Morgan and Osterbrock, 1969) emphasizes the correlation between morphologies and stellar populations. For spirals, this system is based simply on the central concentration of light, and it is found that highly concentrated galaxies have late-type nuclear spectra (indicating a mixture of G, K, and M stars), while those with little central concentration of light have early- type spectra (dominated by B stars). The Yerkes types of galaxies are correlated loosely with Hubble types , which is not surprising since the Hubble classification is based partly on the amount of light concentrated into a nuclear bulge and partly on the tightness of the spiral structure. The increasing prevalence of blue, young stars as one goes from ellipticals to irregular galaxies is reflected in a general progression from redder to bluer integrated colors.

From studies of the integrated spectra and colors of galaxies, we conclude that nearly all galaxies contain some very old stars, and their different proportions of red and blue stars, as indicated by their integrated light, are mainly due to different current rates of star formation.

Most (if not all) galaxies appear to be many billions of years old, but whereas significant star formation ceased billion of years ago in the ellipticals, it has occured at a roughly constant rate in the latest types of galaxies. Theories of galaxy formation, and star formation within galaxy morphology, are challenged to explain this close correlation between forms

of galaxies and their histories of star formation.

Some galaxies fit nowhere into a tidy sequence of types, and they are classified as simply peculiar or as one of the special types of peculiars such as ring galaxies or Irr–II. Many of peculiar galaxies are interacting galaxies, distorted by tidal effects (Toomre and Toomre, 1972). Sometimes the colors of peculiar galaxies are so blue that any underlying old population is completely outshone by newly formed stars, and sometimes they are so red that most of the activity must be hidden in dust clouds. Although these peculiar galaxies are rare, they are of special interest since some of them may be undergoing the kinds of violent changes and rapid star formation that characterized normal galaxies in their youth (Larson, 1976).

The chemical compositions of galaxies in general show much less diversity than their populations. Few instances are known of interstellar gas that is deficient or overabundant in heavy elements by more than a factor of four relative to the Sun, and, although stellar metallicity ranges over more than two orders of magnitude, they are usually within a factor of three of solar. Many of the differences among chemical composition are systematic: metallicity of both stars and gas tend to decrease outward from the centres of galaxies, and average metallicity tends to increase with galaxy luminosity.

Many more details are known about the stellar populations in the solar vicinity of our galaxy than anywhere else, and some of these details contain clues to large-scales processes of galaxy formation. For example, stars with high space velocities that make them members of halo population are metal poor by a factor of ten or more relative to the Sun, while stars with disc motions have metallicity almost within a factor of three of the solar one.

Fig. 1.1: The h and χ Persei galactic open cluster.

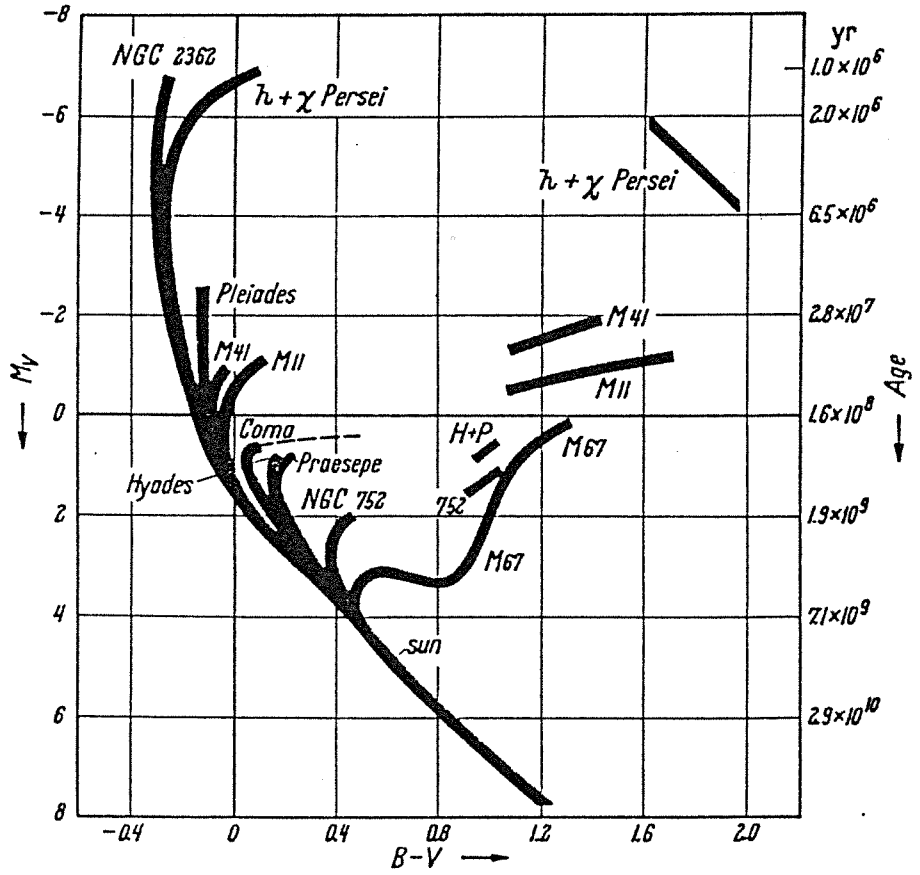

Fig. 1.2: Observed color-magnitude diagram for several representative galactic clusters. (Adapted from a diagram by Sandage, 1957)

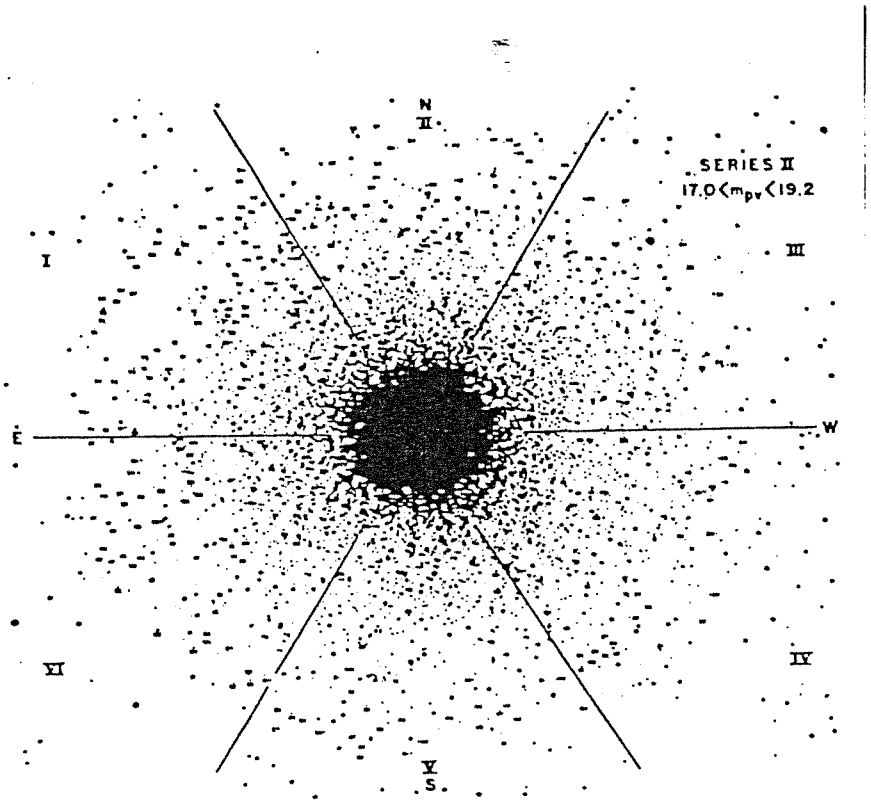

Fig. 1.3a: Photograph of the globular cluster M 3 from Johnson and Sandage, 1956.

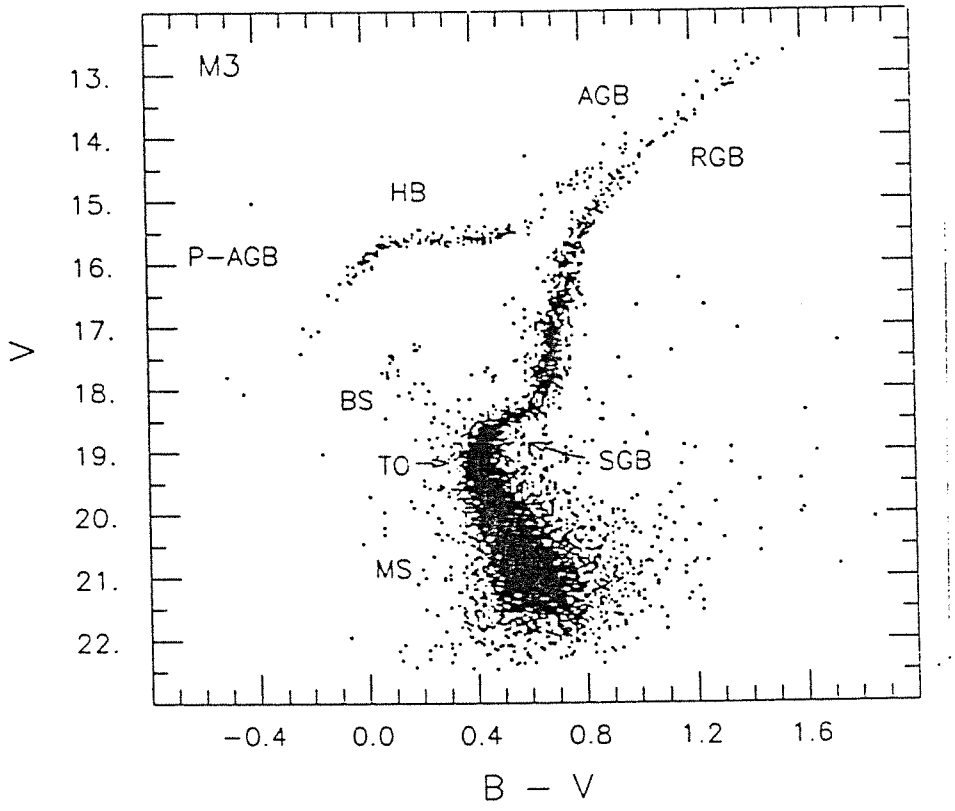

Fig. 1.3b: CM diagram for M 3 (MS: Main sequence; SGB: Subgiant branch; TO: Turnoff Point; BS: Blue straggler; RGB: Red-giant branch; ABG: Asymptotic branch; HB: Horizontal branch; P-AGB: Post-asymptotic branch).

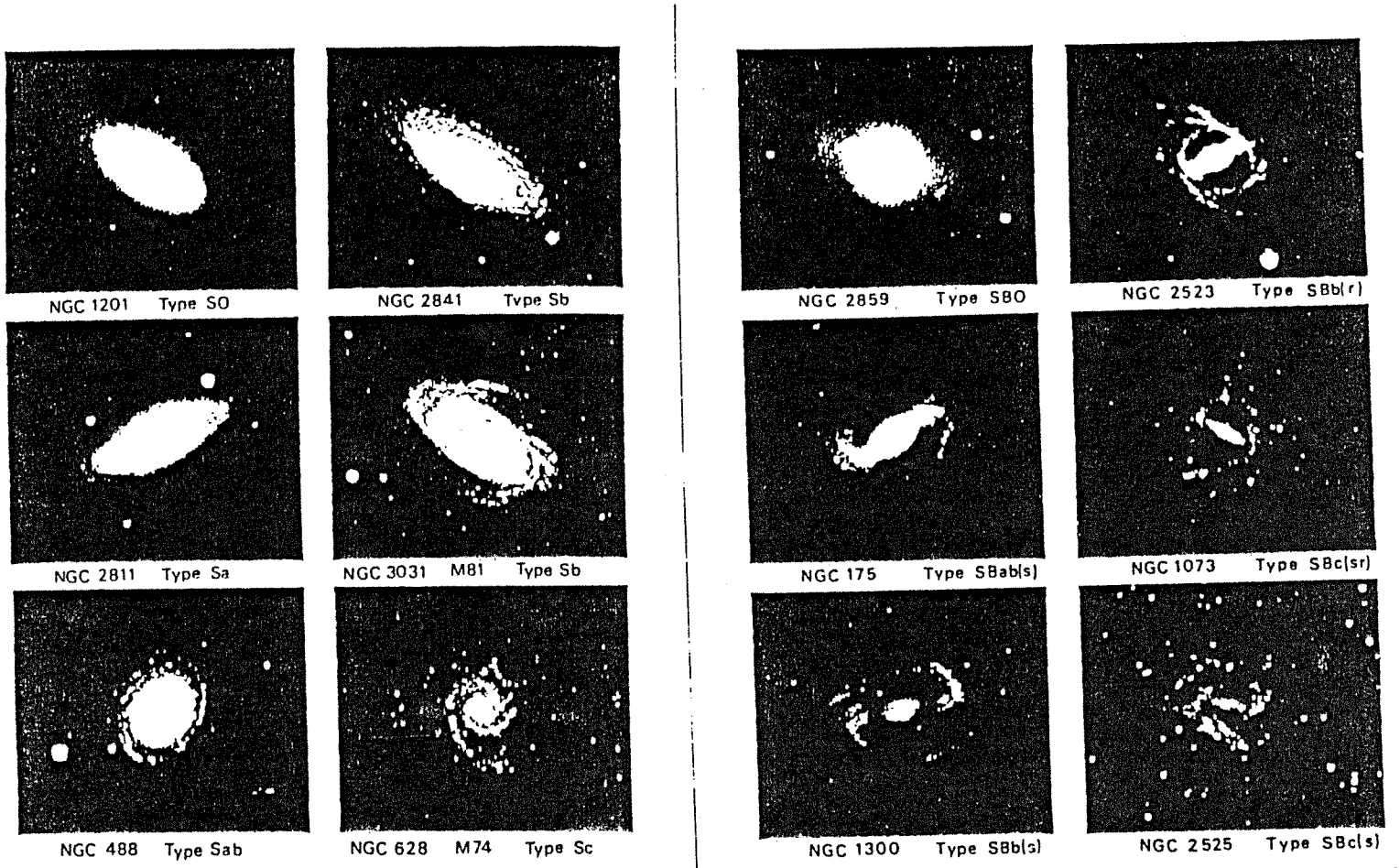

Fig. 1.4: A photographic sample of spiral galaxy types.

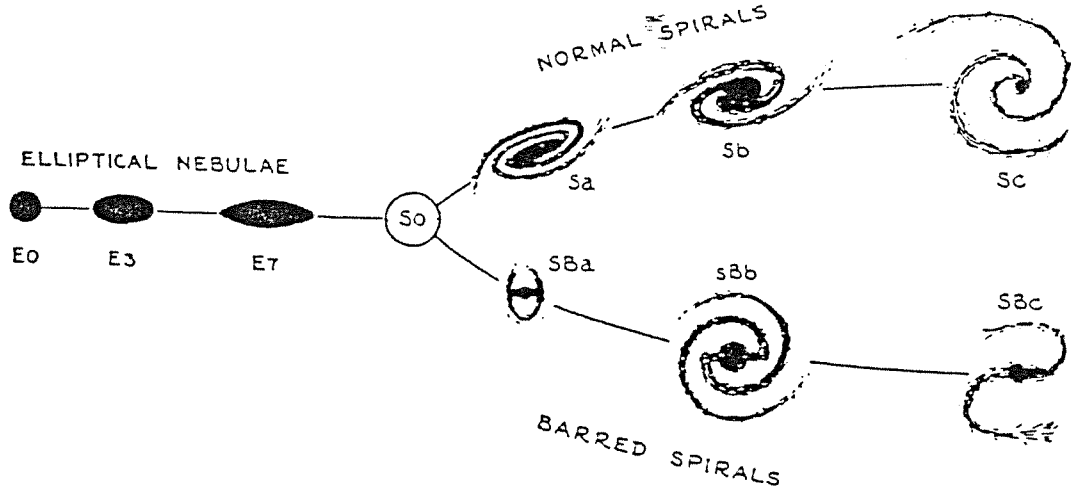

Fig. 1.5: Hubble's classification of galaxy types.

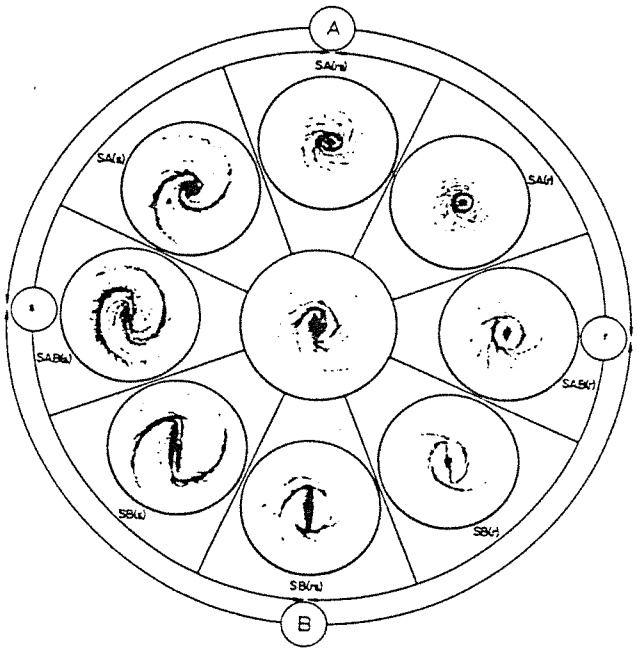

Fig. 1.6: de Vaucouleurs's classification of spiral galaxy types.

2 THE STELLAR POPULATION CONCEPT

The concept of stellar population as introduced by Baade (1944) has proved to be useful in a variety of contexts, as it ties together a number of intricate details and diverse parts of a particular field.

For the last four decade the simple idea has been expanded and modified to such a large extent that Sandage (1986) summarized the situation: "all of this impacted on the population concept, adding detail and complication.....until it was said that everyone means different thing when they talk about stellar population". The historical development of the concept of stellar population has been thoroughly reviewed by Sandage (1986).

In fact, the revolution in theoretical concepts and in observational techniques have given a new shape to the understanding of stellar populations. On the observational side, after the advent of sensitive detectors, it has become possible to build color-magnitude diagrams (CM) for faint stellar systems thus reaching deep distances in the galaxy. On the theoretical side, there is a rapid growth of insight into basic physics of energy generation and energy transport in the stars; in addition, the availability of high speed computers makes feasible the detailed computation of evolutionary tracks for individual stars in the color-magnitude diagram.

At present, this concept tends to answer the various questions, such as the age differences among different galaxy components and dependence of differences on metallicity, kinematics, and position in a galaxy.

The ultimate aim of work in stellar populations is to achieve the understanding of the structure and evolution of galaxies. In this section, we do not intend to discuss this topic in great detail, but we want to sketch the broad outlines, on which later ideas of stellar population synthesis will be

built.

2.1 Classification and Characteristics

The historical development in classification of stellar populations had its starting in the work of Baade (1944), who, having resolved the red giants in Andromeda and its satellite galaxies, appreciated the basic difference between these objects and mixture of stars in the solar neighbourhood. He demonstrated that red giants in these galaxies could be identified with those in the galactic globular clusters, while they are completely different from luminous blue supergiants found in the spiral arms.

According to Baade, stars in a galaxy can be classified into two distinctive types:

Population I;
Population II.

In Baade's original work, the distinction between the two types was primarily based on the physical properties, such as spectral class and luminosity, in combination with the position of the objects in the stellar systems.

The enlargement of data and concepts through empirical and theoretical understanding of the H-R diagram, and the introduction of age as the fundamental parameter, have called for a modification of stellar classification in the famous 1957 Vatican Conference on Stellar Population (O'Connell, 1958).

Typical Population I are those objects which are closely associated with spiral arms, e.g. young hot stars of spectral type O and B, ionized hydrogen regions, and the classical cepheids. As we saw in the section 1.1 the open

clusters span a wide range of ages, so Population I objects also cover wide range of ages. This means that some Population I objects are as old as the youngest globular clusters and others are forming-new-stars at the present time.

Kinematical evidences have shown that Population I objects move dominantly in nearly circular orbits around the galactic center with a small random velocity dispersion around the exact circular velocity. The space distribution of Population I objects is strongly flattened.

Population II objects are those which are observed in the spheroidal components of the galaxies, e.g., objects in the nuclear bulge, and in the halo. The most characteristic members of Population II are RR Lyrae stars. The field Pop II stars fit into the same CM diagrams of the galactic globular clusters, so they are old objects, having age nearly equal to the estimate age of the Universe.

This simple concept encountered difficulty when the age criterium in the case of M67 could not differentiate Population I objects from Population II, since stars at the turning point of the cluster M67 in the CM diagram are at the same position of globular cluster stars. But spectroscopic analyses indicate that most of stars in M67 have normal spectra, while stars in globular clusters have weakening of metal lines. This suggests that stars in M67 belong to Population I. Furthermore, on the two-colors (U-B) vs (B-V) plane, stars of the globular clusters deviate substantially from the track of normal stars in the sense of having ultraviolet excesses.

In addition to the age parameter, the other parameter which is attached to the definition of stellar populations is metallicity.

In broad terms, Population I stars are younger and more metal rich,

with metal abundance similar to that of the Sun, than Population II stars which are old and metal deficient by about a factor of one hundred or more relative to the Sun.

Population II objects have a low systematic rotation velocity and a very large random velocity dispersion, this implies that they move on highly eccentric orbits through large ranges of galactocentric radial distance. They have unflattened space distribution.

By the time of the Vatican Conference of 1957, the available data on spatial, kinematical, and chemical properties suggested a more refined subdivison of original Baade's classification. Accordingly, the intermediate "Disk Population " was added to Pop I and II, and Pop I had been bifurcated into "Extreme Population I"and "Older Population I", while Pop II was further subdivided into "Halo Pop II " and "Intermediate Pop II". These five categories are represented by a more or less continuous distribution of properties, ranging from "Halo Population II" to "Extreme Population I" (see Tab. 2.1).

Combining together the subsequent evidences , Eggen *et al.* (1962) (hereafter ELS) presented a scenario of the formation of the Galaxy by a rapid intial collapse from a gaseous protogalaxy to a disk/halo configuration on a time scale on the order of 10^8 years. Their argument was actually based on the strong correlation they found between chemical abundance and orbital eccentricity, in the sense that stars of lowest metallicity were invariably on the plunging orbits. In the light of this correlation the sequence of populations thus formed are thought to be fundamentally one-dimensional with all relevant properties being function of a single parameter, i.e. stellar age. According to this hypothesis, the first stars that formed were

widely distributed in an unflattened system of low rotation velocity, out of material with very low metal content. Subsequent groups of stars, each corresponding to a definite population subdivison, formed a sequence of systems that were more flattened, contained stars that moved on nearly circular orbits, and were composed of metal-rich material. It was thought that this sequence started from Halo Population II and passed through the Intermediate Population II and ended with Disk Population. After the formation of disk, it was assumed that star formation occured at slower rate; the spiral-arm now forming stars were called Extreme Population I, while somewhat older metal-rich field stars, such as the Sun, were called Older Population.

This scenario encountered contradictions and serious ambiguities due to the following reasons:

1) as Mihalas and Binney (1981) pointed out, there are large selection effects at work in the sample of ELS that forms the basis of the correlation between metallicity and eccentricity. This simple model was unable to explain that stars in the nuclear bulge of our own Galaxy and in the central region of elliptical galaxies, which are Pop. II by kinematic criteria, are found to be metal rich;

2) detailed analyses of stars in the solar neighbourhood showed that this correlation does not hold. It is shown that stars with identical values of metallcity fall neatly into two kinematics subgroups, one clearly having Halo Population characteristics (high vertical velocity, eccentric orbits) and the other having Disk Population characteristics (low vertical velocity and circular orbits).

Above all, many perceptions of the scheme that were self consistent

in the solar neighbourhood gave rise to contradiction when applied to the other parts of the Galaxy.

By the 1970s and 1980s the emphasis had shifted towards a description of the Galaxy in terms of a disk and a spheroid, all embedded in a dark corona commonly called as the dark halo (Searle, 1986 and Freeman, 1986).

The spheroidal component (SC) includes the halo, bulge and nucleus, and is relatively simple, although it differs significantly from Baade's original conception. The space distribution of SC stars is nearly spherical, they are strongly concentrated at the center, with number densities of all objects rising as $\propto R^{-3}$ for R in the range 100 $pc \leq R \leq 30$ kpc. Globular clusters and RR Lyrae stars are typical members of SC that can be identified throughout its volume. In the solar neighbourhood, the SC is also represented by the extreme subdwarfs, which of course may exist everywhere within it, but can be detected only locally. All of these objects are old, 10 to 15 billions years. The masses of SC stars are about 0.8 $M_{\odot}$ or less, more-massive stars having already evolved to white dwarfs. The SC contains little dust or interstellar gas, except in the galactic nucleus.

There is a strong dependence of metallicity on the radial distance, in the sense of increasing metallicity toward the galactic center. There is large scatter of metallicity in the outermost regions of the SC.

In terms of metallicity the SC can be divided into the following metallicity groups: a metal-poor halo, a metal-rich bulge and, in between, one or more intermediate spheroidal component systems. Each of these metallicity groups fill almost the whole volume from the center out to some maximum distance, because SC objects move in highly eccentric orbits.

Kinematically, the SC is a system having a low rotation velocity around

the galactic center and a large velocity dispersion. Both SC stars and globular clusters move on highly eccentric orbits, but in principle we determine the orbits only for halo subdwarfs and RR Lyrae stars found in the solar neighbourhood for which the required measurements can be made.

The age estimate of disk components suggests that the disk may be significantly younger than the spheroidal components. It is likely that disk was formed out of the material processed by SC stars. Star formation in the disk apparently delayed until the gas had already been circularized by inelastic cloud-cloud collisions, so that even the oldest disk stars were formed in nearly circular orbits.

The stars at a given position of the disk in the solar neighbourhood are composed of a broad mixture of disk populations of widely varying ages and properties, plus stars from background of the spheroidal component within which it is immersed. The stars in the disk population are classified into three subclasses: (1) Young Population; (2) Intermediate Population; and (3) Oldest Population.

The very youngest stars in the solar neighbourhood belong to the spiral-arm population. These stars are concentrated groups (open clusters and associations) in the galactic plane in a dust- and gas-filled environment, from which they were recently formed when the interstellar material was compressed and star formation was triggered, and they have solar or above solar metallicity. The spiral-arm population includes stars of all masses, and it has few or no white dwarfs. Its brightest members are blue supergiants and upper-main sequence stars, and their main sequence will be like that of NGC 2362 and h and χ Persei (Fig 1.2). These are bright luminous objects and there presence is detected easily. Spiral-arm stars move on essentially

circular orbits around the galactic center and have small random velocity dispersion relative to the interstellar clouds. These stars are more closely confined to the galactic plane and their correlation with the distribution of molecular clouds suggest that they form out of these clouds.

Intermediate disk population are older than younger disk population, they are generally found in a group 5 billion years old: during this period the A and F stars have evolved out of the MS and are accounted for in an increased number of white dwarfs. The mean mass of the sample is smaller than for young disk stars. The H-R diagram of these stars would be like that of M67 (Fig. 1.2), and their metallicity probably ranges from perhaps a factor of two below the solar one up to solar chemical composition. Most of field G dwarfs belong to this group, and some of the field K and M dwarfs and white dwarfs are in this group. A typical member has an appreciably eccentric orbit, and thus it can move over a large range of galactocentric distances within the disk.

The oldest disk population stars may be as old as 10^{10} years, but they are probably somewhat younger. The members of this group are late G, K, and M dwarfs on the main sequence, large numbers of white dwarfs, and a good representation of subgiants and red giants. Their H-R diagram might resemble that of NGC 188 (Fig. 2.1), and we would expect their average metallicities to be a factor of three to five lower than the solar one. The orbits of a fair fraction of these stars will be quite eccentric.

Later on, the investigations of Gilmore and Reid (1982) and Zinn (1985) have shown that the disk is a more complicated structure than had been thought before. They suggested that the disk is composed of not only a thin component, but also a thick component.

From all these discussion, it should come as no surprise that our picture of populations of the Galaxy is still incomplete. Argument continues, for example, as to the nature of the thick disk. Much work is being undertaken on the Galactic bulge. What is clear, however, is the deriving incentive behind the desire to define the basic populations of the Galaxy. If we can comprehend the nature and interrelationships between the different populations we shall have an understanding of the formation and evolution of the Galaxy itself.

Tab. 2.1: The classification of stellar population at the Vatican conference of 1957.

	Population II		Disk Population	Population I	
	Halo Pop. II	Intermediate Pop. II		Older Pop. I	Extreme Pop. I
	Subdwarfs Globular clusters RR Lyrae stars with periods longer than 0.4 days	High-velocity stars with z-velocities> 30 km/sec Long-period variables with periods <250 days and spectral types earlier than M5e	Stars of galactic nucleus Planetary nebulae Novae RR Lyrae stars with periods <0.4 days Weak-line stars	A-type stars Strong-line stars Me dwarfs	Gas Young stars associated with the present spiral structure Supergiants Cepheids T Tauri stars Galactic clusters of Trumpler's class I
$\langle\|z\|\rangle$ (parsecs)	2000	700	400	160	120
$\langle\|Z\|\rangle$ (km/sec)	75	25	17	10	8
Axial ratio of spheroidal distribution	2	5	25?	?	100
Concentration toward center	Strong	Strong	Strong?	Little	Little
Distribution	Smooth	Smooth	Smooth?	Patchy, spiral arms	Extremely patchy, spiral arms
$Z_{b.g.}$	0.003	0.01	0.02	0.03	0.04
Age (10^9 years)	6	6.0 to 5.0	1.5 to 5.0	0.1 to 1.5	<0.1
Total mass (10^9 ⊙)	16	47		5	2

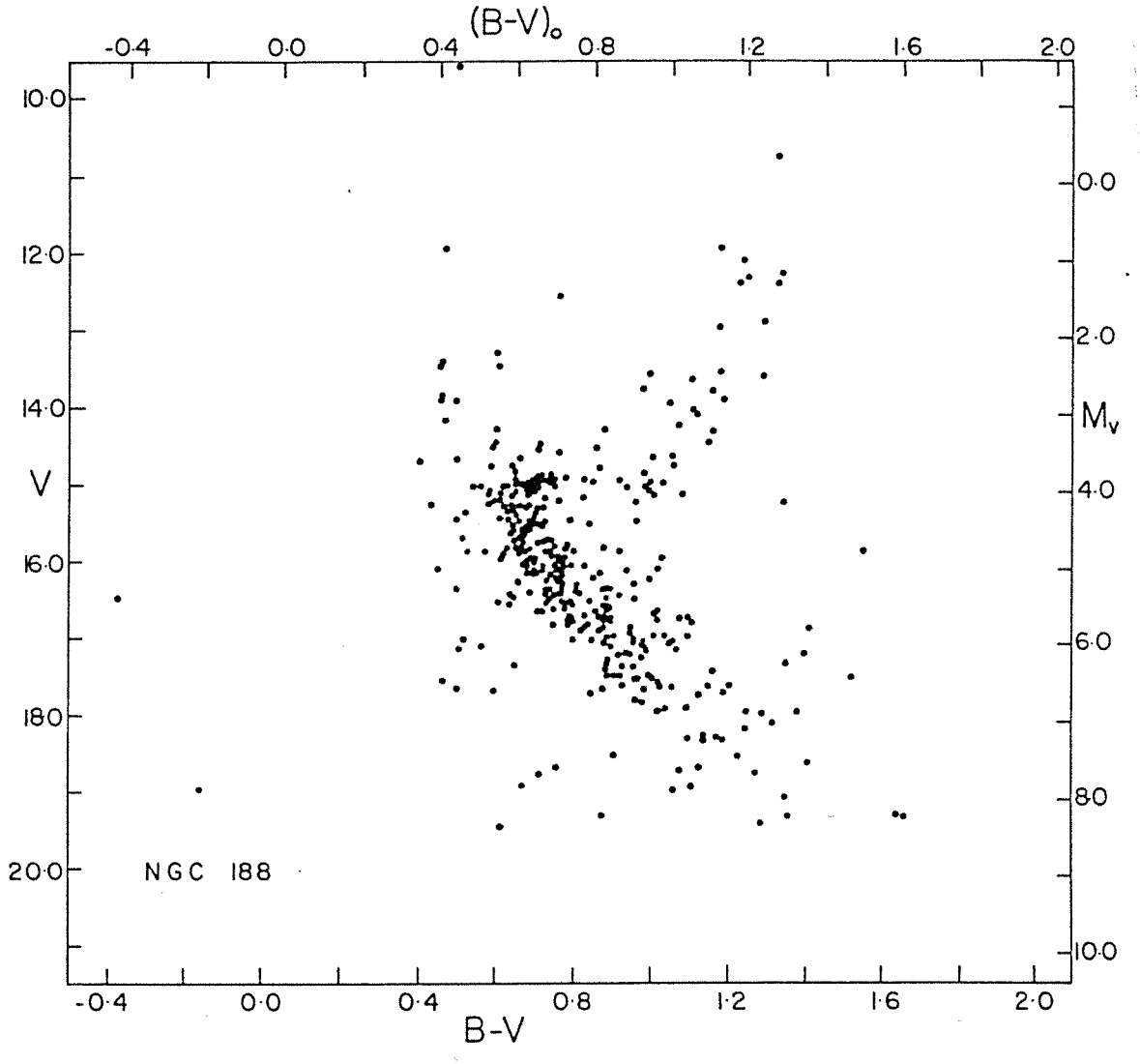

Fig. 2.1: CM diagram for the open cluster NGC 188.

3 THE ANALYSIS OF COMPOSITE LIGHT

Most of our knowledge about the extragalactic systems comes from the composite light of the objects that compose the systems. It is difficult to resolve directly the integrated light into individual components. Therefore, we need some methods which allow the analysis of integrated light to ascertain the nature of unresolved objects responsible for the radiation. Although this problem has been faced first by Whipple (1935), only recently quantative and qualitative solutions to this problem have been developed on the basis of improved knowlegde of theoretical models and the availability of high quality observations.

In the composite light of nearby stellar systems, the contribution of light at short wavelengths comes from the bluest stars, while at the long wavelengths comes from the reddest stars. The strengths of the spectral features, due to the contribution of a variety of spectral types, will be weaker than in individual stars, in the sense that there is dilution of continuum light from stars that are weak-lined at the feature of interest. The continuum and line spectrum at short wavelengths will be dominated by the earlier stars in the systems, and conversely at long wavelengths.

The problem of the analysis of the composite light can be tackled in qualitative and quantitative ways. Even though the qualitative methods give only a crude estimation of stellar populations, they can supplement the information to the quantitative methods.

In the light of stellar evolution theory, spectral synthesis technique evolved into two different methods: 1) Population synthesis technique, also known as "optimized synthesis", and 2) Evolutionary synthesis.

In "evolutionary synthesis" one predicts the spectral energy distribution

(SED) resulting from a particular evolutionary scenario or from empirical data. This technique is reviewed by Tinsley (1980), Barbaro and Olivi (1986), Renzini and Buzzoni (1986) and Buzzoni (1987). It is simple mathematically and generally used to explore only a limited parameter space, typically involving no more than 2-3 parameters. It is especially useful in examining the range of spectral properties which can be induced by variation of the dominant population parameters.

In the context of population synthesis, one starts from an opposite point of view with respect to the evolutionary approach: one estimates the most probable color magnitude diagram responsible for a given spectral energy distribution (SED). Historically, this technique began with relatively unconstrained additions of groups of stars in the CMD by trial and error to fit galaxy SED's (e.g. Roberts, 1956, de Vaucouleurs & de Vaucouleurs, 1959). It steadily evolved to the point where a very large volume of parameter space or range of population mixtures may simultaneously be explored by sophisticated automatic optimizing algorithms (Pickles, 1985, and O'Connell, 1986). The types of linear or quadratic programming methods used have wide utility in astrophysics (e.g. Schwarzschild, 1979).

In both of these approaches, stellar physics plays an important role. We will describe the stellar ingredients, in particular the role of stellar atmospheres, in the second part of this thesis. In this section we will describe the latter method in detail, while the evolutionary synthesis approach (Buzzoni, 1989) will be discussed at greater length in section 4.

3.1 Qualitative approaches

The following qualitative approaches are used to estimate the contribution of different spectral classes to the composite light:

(1) Count-to-Brightness Ratio;

(2) Integrated Spectral Type;

(3) Mass-to-Luminosity Ratio;

(4) Broad-Band Colors;

Each of them will be outlined in brief.

3.1.1 Count-to-Brightness Ratio

Baum (1959) had used this photographic method to resolve bright giants and supergiants in nearby galaxies. He considered the ratio of photographically resolved stars per unit area to surface brightness; the resolution limit at the distance of M31 was $M_v \sim -2$. He predicted that the ratio would be higher in globular cluster-like population than in a population like that of the solar neighbourhood, and that it would be lower in an old population where there are no bright blue stars but many unresolved old dwarfs. By these counts Bauum was able to show that the disk of M31 is probably dominated by Pop II. Although this is obviously a rather crude type of analysis, it can usefully complement others in checking predictions as to how many individual bright stars should be seen in a region of a nearby galaxy.

3.1.2 Integrated Spectral Type

On the basis of spectrograms of integrated light of various regions in giant galaxies, Morgan and Osterbrock (1969) classified the stellar populations

according to the appearance of the spectra. These types are correlated with the Yerkes classification of galaxies. This information allows us to understand the correlation between the process of star formation and the dynamical properties of galaxies. On this basis three principal categories were defined:

a) *The Orion population*: This has spectra showing emission lines, like the Orion nebula, superimposed on an early-type continuum with B-F type absorption lines. Such spectra are found in irregular galaxies with many H II regions, much gas, and bright blue stars, but little sign of later types.

b) *The Intermediate Population*: This has a spectral type near F8 in the blue-violet, but the spectrum is clearly composite, showing contributions from F-K stars; in other words, one sees spectral features that are strong in many different types of stars, but because of the diluting effect of other types, none of the lines is as strong as in individual stars. Populations with this kind of spectrum are found in the nuclear regions and main bodies of giant spirals of Yerkes classes fS and fgS.

c) *The amorphous population*: This is characterized by spectral type KO in the blue-violet, with very strong giant characteristics, of type near K5 in the green, and M in the red. The change of spectral type with wavelength illustrates clearly the expected change in stellar types that makes the dominant contribution; the rather late type at short wavelengths tells us that early (young) stars are a very small component of the population, if any. This population type is found in the entire bodies of giant galaxies, and in the inner regions of centrally condensed spirals.

Morgan and Osterbrock (1969) used this technique of making composite spectrograms, photographically adding those of different stars, to compare

with the spectra of galaxies. This method gives important qualitative information about the stellar population, but cannot be used to define a unique combination of stars capable of explaining the composite spectrum.

3.1.3 Mass-to-Luminosity Ratio, M/L

This quantity is determined, though seldom with great accuracy, for many galaxies and regions of galaxies. The most striking fact is that the integrated M/L of galaxies is nearly always greater than that of the stars found (spectroscopically and photometrically) to dominate the light; in other words, most of the mass resides in material that does not contribute to the light (at least in B and V, where M/L is determined). For example, the central regions of giant elliptical galaxies have$M/L_B \sim 0.01$. The nature of hidden mass is an interesting problem. We should clear away the common misconception, that the smallest objects we can imagine in the system are stars of mass $0.1M_\odot$ (This is the lower limit for hydrogen burning to occur) whose M/L is several hundred. The physical processes that determine the distribution of masses into which a gas cloud fragments are completely independent of those determining the mass limit for hydrogen-burning,i.e. for being a luminous star for an appreciable length of time. Thus there is no a priori reason why stellar population should not contain any amount of non-luminous sub-stellar objects, and we should not be concerned if spectroscopic data do not show the presence of enough late dwarfs to account for M/L.

3.1.4 Broad-Band Colors

The colors U-B and B-V have been measured for very large sets of galaxies, and their distribution across galaxies has been widely studied. Fewer data are available for colors at long wavelengths, and mostly for the nuclear regions only. Fig. 3.1 shows an average two-color diagram for galaxies compared with that of main sequence stars. The composite nature of the galactic light is obvious here: U-B is bluer for a given B-V in galaxies than in stars, because in galaxies bluer stars are contributing more in the U band than in V. For individual stars, UBV colors can be used to obtain an indication of the metal abundance and/or luminosity class. But for galaxies, it is generally not possible to derive such information from two-color diagram because one cannot disentangle blanketing effects from those due to an unknown mixture of different stellar temperatures and gravities. The integrated UBV colors of globular clusters do give useful information on the metal abundance, however, because one already knows more or less the distribution of stars in the H-R diagram; the reddening–free index Q=(U-B)-0.72(B-V) is a useful metallicity index, since it is determined by the colors of the giant branch and of the horizontal branch.

Recently, broad-band photometry has been constructed in the light of evolutionary synthesis coeval models. Fig. 3.2 illustrates the (U-B), (B-V) plot for the extensive time, metallicity (t, Z) grid of Rabin (1980), which is actually based on the corrected version of Yale isochrone (1977). For $Z \leq 0.5\ Z_{\odot}$, a good (t, Z) separation is possible. But loci become degenerate and thus indistinguishable for old metal rich populations, and UBVK colors are no less degenerate. The nuclei of luminous early-type galaxies fill the toe of the dashed line, and it is evident that the age assigned

to populations in this region will be a very strong function of Z. The red envelope of nuclear colors corresponds to 15 Gyr if $Z = Z_{\odot}$, but only to 7.5 Gyrs if $Z = 2\ Z_{\odot}$. However, the colors do provide the interesting limit that $Z \geq 0.5\ Z_{\odot}$, if $t \leq 20$ Gyrs. The main problem with this method is to disentangle the age effect from metallicity.

3.2 Quantitative methods

3.2.1 Intermediate- and Narrow-Band Spectrophotometry

This method is based on the pioneering work of Spinrad and Taylor (1971), who measured continuum colors over a wide range of wavelengths, thus sampling the stellar populations at a wide range of spectral types. Moreover, measurements at the wavelengths of suitable spectral features can give quantitative information of the kind discussed in Sec. 3.1.2 ; with care, one can obtain useful information on the metal abundance of the dominant stars, and information whether they are giants or dwarfs.

To establish the basic concepts, let us consider a population that, we have reason to believe, contains mostly old stars, distributed in the H-R diagram like in an old galactic cluster, with perhaps a few stars above the main sequence turnoff. We imagine the H-R diagram to be populated, as shown in Fig. 3.3, at K discrete points $(k = 1, 2, ...K)$ with n_k stars at k point. The numbers n_k are the unknown we wish to determine. Let the photometric system consists of fluxes, for which it is clear that the absolute calibration does not matter, in J filter bands, $j = 1, 2, ...J$. Let f_{kj} be the flux of a star of type k in filter band j, and let F_{gj} be the observed integrated flux of the galaxy population in that band. Generally the data are given in the form of luminosities (or magnitudes) at one band j_o and

the color relative to j_o; i.e., for stars of type k, the j-th color is

$$C_{kj} = -2.5\ log\ (f_{kj}/f_{kj_o}) \tag{3.1}$$

and for the galaxy, the $j-th$ color is

$$C_{gj} = -2.5\ log\ (F_{gj}/F_{gj_o}) \tag{3.2}$$

For a given assumed population, i.e. a set of values of n_k, one obtains the synthetic total fluxes, in bands j,

$$F_{sj} = \sum_{k=1}^{K} n_k f_{kj} \tag{3.3}$$

and the synthetic colors,

$$C_{sj} = -2.5\ log\ (F_{sj}/F_{sj_o}) \tag{3.4}$$

the problem is to find the best set of values n_k, by comparison of C_{sj} and C_{gj}.

Several methods have been used to solve this problem:

(a) *Blind algebraic method*

If $K \leq J$, it is possible to write the equations $C_{sj} = C_{gj}$, for K values of j, and solve them directly for n_k. However, because of observational errors, this procedure generally leads to non acceptable solutions, with astrophysically implausible distributions in the H-R diagram (e.g. K giants with no K0 progenitors) and even negative number of stars. This method have been rejected by most authors who have tried it.

(b) *Trial and error with astrophysical constraints*

This method can be used even if $K > J$. One imposes plausible constraints, such as that the values of n_k should increase down the main sequence, should be comparable to a cluster luminosity function on the giant branch, and should be small above the present-age main sequence turnoff. Then by the trial and error method one tries different mixtures until the colors, and perhaps M/L, are matched within the observational uncertainties. Plausible population models have been derived by Wood (1966), McClure and van den Berg (1968), and especially Spinrad and Taylor (1971). Basic problems with this method are that the uniqueness of the solution is not guaranteed and its sensitivity to observational errors is very difficult to estimate. These two problems, especially that of uniqueness,are the worst difficulties encountered in theoretical synthesis of stellar populations.

(c) *Quadratic programming*

Faber (1972) applied to the synthesis problem a mathematical technique that incorporates a chosen set of constraints objectively, yields a unique best solution for the given set of constraints, and allows the sensitivity of the solution to the observational errors to be tested readily. Of course a unique best synthetic population is not obtained objectively, because the choice of constraints is a matter of judgement.

The best criterion chosen by Faber (1972) is that the weighted sum of the squares of the fractional residuals in all filter bands be minimized, subject to the chosen constraints. The sum to be minimized is

$$\sum_{j=1}^{J} W_j (1 - F_{sj}/F_{gj})^2 \tag{3.5}$$

where the W_j are the weights that may be chosen at convenience; e.g., W_j may be the inverse squares of the observational errors of F_{gj}. The

constraints may include those mentioned for the trial-and-error method, expressed algebraically; e.g.:

(1) no negative numbers of stars are allowed:

$$n_k > 0. \tag{3.6}$$

(2) ratios of n_k can be constrained to lie within certain limits given by constants A_i:

$$A_1 < n_k/n_{k'} < A_2 \tag{3.7}$$

(3) the contribution of certain types of stars to the light in some filter band may be constrained to lie between certain values, perhaps suggested by spectroscopic criteria not contained in the filter photometry:

$$A_3 < n_k f_{kj}/F_{sj} < A_4 \tag{3.8}$$

(4) the M/L ratio in filter j may be constrained to lie within empirical limits:

$$A_5 < (\sum_{k=1}^{K} n_k m_k/L_{sj} < A_6, \tag{3.9}$$

where m_k is the mass of the star of type k. In view of the possibility of non-luminous matter, it is only safe to constraint M/L to lie below an upper limit given by the dynamically-determined mass of the system.

The mathematical method is described by Faber, and is straight-forward. It is found in practice that a unique solution results from a given set of constraints, even if $K > J$, because other solutions are excluded by the

constraint $n_k > 0$. The sensitivity to uncertainties in input data is tested by finding solutions for altered data in a series of numerical experiments.

Faber (1972) has applied this method to Spinrad and Taylor 36-color photometry, and to her own 10-color photometry of elliptical galaxies; the number of stellar ingredients allowed was $K = 38$.

(d) *Evolutionary synthesis*

We know theoretically that the stellar population of a system depends upon the past history of star formation and of chemical composition of the gas from which the stars formed. In order to avoid the problem of chemical composition, let us assume that all the stars are of solar abundance. The stellar birthrate is then a function of stellar mass m and time t, written as $b(m,t)dmdt$, which is the number of stars in mass interval $(m, m + dm)$ born in the time interval $(t, t + dt)$. The evolutionary approach to population synthesis asks: what function $b(m,t)$ will give rise to the population whose integrated radiation has the properties now observed ? The unknown quantities, which were n_k in the previous method, are now the parameters defining the function $b(m,t)$; the constraints are now the evolutionary tracks in the H-R diagram of stars of mass m. If the latter were perfectly known, then photometry in J filter bands might allow us to determine J parameters for the birthrate, which is an impressive amount of detail if $J \sim 36$. However, there are serious uncertainties in these constraints, so one has to content oneself with parametrization. For example, the birthrate may be separated into functions of mass and time:

$$b(m,t) = \Phi(m)\Psi(t) \tag{3.10}$$

where $\Phi(m)$ is the initial mass function (IMF); and $\Psi(t)$ is the star forma-

tion rate (SFR). Then one might adopt a power law for the initial mass function (IMF),

$$\Phi(m) = x m_L^x m^{-(1+x)}, m_U \geq m \geq m_L \tag{3.11}$$

$$\Phi(m) = 0, m > m_U, m < m_L \tag{3.12}$$

(where x is the slope of the IMF) which is normalized so that $\int_{m_L}^{m_U} \Phi(m) dm = 1$; where m_L and m_U are the lower and upper mass limits, respectively, and an exponential decline for the time dependence,

$$\Psi(t) = \Psi_o exp(-t/\tau) \tag{3.13}$$

The unknowns of the problem would be x (the slope of the IMF), m_U and m_L (the limits of stellar mass, where m_L might be substellar), Ψ_o (a parameter representing the efficiency of star formation), and τ (the time scale for star formation to decline). The procedure is to choose a discrete set of stellar massses, distribute stars on the zero-age main sequence at each time step according to $b(m,t)$; and follow their positions in the H-R diagram at later times, according to a prescribed set of evolutionary tracks. This procedure gives values of n_k, as before, and synthetic colors are derived. No objective method for choosing the best set of parameters has yet been used with this method, since the number of parameters is so small that the best agreement with observations can be checked by direct inspection of results.

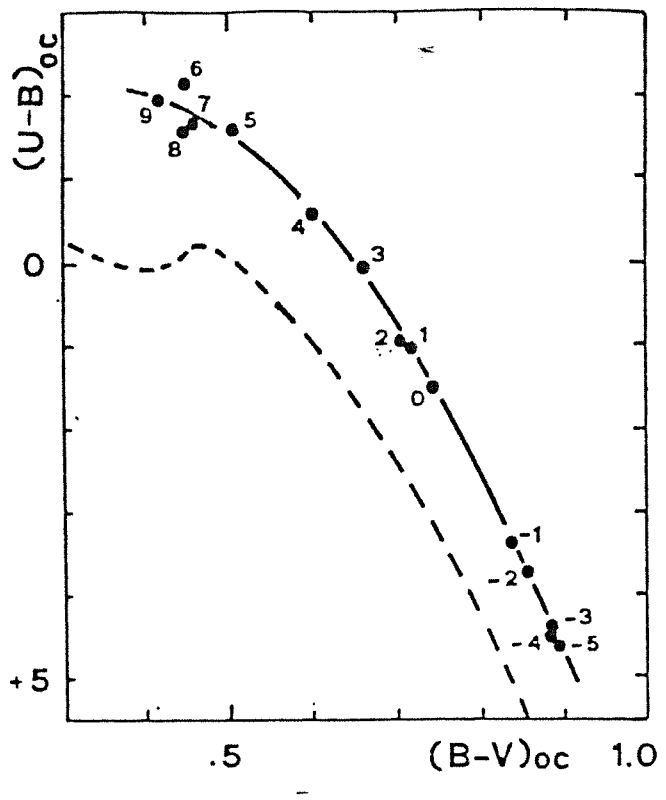

Fig. 3.1: Mean Two-color diagram; numbers refer to galaxy types. Dashed line is the stellar main sequence. (Adapted from Tinsley, 1975)

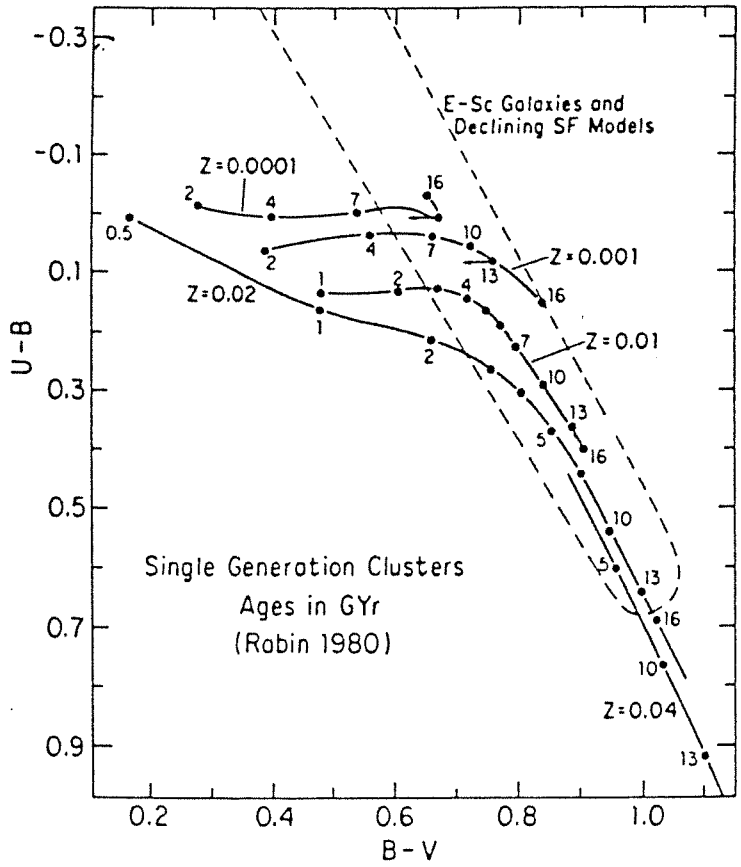

Fig. 3.2: A two-color diagram of evolutionary models for single generation star clusters of different metallicity.

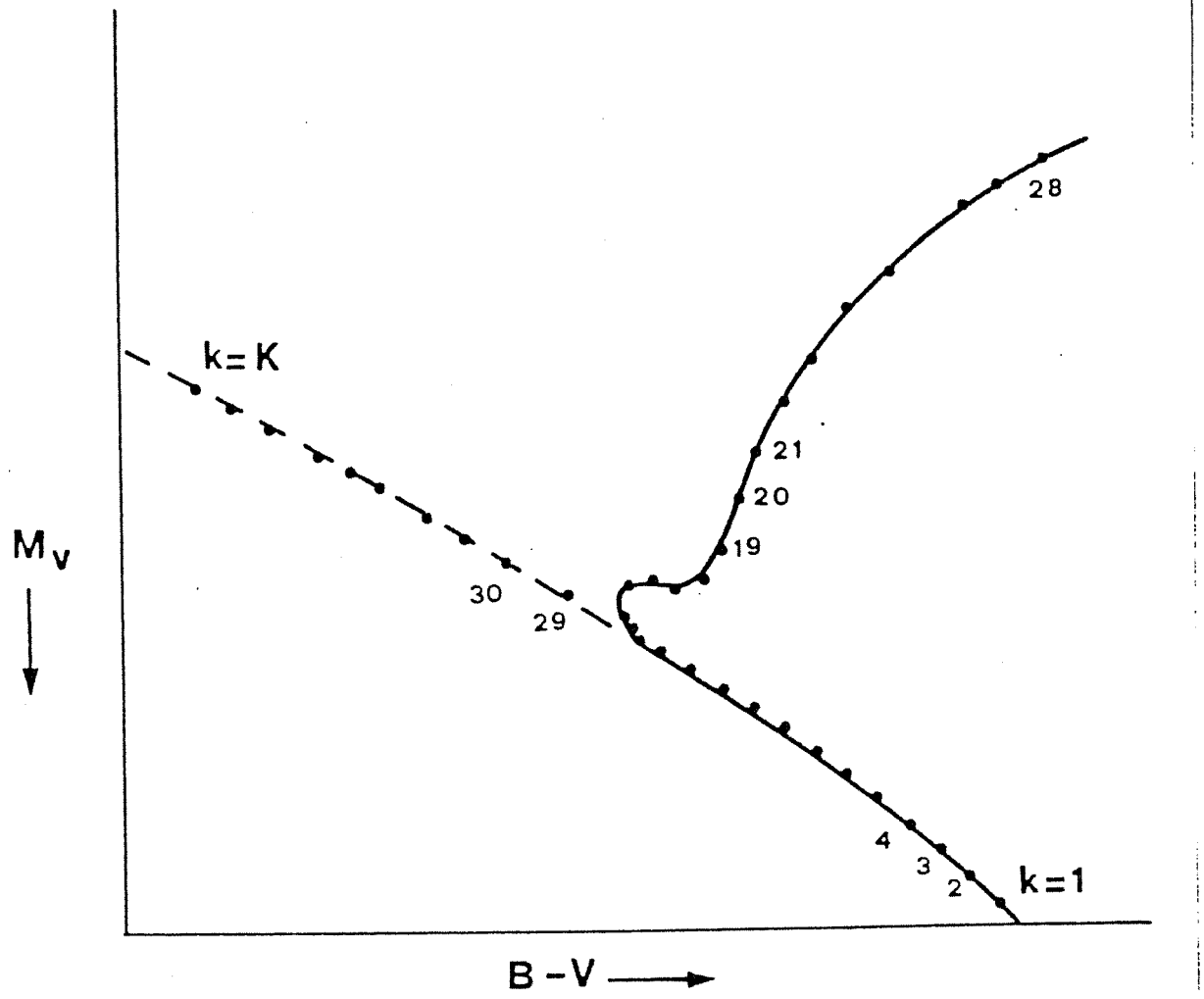

Fig. 3.3: The distribution of stellar ingredients on the H-R diagram for synthesis of predominantly old population. (Adapted from Tinsley, 1975)

4 EVOLUTIONARY POPULATION SYNTHESIS

Evolutionary population synthesis (EPS) is a powerful tool in exploring not only the nature of the stellar populations and spectral energy distribution (SED) of stellar systems at the present time but also for the reconstruction of their past history.

In evolutionary synthesis technique, one starts from the basic assumptions that both the initial mass function and the star formation rate can be expressed by simple analytical functions. These two functions give the number of stars of a given mass born during a given time interval. Evolutionary tracks provide the amount of time spent by stars of different masses at different positions of the H-R diagram, and stellar atmosphere models provide the spectral energy distribution. Once the stellar population content of a model is calculated, the predicted spectrum is easily found.

This technique has been reviewed by Tinsley (1980) and Barbaro and Olivi (1986). Recently, Buzzoni (1989) has computed a set of EPS models for old simple stellar populations (SSP), which takes into account the effects of relevant parameters like age, chemical composition, slope of the initial mass function (IMF), and efficiency of the stellar mass loss on the SED's. Moreover, the computational code completely incorporates in a quantitative way the contribution from all the relevant stellar evolutionary phases according to the theory of stellar evolution. This is an important step, since previous works on EPS systematically missed a realistic description of the evolutionary scenario ignoring the contribution from stars in some important stages of their life, like the Horizontal Branch (HB), the Asymptotic Giant Branch (AGB) and the Post Asymptotic Giant Branch

(P-AGB), (Tinsley and Gunn, 1976, hereafter TG76, Tinsley, 1978, Gunn, Stryker and Tinsley, 1981, Bruzual, 1983, Arimoto and Yoshii, 1985). In some cases the lack of this knowledge was partially recovered by means of qualitative or semi-empirical corrections (Sil'chenko, 1983). With the improved knowledge of stellar evolutionary concepts, it has become essential to incorporate these phases of stellar evolution into EPS. In this section we will present the theoretical approach of EPS, in particular reference will be made to Buzzoni's models (1989) which we are using for the analysis of synthetic spectra and ingredients involved in this approach.

Obviously, the evolutionary population synthesis approach proves itself more convenient for the study of spectral evolution, and it is the one which will be used in our investigation. On the other hand, the population synthesis approach does not provide with any information about how the stellar content of stellar systems came to be what the model predicts, and there is no unique way to derive the past history of a galaxy.

4.1 The Theoretical Approach

The synthetic approach is generally based on the following assumptions:

(1) the non-thermal emission from the interstellar gas is negligible; this automatically rules out the possibility of modelling active galaxies, whose activity cannot be assigned to the stars;

(2) the thermal emission from the interstellar gas is negligible; Huchra (1977) has shown that the continuum emission from the interstellar gas is negligible compared to that of stars;

(3) the absorption of light from gas and dust can be neglected. Although this assumption seems justified for the early type galaxies, it is not true for

late-type galaxies, where gas and dust are present in considerable amount.

(4) a simple stellar population (SSP) is generally considered: it is an assembly of coeval, intially chemically homogenous, single stars; galaxies are not SSP, as they contain stars of different metallicity and of different ages (perhaps excluding the elliptical galaxies), and binaries are common objects. However, the complex systems can be expressed as series of SSP, and therefore the case of SSP must be understood before attempting more complex systems.

As a result of these assumptions the integrated bolometric luminosity of SSP is contributed by stars in different phase of evolution. The contribution to the integrated bolometric luminosity arises from the main-sequence (MS) and post main sequence (P-MS) stars. The P-MS can be subdivided in whatever manner we wish to do it.

The first step towards the construction in EPS models is the correct determination of the distribution of stars along the different evolutionary tracks in the H-R diagram.

We know that the number of stars in the post-main sequence phase is proportional to the lifetimes spent during this stage of evolution, but depends primarily on the IMF in the main-sequence. In order to evaluate the star counts on the H-R diagram, the continuous distribution along each sequence is to be ensured.

In the case of simple stellar population model, the IMF is assumed to be represented as:

$$\delta N = N(M)\delta M = AM^{-s}\delta M \tag{4.1}$$

with the Salpeter exponent s=2.35 derived from empirical star counts in

the solar neighbourhood. The right hand side of Eq.4.1 gives the number of stars in the mass range $M \div$(M+δM). The coefficient A in the equation is a normalization factor, possibly related to the star formation rate (SFR) which in turn depends upon time. In the case of a single burst population, the SFR is virtually a δ-function, A is a constant related to the total number of stars (N_{tot}) or the total mass (M_{tot}) of the SSP in a simple way:

$$A = (1-s)\frac{N_{tot}}{[M^{1-s}]_{M_l}^{M_u}} \quad s \neq 1 \tag{4.2a}$$

$$A = \frac{N_{tot}}{\ln(M_u/M_l)} \quad s = 1 \tag{4.2b}$$

or

$$A = (2-s)\frac{M_{tot}}{[M^{2-s}]_{M_l}^{M_u}} \quad s \neq 2 \tag{4.3a}$$

$$A = \frac{M_{tot}}{\ln(M_u/M_l)} \quad s = 2 \tag{4.3b}$$

where M_u and M_l are the masses of the upper and lower cut off in the IMF.

It is well known that the stellar lifetime is a function of the stellar mass, and a star spends most of its lifetime while burning hydrogen on the main sequence. For a SSP of age t, the turnoff mass, M_{TO}, is defined as the mass of a star which is on the verge of exhausting hydrogen at the center. Therefore, stars with initial mass $M_i < M_{TO}$ are still burning hydrogen at the center, and stars with $M_i > M_{TO}$ are in more advanced stages of evolution, or have already completed their evolution. Since the turnoff mass is a function of the age of the SSP, from the evolutionary models (Becker and Iben 1979, Mengel *et al.* 1979) one can derive the following analytical expression (numerical constants are given for $(Y, Z) = (0.28, 0.02)$):

$$\log M_{TO}(t) = 0.0558 \log^2 t - 1.338 \log t + 7.764 \tag{4.4}$$

where M_{TO} is in solar masses and t is in years.

So, expressing mass as a function of time, Eq. 4.1 can be written as:

$$\delta N = AM^{-s} |dM/dt| \, \delta t \tag{4.5}$$

Eq. 4.5 is satisfied on the basical assumption that the time interval δt is short enough to ensure a variation δM on M such that $\delta M \ll M$. One of the useful applications of Eq. 4.5 is that it can be used to derive the star counts in PM-S. Since, the mass of stars evolving across the TO depends on the time i.e. $M_{TO} = f(t)$, we find from the models that it is of the same order of M_{TO}/T where T is the age of the population for a given M_{TO}. Moreover the P-MS evolutionary time, t_{pms} , for a star of mass M_{TO} is always shorter than T (the ratio t_{pms}/T ranges between 1/3 and 1/5). This means that the difference δM in the initial mass between dying stars and those leaving the TO at a given age can be evaluated as: $\delta M = t_{pms}(dM_{TO}/dt) \sim M_{TO}(t_{pms}/T)$ thus satisfying the condition $\delta M/M \ll 1$. In a SSP we are dealing at any time with a P-MS evolution of stars of initial mass nearly identical to M_{TO}. Thus Eq. 4.5 provides the right distribution of stars along the different evolutionary branches, once we divide them into discrete bins of known duration δt.

We can also write:

$$\delta N_{pms} = b \delta t_{pms} \tag{4.6}$$

where

$$b = AM_{TO}^{-s}|dM_{TO}/dt| \tag{4.7}$$

is the "evolutionary flux " of the SSP.

Another quantity, which is equivalent to b but more useful in the practical application is the "specific evolutionary flux" defined as:

$$B = b/L_{tot} \tag{4.8}$$

where L_{tot} is the bolometric luminosity of a SSP having a given $b - flux$. Since L_{tot} scales with the same value of A as b does, their ratio is an intrinsic parameter of the SSP allowing a direct link betwen star counts and evolutionary lifetimes for real populations of the integral observed luminosity L_*:

$$N_{pms} = BL_*t_{pms} \tag{4.9}$$

It was shown by Renzini and Buzzoni (1986) (hereafter RB86), that B does not depend very strongly on the other parameters and it can be regarded as a cosmic constant. Its value is about $(1.7\pm0.4)\times10^{-11}[L_\odot^{-1}yr^{-1}]$

Concerning the inner consistency of the EPS models, there is another important condition to be fulfilled. Eq. 4.6 implies that the contribution in bolometric luminosity coming from the stars in the P-MS phases (L_{pms} is given by

$$L_{pms} = b\int^{pms} L_t dt \tag{4.10}$$

where L_t is taken over the evolutionary track of a star of mass M_{TO}. The physical meaning of Eq. 4.10 is that the P-MS luminosity of a SSP is simply

proportional to the nuclear (and gravitational) fuel available to stars having $M = M_{TO}$. This condition, originally stated in Tinsley and Gunn (1976) and now known as the "Fuel Consumption Theorem", is a powerful tool to check the consistency of the monochromatic contribution from stars in some exotic phases, like for instance the AGB. In these cases we can approximate the knowledge of the evolutionary path of the stars in the H-R diagrams by means of the constraints on their total fuel available, which is usually rather well defined for the stellar models.

As mentioned above, the theoretical SSP's closely resemble the real cases of single burst SFR's but in principle all arbitrary complex histories can be constructed by properly combining these basic models. In the case of SSP's, the star formation rate (SFR) is SFR=δ_T, otherwise, in real cases, it is convolution of some SSPs weighted by their SFR. In the general case that SFR $\neq 0$ in a short time $\tau \ll T$, our δ-function simplification holds as long as the expected variation of the SSP at the relevant wavelength of observation can be supposed to be negligible over the age interval $[T - \tau, T]$. This condition is usually met, but complications can arise when approaching the creation event, i.e. $T \rightarrow \tau$, or in the case of a sudden phase transition in the overall evolutionary phase when the time scale is comparable with τ.

Another question which deserves more attention in comparing theoretical and observed SED's, concerns the stochastic fluctuations in the emitted flux due to the discreteness of the real populations. Stochastic fluctuations could play a role for instance in the globular clusters, despite there are about 10^5 stars, a number large enough to assure a smoothed contribution to the total SED (Buzzoni, 1988).

4.2 INGREDIENTS FOR EPS

In an effective EPS approach two sets of data should be properly linked:

(1) we need a set of isochrones providing a good representation of the distribution of the stars in the H-R diagram, and

(2) we should be able to reproduce the SED of each star along the isochrone in order to take into account all the possible contributions to total light of the population.

Concerning the isochrones, we must ensure continuity in luminosity, temperature and star counts along the MS, the sub-giant branch, the red-giant branch and the subsequent phases for which we use evolutionary tracks at constant mass. The parameters involved in the calculation of Buzzoni models are as follows: Metallicity cover the range of $0.0001 \leq Z \leq 0.03$. Helium abudance is taken to be $Y = 0.23$ for the metal poor condition, and $Y = 0.25$ for $Z \geq 0.01$. The first value well accounts for the abundances estimated in the globular clusters (Buzzoni *et al.*, 1983). Three different exponents for the IMF are considered: 1.35, 2.35, and 3.35. Mass loss parameter is parameterized by means of the coefficient η (Reimers, 1975). It assumes the values 0.3, 0.4, and 0.5 (the commonly accepted value of 0.4 comes from the empirical calibration based on the galactic globular clusters, Fusi Pecci and Renzini, 1976,1978).

Ages of the models are chosen to cover the old SSPs, dominated by low mass stars; they span from 4 to 18 Gyr. In Tab. 4.1, the grid for calculated SSP's models is given.

4.2.1 Main Sequence

In constructing EPS models, we need a wide range of isochrones which cover the distribution of stars in CM digram to all phases of evolution. Among the existing ischrones, VandenBerg and collaborators (VandenBerg 1983,1985, VandenBerg and Bell, 1985, VandenBerg and Laskarides, 1987) isochrones are preferred. This set is commonly accepted as the most effective in reproducing the observed features of the CM-diagrams of the globular clusters. In particular it takes into account the influence of the stellar convection, through the variation of the mixing length parameter α. The basic difference between the new set and the most popular one used so far in EPS, i.e. the Yale isochrones (Ciardullo and Demarque, 1977), is the fact that by increasing α from 1.0 as previously used to $1.5 - 1.6$, stars become slightly bluer. The effect of increasing efficiency in the convection mimics an increase in the mass of the convective envelope of the stars, thus increasing the gravity. This forces stars to reach thermodynamical equilibrium at lower radii and at slightly higher temperatures. The shift becomes important where a large convective envelope is present, namely around the TO for the low mass stars ($M < 1.5M_{\odot}$) and at the base of the RGB. It increases for high metallicity mixtures due to the direct influence of the opacity on the radiative gradient, which constraints convection.

As a result, relevant consequences are induced in the EPS models. It is well known that the MS are the main contributors to the short wavelength emission of galaxies, since the stars around the TO are usually among the bluest members of a SSP. In fact the comparison of the observed and the theoretical SEDs around the 4000 $\AA$ break is a very popular procedure to estimate the age of the elliptical galaxies (O'Connell, 1980, Pickles, 1985,

Pickles and Van der Kruit, 1988). Therefore it is clear that synthetic models that miss the right blueness of the MS are expected to underestimate the true age of the galaxies since younger isochrones are needed to fit the observed SED. Fig. 4.1, shows the theoretically predicted relative contribution as function of age turnoff mass M_{TO}: it shows that, for young populations, relative light contribution from the main sequence is dominant.

Due to their wide spread in temperature, MS stars are effective contributors also to all the different bands of the total SED. In particular, the near infrared could be modulated by the red dwarfs, especially in the case of a steep IMF. Since VandenBerg's isochrones do not cover the range of luminosity to the faint tail of MS, this can be extended by other authors using the set of evolutionary tracks for red dwarfs calculated by VandenBerg, Hartwick, and Alexander (1983); Copeland, Jenson and Jorgensen (1970); Seinkiewicz (1982), D'Antona and Mazzitelli (1985).

Red dwarfs are almost unevolved stars and they are still expected to populate the ZAMS; nevertheless, in order to ensure continuity, a little enhancement is necessary, slightly increasing luminosity and temperature of the dwarfs from their location on the ZAMS. A lower cut off in mass at M_l is adopted for the MS, which accounts for the limit on the nuclear reaction to occur. It has been tested that the variation of M_l does not affect the synthetic SED of the SSP, while M_{tot} (and then the M/L ratio) is affected.

4.2.2 The Post Main Sequence Link

In accounting for the P-MS evolution, great care must be excercised to correctly match evolved stars with the bulk of the SSP represented by the MS.

Continuity in the star counts has to be guaranteed in order to avoid fatal misinterpretations of the contribution from the bright stars. The main-sequence is linked to the P-MS sequence stage through the turnoff point, which is the core of the stellar evolution clock. Even the reliablity of MS models is tested by looking at the implication at the TO point. For the old stellar populations, PM-S phases provide roughly 70% of the total luminosity of a SSP. They radiate mainly in the infrared but their contribution at short wavelengths cannot be neglected when we try to discriminate the age of a SSP from the study of its SED in the blue. Correct scaling of the P-MS rests on the basic relation defined above: in particular by means of Eq. 4.6 we are able to convert the extremely thin spread in mass into star counts, through the IMF. The only crucial quantity to be known in this regard is the evolutionary flux b. This provides the right scaling factor since it contains the information on the total mass of the SSP, through the constant A of Eqs 4.3 and 4.4. In sequences of models, A remains constant when varying the age, and the evolutionary flux is modulated only by the factor $M_{TO}^{-s}|dM_{TO}/dt|$ which is time dependent. The other post-main sequence stages are discussed in the following subsections.

4.2.3 Red Giant Branch

The RGB is perhaps the most prominent feature of old stellar populatiom and RGB stars provide a good fraction of cluster radiation (see Fig. 4.1). The models of Sweigart and Gross (1978) cover a wide range of tracks and follow the stars until the tip of the RGB evolution. However, Sweigart and Gross's models were calculated for mixing length parameter $\alpha = 1$ as they were extension of the tracks by Mengel *et al.* (1979) that formed the base

of Yale isochrones. Buzzoni has used the linear slope of the $\log L$ vs $\log T$ from Yale isochrones, then adjusted the offset so as to match the Vanden Berg's isochrones. Thus the new RGB's relation becomes:

$$\log T = (-0.13 \log Z - 0.92) \log L + offset \tag{4.11}$$

4.2.4 Stellar Mass Loss

The mass loss from the stars involves the outer layers of the stars, thus removing the fresh fuel from their envelopes. As soon as the nuclear burning proceeds outwards, the evolution is suddenly truncated; this is believed to occur in the AGB phase.

In RGB the mass loss is not expected to strongly affect photometric features of the evolution but, since the mechanism involves the stellar envelope, the actual mass of the stars reaching the subsequent HB phase is slightly reduced. It is expected that scatter along the HB phase could be due to variable mass loss. Buzzoni (1989) took into account the mass loss by following the relation of Reimers. Its rate is supposed to depend on radiation pressure and gravity:

$$\frac{dM}{dt} = -4 \times 10^{-13} \eta \frac{L}{gR} \, [M_\odot / yr] \tag{4.12}$$

where η is a tuning factor, of the order of the unity, and the other quantites are to be expressed in solar units.

4.2.5 Horizontal Branch

The HB is one of the intriguing phase of evolution for the low mass stars. A variety of evolutionary tracks are already available, covering a large spread

in total mass and metallicity, and computational details seems to be well under control (Sweigert and Gross, 1976; Seidel, Demarque and Weinberg, 1987; Sweigert, 1987). Nevertheless difficulties still arise in explaining the HB morphology as it is seen for the globular clusters. Two requirements seem to be fulfilled to reproduce the observations: i) slightly lower masses than the TO mass, and ii) a spread in the actual mass of the HB stars.

Point i) is easily satisfied once the mass loss is taken into account, and point ii) is related to the so-called "second parameter effect", and at present we do not have a satisfactory solution for this problem (Sandage and Wildey, 1967; Rood, 1973; Fusi Pecci and Renzini, 1978; Crocker, Rood and O'Connell, 1988). Instead of ignoring this phase, some approximation may work:

1) independently of the mechanism at work, the net effect is a spread in colors along the HB observed in some globular clusters;

2) this effect should be induced by a spread in the actual mass of the stars, in the sense that stars at lower mass populate the HB at the bluer colors;

3) assuming the real HB to be conveniently described by the distribution of the stars along the ZAHB (zero age horizontal branch) (Iben and Rood, 1970), a narrower spread in mass is required to produce a given spread in color when metallicity increases;

4) HB morphology in the globular clusters seems to be related to the metallicity of the population, in the sense that HB becomes bluer by decreasing Z.

4.2.6 Asymptotic Giant Branch

There are basically two problems to be solved to correctly insert AGB evolution in the SSP models:

i) we do not know the detailed path of the stars along the AGB for various combinations of age and chemical composition;

ii) stellar evolution can be strongly affected by some new mechanisms, for instance mass loss, that introduce additional degrees of freedom to be parameterized and explored.

At present, a very limited data-base of AGB evolutionary tracks is available: because difficulty in properly reconstructing the whole structure of these stars due to their two sources of energy, ie. hydrogen and helium shell burning. This happens under very peculiar conditions and some abrupt instabilities can arise. At present, all our theoretical acquirements concerning the AGB evolution of low mass stars comes from works by Gingold (1974, 1976), Paczynski (1970, 1971, 1975) and Iben (1982), who provide some quantitative hints about the evolutioanry lifetimes and the expected luminosity function for stars of different chemical composition. In particular Gingold and Iben let evolve population II stars ($Z = 0.001$) with masses between 0.5 and 0.7 $M_{\odot}$, while Paczynski provided a useful relation between core mass and luminosity for population I stars ($Z = 0.03$). This relation fairly accounts for the path of the stars along the upper part of the AGB, when thermal pulses occur.

The better understanding of the inner structure of the AGB stars and in particular of their nucleosynthesis and energetics comes from Iben and Renzini (1982a, b, 1983) and Renzini and Voli (1981). This highly facilitates in setting reasonable constraints to the contribution of the AGB stars to a

SSP via the fuel consumption theorem.

4.2.7 Post Asymptotic Giant Branch

The fast ejection of most of the stellar envelope moves stars rapidly away from the AGB to the opposite side of the H-R diagram. P-AGB evolution of low mass stars are believed to coincide with the planetary nebula phase, having the nebula formed by the lost envelope (Wood and Cahn, 1977). Stars in P-AGB phase can reach up to temperatures $T > 10^5 K$ and spend most of their fuel above T = 20,000 K. The associated energetic is not relevant, since RB 86 find just $\sim 1\%$ at the most in the bolometric emission of an old SSP (see Fig. 4.1). But it is remarkable to note that this light is mainly emitted in the far UV, at the wavelengths shorter than 2000$\mathring{A}$. Here P-AGB might contribute in a more effective way to the SED of a SSP. Basically, the treatment of the P-AGB was computed by Paczynski (1970, 1971), who gave the evolutionary tracks for three masses, i.e 0.6, 0.8 and 1.2 $M_{\odot}$. Schonberner (1979, 1981) has computed models for low mass stars.

There is no doubt that ellipticals must contain hot post-AGB stars, since dying stars necessarily go through this stage before becoming degenerate dwarfs. From the fuel consumption theorem, the relative contribution of hot P-AGB stars is proportional to the amount of fuel which is burned during this stage. Stars leave the AGB and go to P-AGB only after having ejected most of their H-rich envelope. Hence they retain very little fuel to burn but they do so at the expense of high effective temperature.

Tab. 4.1: Grid of parameters for which Buzzoni (1989) computed evolutionary population models.

Chemical Composition (Z,Y)		Age (Gyrs)							
0.0001	0.23				8	10	12.5	15	18
0.001	0.23				8	10	12.5	15	18
0.01	0.25	4	5	6	8	10	12.5	15	
0.017	0.25	4	5	6	8	10	12.5	15	
0.03	0.25	4	5	6	8	10	12.5	15	

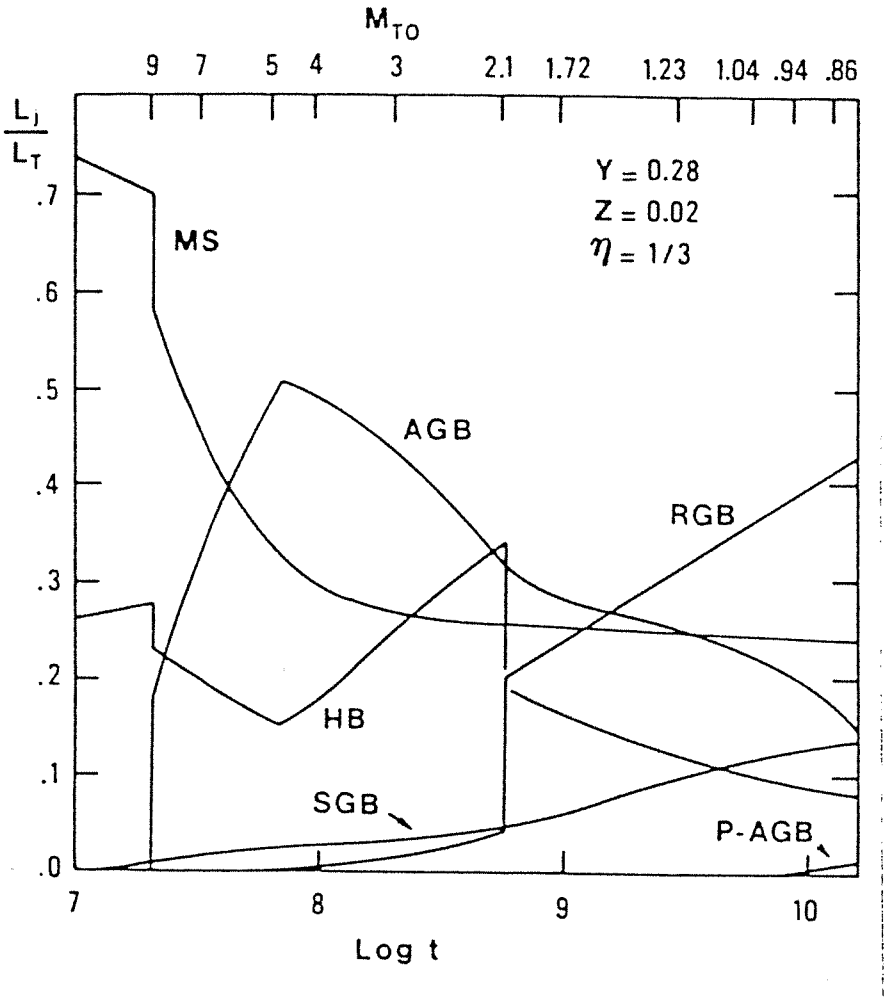

Fig. 4.1: The relative contribution of the various evolutionary stages to the integrated bolometric luminosity of a simple stellar population as a function of age (lower scale) and turnoff mass (upper scale). The various evolutionary stages are indicated in Fig. 1.3b.

5 SPECTRAL FEATURES DESCRIPTION

One of the most intriguing problems concerning the study of the evolutionary status of the stellar populations in stellar systems is to differentiate between observational effects due to the age from those due to the chemical composition. A direct comparison of integrated spectral energy distribution of the stellar systems with a reliable set of theoretical models of stellar populations (Buzzoni, 1989) does not allow one to solve the dichotomy in a unique way. For instance, it is claimed that in stellar systems photometric indices corresponding to the Turn Off (TO) temperature in the color-magnitude diagram could provide a good estimate of their age (O'Connell, 1980).

This idea encounters difficulty because the TO temperature depends upon metallicity of the stellar population, since colors of high metallicity isochrones for a given TO temperature mimic those of old low-metallicity at low temperature ones (VandenBerg and Bell, 1985; VandenBerg and Laskarides, 1987). In order to overcome such a difficulty we need suitable data with higher spectral resolution than broad-band colors. As might be expected, the temperature distribution of the population is most strongly dependent on the continuous energy distribution, while the metallicity distribution is most strongly dependent on the line spectrum, though there is enough interaction that these aspects cannot be considered independently (Pickles, 1985). Long wavelength-baseline spectra with resolution of $20 - 30$ $\AA$ and S/N$\geq$ $30 - 50$ appear sufficient to separate the age and metallicity effects (O'Connell, 1986).

In this section, we discuss the spectral features which are strong enough to be detectable in stellar systems at large distances; and the correlation

between feature strengths and physical parameters of stellar populations, such as effective temperature, gravity and chemical abundance. Besides, we will describe our present choice of spectral features; and reference stellar library, which is usually adopted to study the stellar populations in population synthesis techniques.

5.1 Observations

A wide variety of line- and band-strength indices have been defined by choosing different sets of intermediate filters. These filters have typically half widths $\sim$ 100$\AA$, and are strategically placed in wavelength so that one of a pair of filters transmit light at the frequency of a strong spectral feature, while the other measures the brightness in an adjacent continuum band. The difference in the brightness observed in the two filters (expressed in magnitude) provides a measure of the strength of the spectral feature. One of the first systems of this type to be introduced was the David Dunlap Observatory (DDO) six-color system of McClure and VandenBerg (1968). A twelve-color system has been defined by Wood (1965, 1969). Features that can be monitored in this way include the CN absorption near λ4200$\AA$, and Mg absorption near the λ 5200 $\AA$.

Out of these filters, Faber (1973) selected 10-filters (see Table 2 in Faber, 1973) to study stellar systems (elliptical galaxies) of old stellar populations. She found that the strength of the absorption features CN (λ_{eff} 4167 $\AA$, 4181 $\AA$) and Mg "b" plus MgH (λ_{eff} 5162 $\AA$, 5195 $\AA$), together with blanketing by metallic lines increase monotonically with increasing luminosity. This suggests that the mean metal abundance of stellar populations increases with luminosity. Therefore a rigorous attempt at pop-

ulation synthesis would utilize a complete grid of spectral features of stars of different mass, age, and composition. We will discuss this point in Sec. 5.1.1. Faber (1983) concludes that a reddening free line absorption index monitoring CN and Mg can be used to determine the absolute magnitude of the elliptical galaxies with an accuracy of $\pm 0.56\ mag$.

In order to study the stellar populations of old stellar systems, Faber *et al.* (1985) (hereafter referred to as FFBG) have analyzed and intercompared eleven strong features, based on spectra taken at 9 $\AA$ resolution, in a sample of K-giant stars in the solar neighbourhood and in globular clusters. Features measured include CN $\lambda 4170$ $\AA$, the G band, H_β, Mg b, MgH, Mg b + MgH, two Fe lines, Na D, and two TiO bands. The complete list of these features with their central wavelengths and continuum is presented in Tab. 5.1. Their purpose of analyzing K-giant stars and globular clusters is to calculate integrated indices for model stellar populations and to calibrate line strength indices as a function of metallicity.

This approach can be tackled in a purely theoretical way, since the set of representative stars can be substituted by a library of pseudo stars obtained by model atmospheres and synthetic spectra.

The aim of our research project is to calibrate some of the synthetic spectral indices listed above versus metallicity in a combined way, using both the empirical and theoretical approaches. At present, we are working on the computation of model atmospheres for testing the consistency of spectral indices derived from models with the observations.

Observations on the program stars given in Tab. 5.2, have been made, by our collaborators from Brera Observatory, at the European Southern Observatory La Silla, Chile. We defer the discussion on model atmosphere

to the second part of this thesis. The main advantage of using purely theoretical approach over the empirical one is that we can cover a wide range of physical parameters in almost a continuous way, and in particular metallicity. A comparison between theoretical and observational results will give one the credibility of the theoretical tools and of the observations reduction methods.

As a follow up of the line of FFBG, spectral features can be treated in two ways: atomic absorption line are expressed in $\AA$ and molecular bands in magnitudes. In these cases "Continuum regions" are defined on both sides of each feature. The central and continuum bandpasses selected are tabulated in columns third and fourth, respectively of Tab. 5.1. We are following the same approach as developed by FFBG for selecting and measuring the spectral features, so we recall here the method adopted by them.

The strength of the features had been derived by defining a local continuum at the feature itself, a straight line was drawn between the midpoints of the surrounding continua, and the height of this line at the midpoint of the central bandpass taken to mark the local continuum. On the wavelength side, the placement of spectral features was done by marking the apparent centre of the Na D lines, which is assumed to be 5893 $\AA$. The error in the placement of all the feature intervals was ≤ 1.25 $\AA$, with consequent error in any measured index.

The range of the spectral feature were selected so as to match broadened galaxy spectra rather than stars. As a result, the sideband intervals are quite long and include many weak absorption features. This approach minimize the index dilution at large value of the velocity dispersion, an

important consideration for galaxy spectra.

Because of low spectral resolution and long continuum intervals, final indices are not true equivalent widths. They can be transformed to abundances only via a set of calibrated empirical spectra or via theoretical synthetic spectra, after convolution to similiar spectral resolution.

Both the CN $\lambda 4170$ index and the Mg_2 index measure features that have well-defined measurements on other photometric systems. The CN $\lambda 4170$ index corresponds closely to the C(41-42) index of the DDO system, while Mg_2 is similar to the $(Mg)_o$ index used by Faber (1973). The transformation between CN $\lambda 4170$ and $C(41-42)$ is mildly color-dependent, while the transformation between Mg_2 and $(Mg)_o$ is mildly dependent on luminosity.

As far as the errors on the strength of the observational features are concerned, they can arise from the following sources: most of the errors are random or quasi-random from scan to scan, effects in this category include variations in instrumental resolution, mis-centering of intervals in wavelength, photon statistics, and the failure of the tungsten calibration scan to calibrate properly.

The first two types are known to be unimportant. The last one arises from slight motion of the electron images inside the detector as the telescope is moved, owing to imperfect magnetic shielding. This effect sets an absolute minimum to the error per single observation that is achievable with the image dissector scanner. For bright local giants, the greater share of the total error arises from this source while for the much fainter globular cluster giants is photon statistics.

An additional, non-random error arises from the way in which the data

are standardized. This error has no effect on narrow atomic features but plays a small role in the measurements of the molecular band features, which span a wider wavelength range. It arises from the fact that the scans were not properly corrected but divided by the tungsten lamp flux.

A final and more troublesome error arises from the fact that the 7.5 mag neutral-density fiters used for the brightest stars were not perfectly gray and thus perturbed by the spectral shape. Only the Mg_1 and Mg_2 are affected by this error. More stars are not observed through one or another of these filters.

5.1.1 Feature Strengths as Functions of Physical parameters

In this section, we investigate the dependence of line strengths on temperature, metallicity and gravity. The information on metallicity in the sample of FFBG comes from low-dispersion spectra. Such a low resolution study had been made by various authors (Gottileb and Bell, 1971, hereafter GB; Gustafsson, Kjaergaard, and Anderson, 1974, hereafter GKA; Hansen and Kjaergaard, 1971, hereafter HK). The methods used by these authors differ widely. GB use synthetic spectra to model the narrow-band photometric indices of Spinrad and Taylor (1969, hereafter ST) and thereby derive atmospheric parameters and heavy-element abundances. GKA also analyze photometric indices by means of model atmospheres but use very narrow bands at 4800 $\AA$ and 5800 $\AA$ measuring predominatly weak neutral iron lines. They derive an iron abundance specifically rather than total metal abundance; their results are found to be comparable with other determinations. HK study correlations between atmospheric parameters and a collection of narrow-band photometric indices published by Dickow *et al.*

(1970). They construct linear expressions relating these indices to $R-I$, [Fe/H], and absolute magnitude. Despite the very different methods used in these studies, the values tderived for [Fe/H] of stars in common agree very well. FFBG used these values to calibrate the feature strengths. They used metal abundance for the globular clusters from Kraft (1979). For cool stars with $V-K > 3.30\ mag$, it is found that line strengths are very difficult to interpret, and the mean error in [Fe/H] is perhaps twice as large. The final adopted value of [Fe/H] is the weighted average, hereafter referred to as $[Fe/H]_o$.

It is difficult to determine for all the stars the effective temperature by using direct methods, so reference is made to $V-K$ color which is a good temperature indicator for K-giants. Moreover, $V-K$ is relatively insensitive to blanketing and surface gravity (Cohen, Frogel, and Persson 1978). The information on most of the $V-K$ colors comes from the literature, the primary source being Johnson *et al.* (1966). Many stars in the sample were also studied by ST, who determined a blanketing- corrected temperature index T from the scanner passbands in the near-IR. Good values of $V-K$ for these stars could be determined by using transformation between T and $V-K$ based on all ST stars with Johnson $V-K$ colors. The final adopted value of $V-K$ was a mean between these values, where both existed. From the different sources, the typical error on $V-K$ is $\pm 0.05\ mag$.

5.1.2 Temperature Dependence of the Indices

In order to see the dependency of spectral indices on T_{eff}, FFBG had plotted the temperature indicator, V-K against each of indices. For illustration the plots are shown in Figs. 5.1 (a to k). In these figures, stars are divided

into five iron-abundance regimes, each of which is shown with different symbols. In each diagram, the line that describes the trend of solar metallicity was first drawn by eye and then refined in an iterative procedure.

In all cases except for CN, Fe $\lambda 5270$, and H_β, a straight line seems an adequate fit to the data although with large scatters.

The following conclusions can be drawn from these figures.

For all indices, except the G band and H_β, there is a clear and positive correlation between feature strength and $[Fe/H]_o$. Except for the G band, there is also a strong trend of feature strength versus temperature. The indices fall naturally into two groups in this regard. For one set, including Fe, TiO, H_β, and CN, metal-poor stars lie along a line with slope approximately parallel to that for solar-metallicity stars. For Na, Mg, and TiO_2, in contrast, metal-poor stars progressively diverge from the mean solar line at low temperatures. Residuals in Fe, TiO, H_β, and CN can therefore be used directly without any scaling versus temperature, whereas for Na, Mg, and TiO_2, the raw residuals must first be scaled to a fiducial value of $V-K$.

As indicated above, the G band (Fig. 5.1a) behaves differently from all other indices in showing no clear temperature dependence. The majority of local field stars clusters around G-band stregths of $6-7$ $\AA$ for all $V-K$'s, and furthermore there is no apparent differentiation due to $[Fe/H]$ for these stars. Among the more metal-poor stars, there seems to be a well-defined temperature trend, but authors thought that this could be due to unlucky sampling of weak- and strong-G-band objects. Stars above the level of the horizontal branch in metal-poor globular clusters are known to exhibit wide variation in G-band strength (Norris and Zinn, 1977; Carbon *et al.*, 1982), due to nucleosynthetic processes involving carbon.

The lack of metallicity dependence of the G band among metal-rich stars was also found by ST. Synthetic spectra calculated by Gustafsson and Bell (1978) later confirmed the effect. These authors found that, at high $[Fe/H]$, an increase in overall metal abundance depresses the entire continuum around the G-band, decreasing the contrast of the band against the sidebands.

In order to show the effect of parameters other than temperature, FFBG introduced a new term called a first-order residual (Δ_{raw}). A first order residual is defined as the difference between the feature strength observed in the star and the feature strength of the mean solar line at the star's $V-K$:

$$\Delta_{raw} = (index)_* - (index)_o \qquad (5.1)$$

Since the line indices Na, Mg, and TiO_2 for metal poor stars diverge from the mean solar line, scale factors were estimated by drawing by eye a best-fit line through globular stars of common metallicity in the $V-K$ plots.

5.1.3 Metallicity Dependence: Gravity-insensitive Features

Apart from the effects of temperatures, remaining variations among the Δ-residuals must be due to some combination of abundance and surface gravity, or other physical parameters. Since the dependence on $[Fe/H]_o$ is strong for most features, it is calibrated in the following section and other parameters are investigated too.

In five of the indices, the effects of surface gravity and other physical parameters appear to be either non-existent or smaller than the observa-

tional errors. These gravity-insensitive indices are treated in this section and include the G band, both Fe lines, and both TiO bands. With no dependence on surface gravity or other parameters, the calibration versus $[Fe/H]_o$ is straightforward. Since non-negligible errors exist in both Δ and [Fe/H], the linear least-squares fits are made by using first Δ and then metallicity as the independent variables. Then these fits were weighted according to the errors in order to obtain a mean line. Scatter in excess of observational error is one way to test the extra physical parameters in the data. Another method that tests specifically surface-gravity effects is a check for any systematic offset between subgiants and giants.

Figs. 5.2a and 5.2b show the iron residuals, ΔFe λ5270 and ΔFe λ5335, plotted against [Fe/H]. There is a strong correlation for both indices. This was first discovered by Whitford and Rich (1980,1983), who measured the same features in a sample of 20 local K giants. A good correlation also exists between the present iron indices and those of Williams (1971), which measure a similiar complex of iron lines at 5450 $\AA$. The best straight line fitted through the sample of FFGB gives the equation:

$$< [Fe/H] >= 1/2(\Delta Fe\lambda 5270 + \Delta Fe\lambda 5335) \qquad (5.2)$$

This is adopted as a primary metallicity indicator in much of what follows.

Fig. 5.2c shows a final plot of $< \Delta Fe >$ versus $[Fe/H]_o$. The few stars that fall off the mean line have uncertain $[Fe/H]_o$. A weighted least-squares fit as described above yields the following calibration of $[Fe/H]$ versus $< \delta Fe >$ for the linear regime above $[Fe/H]$= -0.8:

$$[Fe/H] = 0.55 < \Delta Fe > +0.02 \qquad (5.3)$$

The parameter $\delta_{obs}/\delta_{pred}$, which is a measure of scatter in excess of observational error, is 1.0 for this fit supporting the claim above that effects of surface gravity and other variables on $< \Delta Fe >$ are negligible. Further evidence is the fact that subgiant stars show no net offset from the normal giants in Figs. 5.2a-5.2c.

The insensitivity of $< \Delta Fe >$ to surface gravity implies that $< \Delta Fe >$ and V-K alone suffice to estimate a K giant's metal abundance, independent of its mass, age, or surface gravity. The $< \Delta Fe >$ is thus simpler to apply than other, widely used metallicity indicators for K giants, such as CN, which require correction for gravity as well as temperature. For the same reason, $< \Delta Fe >$ is a good choice for metallicity studies based on the integrated spectra of stellar populations, including extragalactic globular clusters and elliptical galaxies.

5.1.4 Metallicity Dependence: Gravity-sensitive Features

Relations analogous to those above are plotted for ΔMg, ΔCN, and ΔNa vesus $< \Delta Fe >$ in Figs. 5.3-5.5. Unlike the previous cases, these indices show excess scatter after metallicity trends are removed, necessitating a change in the previous fitting procedure. Before this, the interest was simply in the good calibration between each Δ-residual and $< \Delta Fe >$, and now it is important to see the residual scatter about these fits and, in particular, in testing whether the net residuals, δ, are somehow related to one another.

To accomplish this, a conventionl least-squares fit of ΔMg_2 on $< \Delta Fe >$ is taken as a point of departure (see Fig 5.3c) and the analogous lines for other indices are adjusted to maximize the second order correlations. The

excess of $\delta_{obs}/\delta_{pred}$ about these lines is striking for Mg and NaD and is significant but not quite large for CN.

All of these indices are common luminosity indicators in K stars, the gravity dependence of CN being opposite to that of Mg and Na (McClure 1970; Deeming, 1960; Spinrad 1962; Price, 1966). The fact that the surface gravity is indeed responsible for the excess scatter is suggested in Figs. 5.3-5.5 by the strong systematic excess displayed by stars in the Mg plots. In order to test further, the correlation among the second-order residuals is studied. If gravity variations are influencing these residuals, there should be a positive correlation in δMg_2 versus δNa but a negative one between δMg_2 and δCN.

The relation of H_β versus metallcity is shown in Fig. 5.6 , where ΔH_β is plotted versus $< \Delta Fe >$. At first glance, it looks that hydrogen abundance is not dependent on metallicity, however, the best-observed stars (triangles) show a weak correlation (dashed line in see Fig. 5.6). This dashed line is considered as an upper limit to any metallicity trend that might exist for the H_β index. H_β index is contaminated by a few metal lines (Burstein *et al.*, 1984). Rabin (1980) has suggested that these lines could conceivably cause spurious positive correlation between the H_β index and metallicity.

Although the scatter in ΔH_β is comparable to the observation error, the subgiants (galactic circle) in Fig. 5.6 are systematically offset to lower H_β values. This fact suggests a possible surface-gravity effect.

5.2 Selection of Features for the Present Work

Among the above mentioned spectral indices, we have selected the H_β and Mg-b indices due to the following reasons. The Mg-index, which involves a

blend of a Mg triplet and the MgH band at $5156-5197\AA$, is a good indicator of metallicity of stellar systems. This index has been already used by Faber (1973), Faber *et al.* (1977), Burstein (1979), and Terlevich *et al.* (1981) to rank empirically stars and stellar systems (globular clusters and elliptical galaxies) versus metallicity. The relevant work recently accomplished by Davis *et al.* (1988) has provided a wide and accurate set of observations of the Mg-index in nearby elliptical galaxies up to 13 magnitude. The use of this index will allow us to establish a reliable calibration versus metallicity both theoretically and observationally. Once we know the metallicity of the stellar systems, we can solve the problem of disentangling the age effect from chemical composition.

On the other hand, H_β is chosen here to derive the temperature of the program stars in a self consistent manner. Furthermore, the strength of this index can resolve the problem of excess contribution of UV-flux in the elliptical galaxies.

5.3 Reference Library of Stars

In constructing the integrated stellar energy distribution (SED) of a given stellar system, it is essential to use a complete library of individual stellar energy distributions, which cover the relevant range of temperatures, gravities, and metallicities, at reasonable intervals in the parameter space. For instance, a good library of stellar SED's for study of giant elliptical galaxies would thoroughly cover a grid of ages 1-20 Gyr and Z's of 0.1-10 $Z_\odot$. No such observational library exists or is likely to be available in the near future. The observational library of Galactic disk population in the solar neighbourhood has been well sampled but covers only $Z \sim 0.5-1.5Z_\odot$

for $t \leq 10Gyr$. Burstein (1985) and Faber et al. (1985) have stressed that such samples tend to select lower gravity giants than would be appropriate for the study of very old populations. Only partial samples of low metallicity stars are available (e.g. Christensen, 1978). It is most likely that few, or no, local analogues exist for some important types of stars in other stellar systems. The best evidence for such " missing components" are the overstrong metallic lines in galaxy nuclei (Faber 1977) or in M31 globular clusters (Burstein *et al.*, 1984), which seem to require the presence of objects more extreme than the "super metal rich" (SMR) stars in the solar neighbourhood. The very metal rich K giants in the Galactic bulge, with [Fe/H] $\sim 0.5 - 1.0$ (Whitford and Rich 1983), may be the counterparts of gE giants, but a complete survey of bulge stars will be cumbersome because of their faintness, image crowding, and the limited low-extinction window available. It is also essential, though even more difficult, to include SMR dwarfs.

To provide more comprehensive libraries for these and other difficult types, we supplement the observational reference library of stars with theoretical model atmosphere calculations. We defer the discussion on model atmosphere to the next part of this thesis. Our approach depends upon both the theoretical as well as the empirical stellar libraries. First, we intend to test the observational strength of stellar features against the stellar parameters, then to test against the features derived from synthetic spectra.

Tab. 5.1: Wavelength intervals for indices.

Identification	Features Measured	Central Bandpass	Continuum Bandpass
		Equivalent Widths	
$G\lambda 4300$	CH	4823.25-4317.00	4268.25-4283.25
			4320.75-4335.75
$Mgb\lambda 5177$	Mgb	5162.00-5193.25	5144.50-5162.00
			5193.25-5207.00
$Fe\lambda 5270$	FeI, CaI	5248.00-5286.75	5235.50-5249.25
			5288.00-5319.25
$Fe\lambda 5335$	FeI, CrI	5314.75-5353.50	5307.25-5317.25
			5356.00-5364.75
$Na\lambda 5895$	NaD	5879.25-5910.50	5863.00-5876.75
			5924.50-5949.25
$H_\beta\lambda 4861$	H_β	4849.50-4877.00	4829.50-4848.25
			4878.25-4892.00
		Molecular Bands	
CN	CN	4144.00-4177.75	4082.00-4118.25
			4246.00-4284.75
Mg_1	MgH	5071.00-5134.75	4897.00-4958.25
			5303.00-5366.75
Mg_2	$MgH+Mgb$	5156.00-5197.25	4897.00-4958.25
			5303.00-5366.75
TiO_1	TiO	5939.00-5995.25	5819.00-5850.25
			6041.00-6104.75
TiO_2	TiO_2	6192.00-6273.25	6069.00-6142.75
			6375.00-6416.25

Tab. 5.2: List of program stars.

HD	V	Teff	Log g	[Fe/H]
1581	4.23	6000	4.50	-0.10
1835	6.39	5793	4.45	0.05
3443	5.57	5419	4.57	-0.16
10380	4.44	4000	1.50	-0.30
10700	3.50	5305	4.46	-0.34
11397	8.95	5663	5.00	0.10
13611	4.37	5143	3.00	0.00
13974	4.87	5600	4.50	-0.30
14802	5.20	5929	4.40	0.00
17925	6.04	5091	4.50	-0.15
18322	3.89	4710	2.80	0.20
20630	4.83	5793	4.45	0.23
20766	5.54	5600	4.00	-0.16
20794	4.27	5362	4.40	-0.25
20807	5.24	5727	4.50	-0.20
20894	5.52	5091	3.10	-0.20
22049	3.73	5040	4.40	-0.23
22484	4.28	6000	3.96	0.04
30495	5.51	6000	4.50	0.10
30562	5.78	5860	3.75	0.13
32147	6.22	4755	4.45	0.02
33793	8.89	3524	4.87	-0.50
36395	7.97	3626	4.80	0.60
37160	4.09	4667	2.57	-0.21
37763	5.19	5040	3.00	0.35
39091	5.65	5663	3.94	0.00
39364	3.81	4383		-0.36
39523	4.51	4667	1.90	0.15
44033	5.69	3294		-0.07
45829	6.63	4200	0.20	-0.08
46407	6.38	4990	2.55	0.03
47205	3.95	4941	3.08	0.07

Tab. 5.2: (Continued)

HD	V	Teff	Log g	[Fe/H]
50778	4.07	3877	1.90	-0.12
50877	3.78	4200	0.40	0.05
56577	4.79	4383	1.30	0.16
60219	8.50	4800	1.70	-0.50
62576	4.59	4308	1.30	0.01
62644	5.06	5143	3.12	-0.35
63302	6.35	4500	0.20	0.17
65699	5.11	4846	1.50	-0.20
69267	3.52	4308	1.87	-0.22
76151	6.00	5600	4.40	-0.02
83548	5.50	5091	2.00	0.10
84810	3.69	4941	1.50	0.30
84903		4500	0.80	-2.60
88218	6.13	5538	3.36	-0.42
88284	3.61	5040	2.86	0.10
89388	3.40	4500	1.60	0.54
91324	4.89	6072	3.90	-0.60
91805	6.08	4846	2.00	0.00
95272	4.08	4032	2.48	-0.12
95345	4.84	4667	2.00	-0.05
96918	3.91	5727	0.40	0.32
97907	5.32	3818	2.07	-0.17
98430	3.56	4846	2.48	-0.33
99491	6.50	5600	4.60	0.09
100407	3.54	4846	2.20	0.00
102365	4.91	5419	4.09	-0.59
102634	6.15	6072	4.30	0.12
102870	3.61	6072	4.30	0.21
111631	8.48	3907	4.50	0.10
188510	8.81	5305	3.80	1.80
189567	6.07	5727	4.08	-0.28

Tab. 5.2: (Continued)

HD	V	Teff	Log g	[Fe/H]
190248	3.56	5600	4.31	0.30
191408	5.32	4893	4.60	-0.07
192310	5.76	4941	4.50	-0.08
192947	3.57	4990	3.00	0.12
196378	5.12	6072	4.10	-0.30
203638	5.77	4541	1.50	0.35
208776	6.94	5929	4.00	-0.14
209100	4.69	4500	4.70	0.04
211391	4.16	4941	2.80	-0.07
212330	5.32	5793	4.20	0.00
213009	3.97	4800	2.00	-0.20
215104	4.85	4755	2.30	-0.20
216437	6.05	5929	4.40	0.10
216763	4.21	4893	2.50	-0.20
219615	3.69	4800	2.42	-0.18
221148	6.25	3210	2.60	0.07
225212	5.16	4200	1.00	0.00

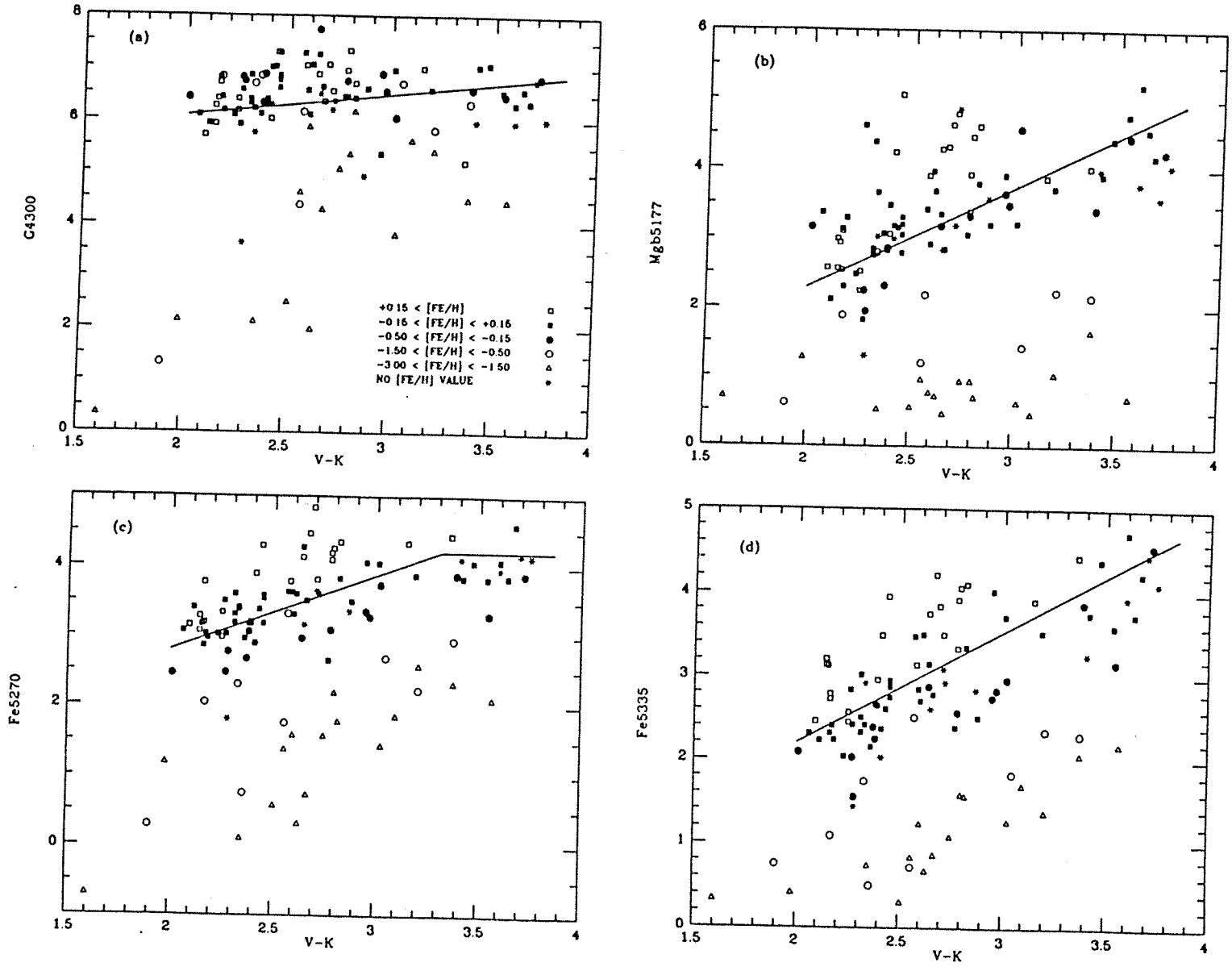

Figs. 5.1a-5.1k: Feature strength vs. $V-K$ for each index. $V-K$ is taken to indicate the effective temperature. Symbols represents stars of different $[Fe/H]_o$. (Adapted from Faber et al. 1985)

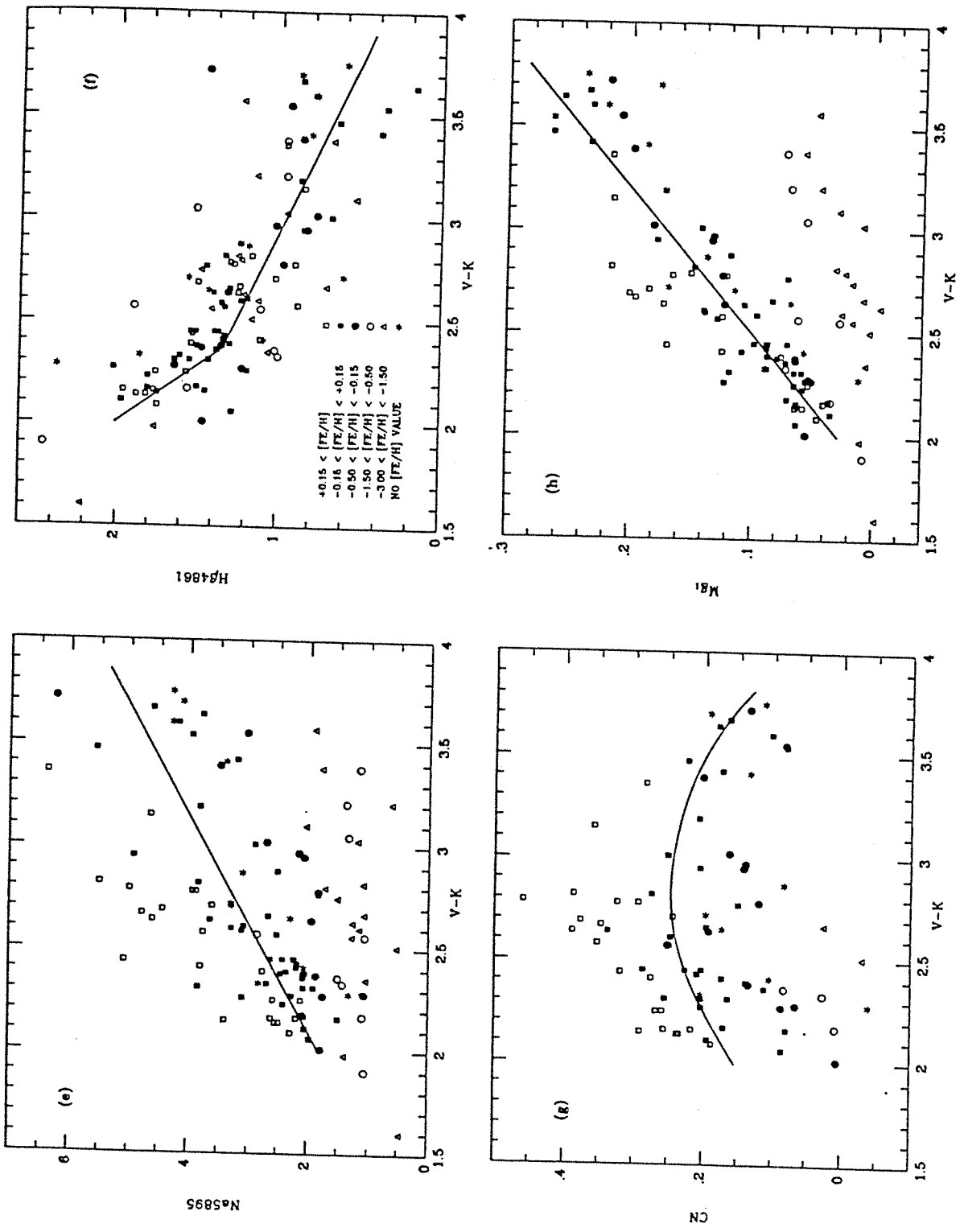
(f)
Hβ4861
V-K
+0.15 < [FE/H]
−0.15 < [FE/H] < +0.15
−0.50 < [FE/H] < −0.15
−1.50 < [FE/H] < −0.50
−3.00 < [FE/H] < −1.50
NO [FE/H] VALUE
(h)
Mg1
V-K
(e)
Na5895
V-K
(g)
CN
V-K

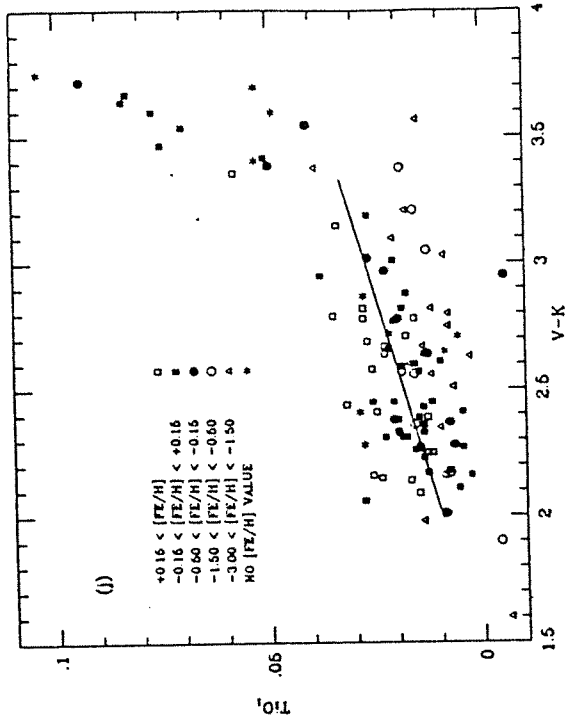
(j)
+0.16 < [Fe/H]
−0.16 < [Fe/H] < +0.16
−0.60 < [Fe/H] < −0.16
−1.50 < [Fe/H] < −0.60
−3.00 < [Fe/H] < −1.50
NO [Fe/H] VALUE
V−K
TiO1

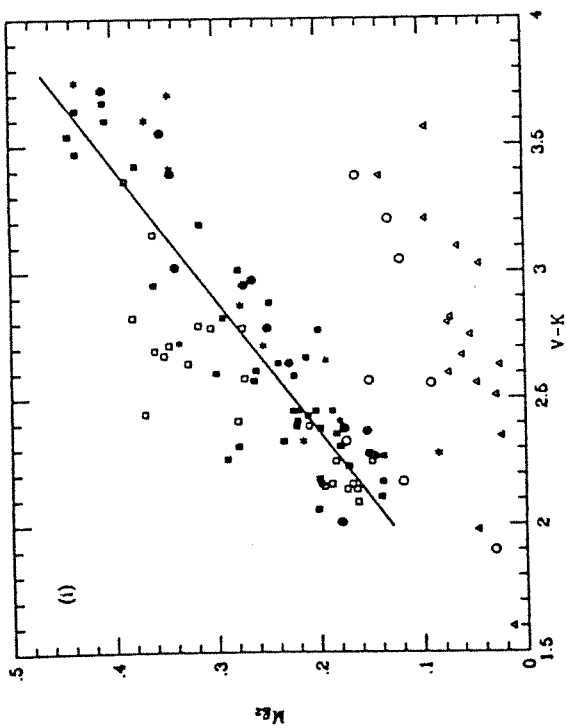
(i)
V−K
Mg2

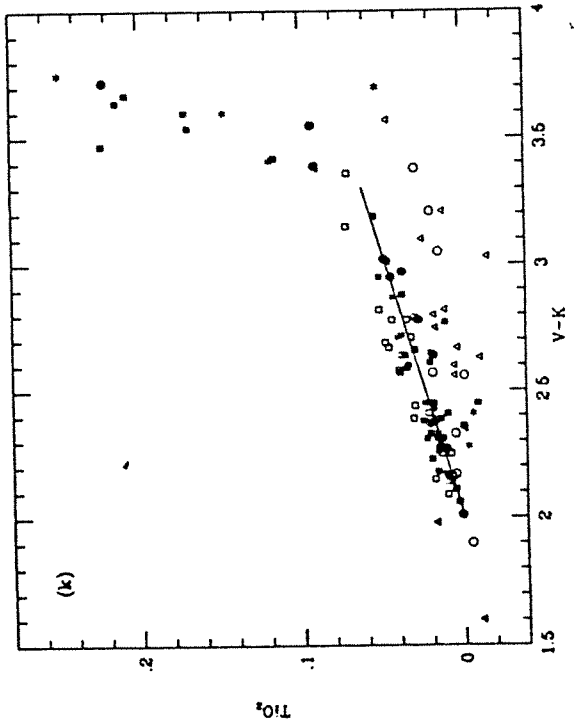
(k)
V−K
TiO2

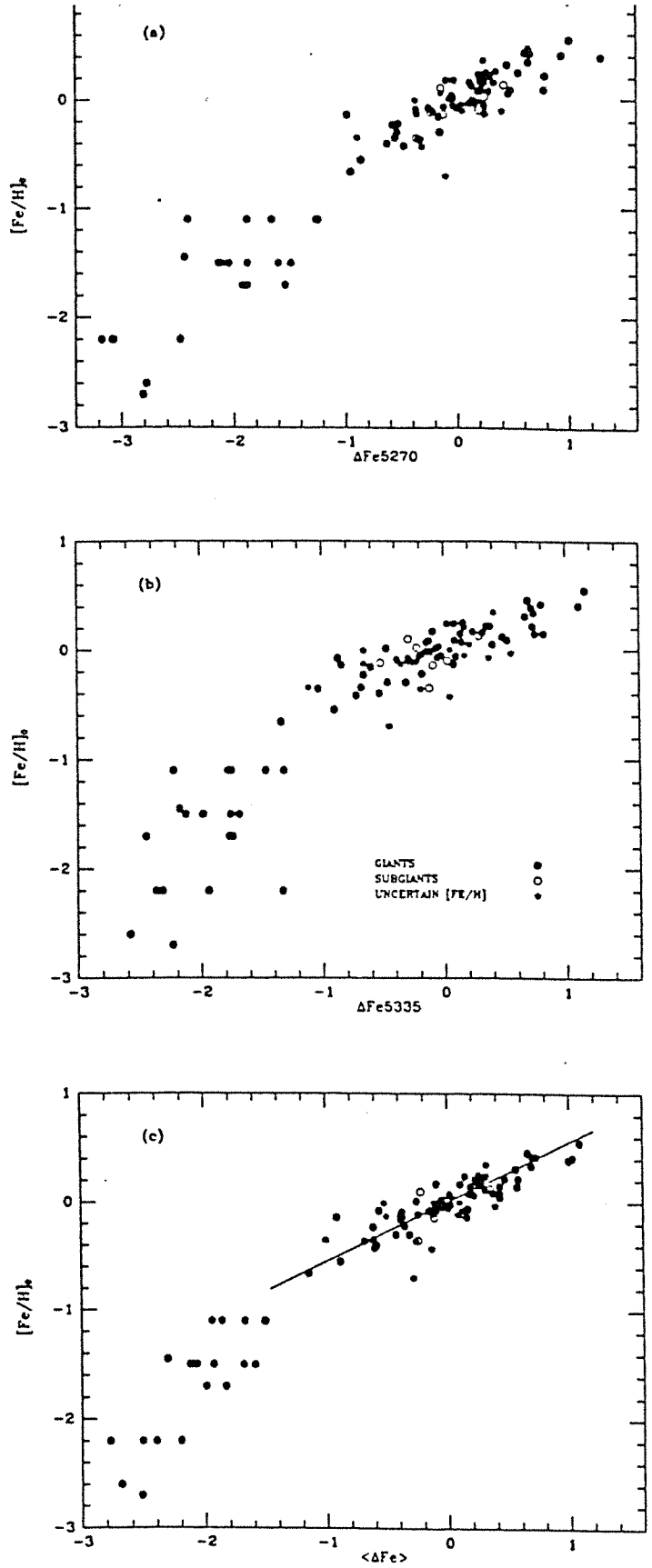

Figs. 5.2a-5.2c: (a) Iron-line residuals ΔFe λ5270 vs. $[Fe/H]_o$. Asterisks have uncertain $[Fe/H]_o$. Open circles are subgiants.
(b) Iron-line residuals ΔFe λ5335 vs. $[Fe/H]_o$.
(c) Mean iron-line residuals, $< \Delta Fe >$ vs. $[Fe/H]_o$.

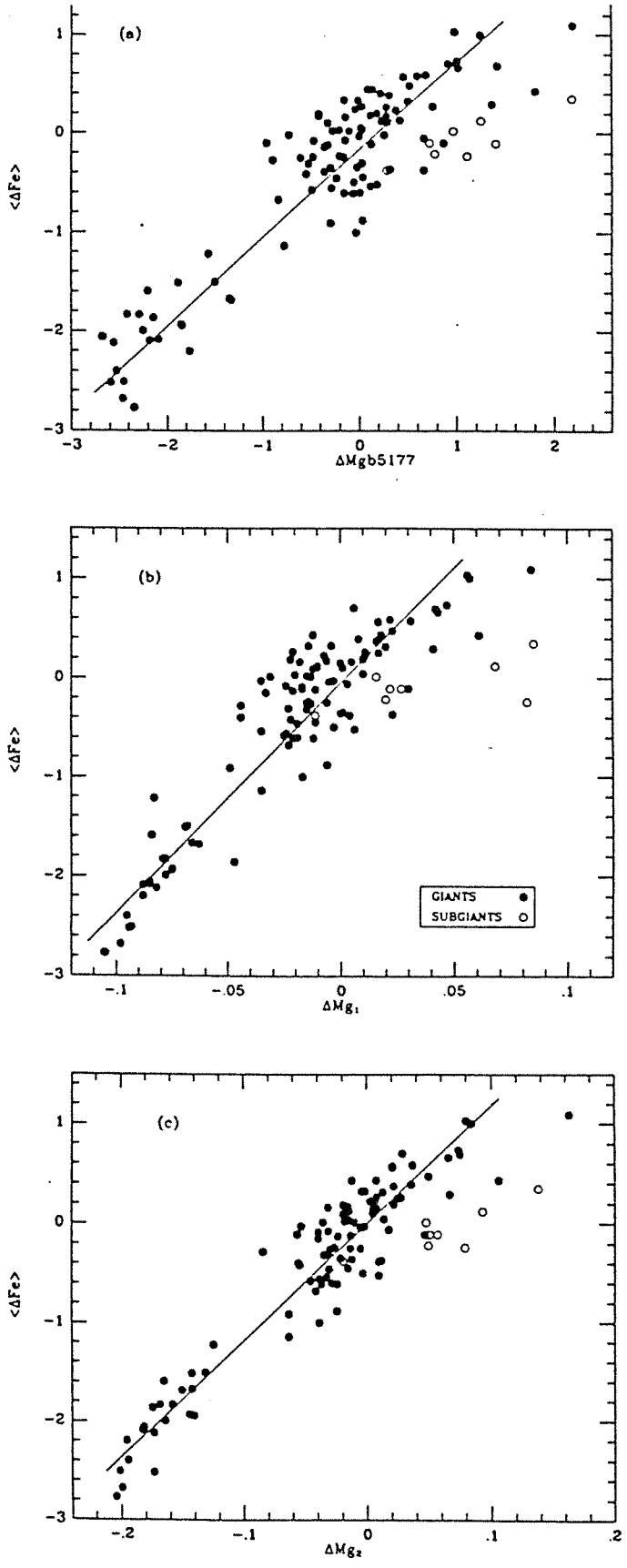

Figs. 5.3a-5.3c: (a) Mgb residuals vs. $< \Delta Fe >$. Open circles are subgiants. (b) Same as Fig 5.3a for ΔMg_1. (c) Same as Fig 5.3a for ΔMg_2.

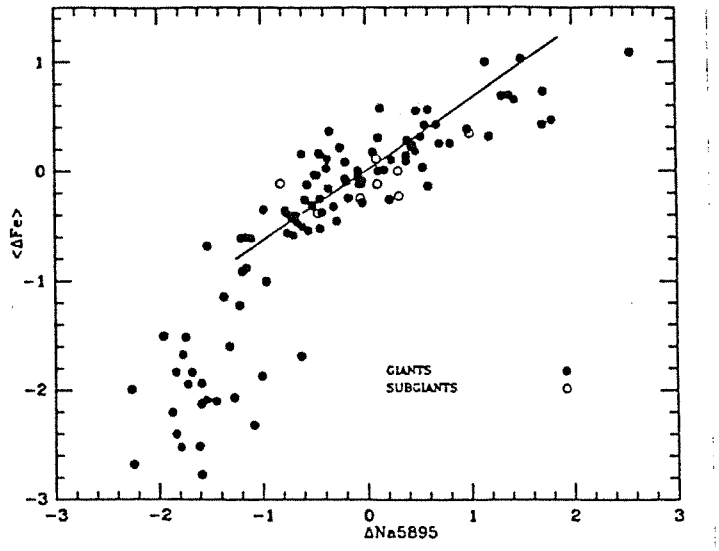

Fig. 5.4: Same as Fig. 5.3a for ΔNaD. Subgiants have slightly high ΔNaD.

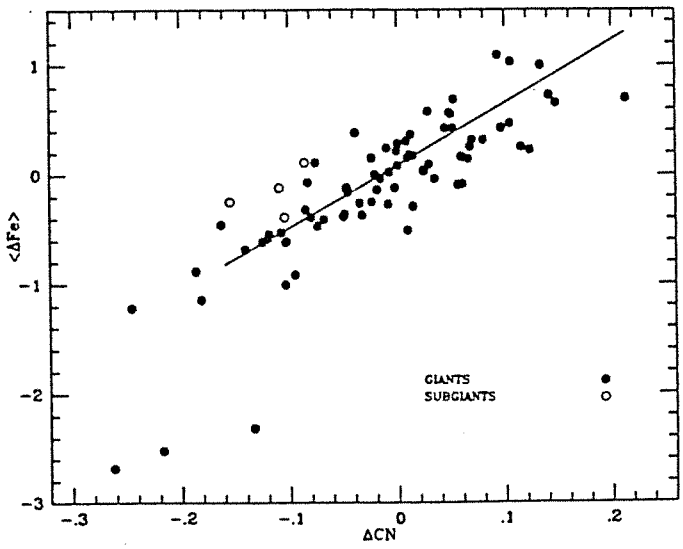

Fig. 5.5: Same as in Fig. 5.3a for ΔCN.

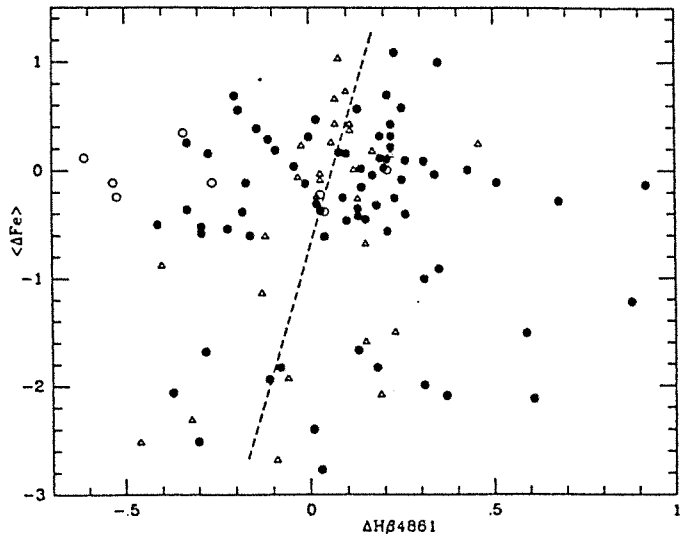

Fig. 5.6: Hβ residual, Δ Hβ, vs $< \Delta Fe >$. Open circles are subgiants; triangles here are stars of higher accuracy (see text).

Part II

MODEL ATMOSPHERE

6 STELLAR ATMOSPHERE MODELS

We have seen in the first part of the thesis, that stellar atmosphere models enter in both kinds of population synthesis techniques. In stellar synthesis, we need to include the models to cover the incomplete temperature and gravity ranges, or to supplement the observed metallicity range; the evolutionary synthesis approach can use stellar atmosphere models alone or refer to empirical stellar libraries (see, for instance, O'Connell, 1973; Jacobi, Hunter and Christian, 1984; Pickles, 1985), supplemented by models.

In this section we will present the main characteristics of stellar atmosphere models, together with their basic assumptions, and the synthetic spectrum approach.

6.1 Grids of Models

Existing models that cover a wide range of stellar physical parameters are due to Carbon and Gingerich (1969); Peytremann (1970;1974a;1974b); Bell, Eriksson, Gustaffson, and Nordlund (1976), hereafter referred to as GBEN; and Kurucz, Peytremann, and Avrett (1974), herafter referred to as KPA, Kurucz (1979).

The Carbon and Gingerich grid was an early attempt to use a distribution function representing the line opacity. They did not have sufficient atomic data to compute the distribution functions, but instead produced empirical three-step distribution functions by varying the parameters so as to match the observed visible blocking of few bright reference stars. They guessed the ultraviolet opacity. In this way, their procedure underestimated the opacity for the early-type stars and produced models with too shallow a temperature gradient.

Peytremann computed a grid of models in which he used a sampling technique to evaluate the integeral over the radiation field, while evaluating the line opacity explicitly at a set of frequency points. However, the line data that were available to him at that time were considerably deficient, therefore he introduced pseudo-lines, to produce a reasonable solar model, thus obtained results biased by the choice of the lines.

KPA computed a grid of models for early-type solar abundance stars covering the range of temperatures from 8000 to 50,000 K. In these models the resolution in temperature and wavelength in tabulating the distribution functions was so coarse as to introduce serious interpolation errors in the derived opacity. This led to an underestimate of the opacity and resulting models with too shallow a temperature gradient. Thus the effective temperatures derived from the KPA energy distributions would be systematically too high.

The GBEN models for later type stars were computed with a statistical distribution function representing the line opacity similar to that adopted by Kurucz (1979). Their line data were determined by empirically fitting the solar spectrum in the visible region of the spectrum and from laboratory data, and include both atomic and molecular lines.

In the following subsection, we will discuss in some detail the main characteristics of Kurucz atmosphere models, which we are using at present for setting up a synthetic stellar library.

6.2 Basic Assumptions

Kurucz models are the classical models of stellar atmosphere with improved line-blanketing computation. These models are based on the following basic

assumptions:

1) plane parallel geometry, in the sense that the thickness of the atmosphere is small as compared to the radius of the star. This approximation fails for the systems with low surface gavity, e.g. supergiants;

2) the layers of stellar atmosphere are assumed to be homogenous except in the normal direction. Magnetic fields, granules, spicules, cells, and spots are ignored;

3) hydrostatic equilibrium, i.e. the pressure at any layer of the atmosphere is balanced by the gravitational attraction, therefore there is no relative motion of the layers in the normal direction and no net acceleration of the atmosphere. No expansion is allowed;

4) the atmosphere is in a steady state. The state of the gas and the transport of the radiation are constant with time. This assumption is a constraint on the equation of state;

5) local thermodynamic equilibrium (LTE): at each depth the state of the gas depends on the local values of the radiation field, and does not depend on radiation fields in other layers. This assumption also affects the equation of state. The LTE assumption has in some cases been shown to be inadequate: the radiation field is not isotropic, the temperature of the outgoing field in the photosphere is generally higher than the local gas temperature and the flux is also often markedly non-Planckian due to wavelength-dependent opacity of the gas;

6) the flux of energy (radiative and convective) is constant with depth in the atmosphere. There is no creation of energy within the atmosphere.

7) the atomic abundances are specified and constant throughout the atmosphere. Molecular components are omitted in the equation of state.

This approximation affects the atmosphere models with low temperature, and therefore is important for late-type stars.

Kurucz (1979) models are useful for a wide range of effective temperature, i.e. from 5500 K to 50,000 K. They have been computed for several values of the metal content ($Z = 1/2\ Z_{\odot}$; $Z = 1/20\ Z_{\odot}$; $Z = 1/200\ Z_{\odot}$)

Kurucz (1979) models are computed by using a modified version of the original computer code ATLAS (Kurucz, 1970), which includes changes in the temperature correction, radiation pressure, convection, and distribtion fuctions. We will describe the procedure to derive models from ATLAS (Castelli, 1988) in the next section.

Kurucz's models have been already widely tested for the stellar continuum and have been found to be in good agreement with the observed spectra of A and F stars (Malagnini et al., 1982) and B stars (Malagnini et al., 1983).

6.3 SPECTRUM SYNTHESIS

The reliability of stellar atmosphere models can be tested against the observations by properly reproducing the fluxes, colors and line profiles. Although the surface fluxes of Kurucz's blanketed models are computed at relatively close wavelength steps, $\Delta\lambda \sim 25\mathring{A}$, they are still inadequate to resolve the important spectral features. Therefore we adopt the spectrum synthesis technique to obtain simultaneously all the lines at high resolution over a portion of the spectrum.

This modern technique has been recently applied to derive the physical parameters of stars by comparing high quality spectroscopic data with synthetic spectra.

With the advent of sophisticated instruments, the data of stellar systems at intermediate resolution are accessible. It is highly desirable to deduce the information about the stellar content in the stellar systems by using the synthetic spectrum technique, since this is the only way to obtain theoretical data with the proper resolution, so as to match the observations. On the observational side, there is much progress and large set of data have been already collected, while, on the theoretical side, this procedure has been applied only to few individual objects, since it is time consuming and depends on the adequacy and accuracy of models used to derive the synthetic spectrum.

This approach has been applied for instance to compute the Mg-index around $\lambda 5175$ $\AA$ and to study old galaxy populations (Mould, 1978; Laird and Levison, 1985).

To compute synthetic spectra, we need atomic lines and molecular line data in the wavelength range of interest. This method works very well when all the observed spectral lines can be identified and have well known oscillator strength (gf) values.

In addition to this, we need to know the mechanisms responsible for the broadening of lines. There are several mechanisms that make lines broadened and remove light in a narrow wavelength range rather than just at the specific wavelength corresponding to an atomic transition.

First, there are the microscopic broadening mechanisms, acting through the distrubance of the energy levels involved in the transition.

Radiation broadening or natural damping is caused by the finite lifetimes of the electronic states of the atoms causing them to decay to lower states in the emission of spectral lines.

van der Waals broadening is caused by electromagnetic dipole disturbances on the energy levels by neutral atoms in the vicinity.

Resonance broadening is caused by the disturbance of line absorbing atom (ion) by other atom (ion) of the same kind.

Quadratic Stark broadening is caused by disturbances form nearby electrons and ionized atoms.

Of these mechanism the last two are not important for late-type stars. Another kind of microscopic broadening is the thermal (Doppler) broadening which is caused by the spread in the line-of-sight velocities of the atom in the gas due to high gas-temperature.

Spectral lines are also broadened by " macroscopic " effects, and the Doppler effect is involved in each: all stars are rotating at some speed, so that, unless we see them from the pole, the different parts of the stellar disk have different line-of-velocities due to the rotation. This in turn will cause the spectrum formed at different parts of the disk to be wavelength shifted by different amounts, and the lines will be broadened in a characteristic way. Late type stars have also convective motions in the gas which has effects on the energy-transport and which require detailed and complicated simulation of non-linear effects in order to be taken into account.

These broadening mechanisms, of course, make the spectral lines to be broadened in a different way, and all but two of them make the lines absorb more light and increase their equivalent widths. These two exceptions are the rotational and the macroturbulence broadening which merely change the shape of the lines. Stark broadening is unimportant at low temperatures. For molecular species, pressure broadening can be rejected.

7 SYNTHETIC SPECTRUM COMPUTATION

The computation of synthetic spectrum is related to the structure of model atmosphere. A model atmopshere describes the variation of temperature and pressure with the depth. From a given model atmosphere, the emergent radiation spectrum can be calculated by solving the equation of radiative transfer. For the last two decades, the introduction of large computers and the development of efficient computer codes have led to compute the synthetic spectrum in any wavelength range of interest.

A major step was taken by Kurucz (1979) and Gustafsson et al. (1975), who computed the flux constant models with convection in the form of mixing length approximation, and the line blanketing included. The model atmosphere computed by them have been widely used for the investigation of different properties of stars. We will not enter into the detail of equations that determine the structure of model atmosphere and spectrum synthesis. In this section we will restrict our discussion to the description of the operations required to obtain synthetic spectra; preliminary results obtained during the course of the present project; dependence of the equivalent width of selected features on atmospheric parameters; and conclusion and future plans.

7.1 Computational Codes

At present, the grid of models atmosphere is limited to the temperature range of 5500-6000 K to represent cool stars for which molecular data are not of overwhelming importance. The computational code, used for deriving the atmospheric model, is the Kurucz's ATLAS code. A complete

discussion on the procedure of extracting models from ATLAS is given in " Kurucz's models, Kurucz's fluxes and the ATLAS code." by Castelli (1988).

ATLAS code, which is being used , is the eighth version of ATLAS, and based on the improvements made on the previous versions. The physical and computational aspects of the model atmosphere calculations are extensively described in the fifth version of ATLAS by Kurucz (1970) in the paper: "ATLAS: A computer program for calculating model stellar atmosphere". The basic assimptions on which this code is based have been presented in section 6.2. The latest version of ATLAS code takes into account changes in the temperature correction, radiation pressure, and convection treatment. Furthermore, the latest version includes the computation of the thermodynamics derivatives. They are more accurately calculated, because the necessary state variables are recomputed before their use in the computation of thermodynamic derivatives. In the previous version of ATLAS, the depth variable is mass per square centimeter and the flux correction determines a mass perturbation that changes the temperature to reduce the flux error. However, the physical variable for the radiation field is an optical depth scale. At high temperature the mass and the optical depth scales vary in a similar fashion because the gas is mostly ionized, but at lower temperatures the optical depth scale becomes a very strong function of temperature because of ionization and Boltzmann population changes. To solve this problem the temperature correction should be changed from a mass to an optical depth dependency.

Modifications are also made to the previous versions of ATLAS in the treatment of the number of depth points . The selection of depth points is a matter of experience. For numerical stability reasons the number of

depth ponits must be large. If the depth-points are ill-chosen the model can blow-up and error message will occur. In this case an usable depth point grid must be obtained with trial and error procedure. The number of depth points suggested by Kurucz are sixty-four and forty, in particular, the new convective models have been computed with sixty-four depth points.

This ATLAS code, written in FORTRAN IV, is available in the simple and double precision formats. It has been pointed out by the author that in some cases problems with exponent underflow or overflow may occur when the single precision is used. It is suggested that double precision version of ATLAS code must be used. In order to make double precision effective, it must be compiled with the G-float option of the VMS. But this version increases the execution time by a factor of 4. We need to use this version while including the molecules in the equation of state.

A characteristic of ATLAS code is the use of tables which contain data computed with other utility programs or taken from literature. These tables are either stored in the program or supplied as input data from input tables.

One of these tables contains the opacity distribution functions (ODF). The ODF tables read from ATLAS come from two different divisons of the frequency range, such as the BIG divison with large intervals of frequencies and the LITTLE divison with small intervals of frequencies. It is preferable to use the BIG intervals for the model calculation because with LITTLE interval the computation time increases by three times than with big interval. On the other hand, little freqency interval is needed for computing the synthetic spectra.

Different ODF's tables must be used for different metallicities and for different turbulence values. If a particular scaled solar abundance is re-

quired, the corresponding ODF's can be obtained by interpolating in a known set of ODF's tables with different metallicities.

The advantage of using ATLAS code is that it not only allows the extension of the grid of models which differ from the existing models, but also permits to change the physical parameters characteristic of stellar atmospheres. For instance, the existing models can be scaled to new values of effective temperature, gravity and chemical abundance.

With ATLAS code, models can be either scaled or be computed directly by supplying the necessary parameters. In order to compute the model, there is a set of input parameters to be supplied in the form of " input cards ". These cards are related to the physical parameters of the atmosphere and the operational procedures. For instance, TEFF and GRAVITY; FREQUENCY SET; ITERATIONS NUMBER; ABUNDANCE SCALE etc.

Regarding the ITERATION NUMBER, the number of iterations can be varied until the convergence criteria is satisfied. A model is considered to be convergent when the absolute values of the percentage error in the flux and in the flux derivative are less than 1 % and 10 %, respectively, for each depth point. The maximum number of iterations allowed with ATLAS is fifteen. However, larger number of iterations are allowed by repeating the card. Iteration 1 must be used while computing the synthetic spectra.

There are other set of optional cards which control the physical processes. These cards are represented in ATLAS by a set of switches that can be either 0 or 1. These switches control, for instance, opacity from different sources, temperature correction, pressure integration, convection, NLTE, etc.

The departure from LTE for the first six-levels of the H atom and for

H^- is allowed. NLTE can be a good approximation only for A and B stars with no more than solar abundances and for cool Pop II stars in which metals will not dominate the electrons.

Concerning the opacity sources, theoretically there are twenty possible opacity sources, but only fifteen are active. They are listed below:

1) The contribution from HI
2) Contribution due to H_2^+
3) Contribution due to H^-
4) Rayleigh scattering by HI
5) Contribution due to HeI
6) Contribution due to HeII
7) Contribution due to He^-
8) Rayleigh scattering by He I
9) Contribution due to cool components
10) Contribution from intermediate components
11) Opacities from low-lying levels of
CII-CIV, N II-V, O II-VI, and Ne I-VI
12) Electron scattering
13) Rayleigh scattering
14) Hydrogen lines, for levels less than 5
15) Lines opacity with ODF's.

There are certain cards which control the output, namely PRINT and PUNCH. Depending on the requirement, a different set of tables can be saved on the output files.

For a given model atmosphere, synthetic spectra are computed using the XNFPELSYN.COM, SYNTH.COM, SPECTRV.COM, ROTATE.COM, BROADEN.COM

PLOTSYN.COM, MERGEPLOT.COM codes. Program XNFPELSYN reads the model file and the frequencies at which the continuum is to be evaluated and produce a file with the partition distribution functions of electrons at each depth point. Line data are read in and processed by the SYNTHE series of programs. SYNTH outputs opacities and line data . ROTATE rotationally broadens the spectrum according to the rotation velocity and writes the ouput file. To compare the observed spectra with synthetic spectra, synthetic spectra are broadened according to the instrumental profile using BROADEN code. Next, each spectrum is plotted by PLOTSYN and in case of two plots, they are merged together into one by MERGEPLOT. Each plot file is just a list of vectors. The ouput is obtained in the form of normalized spectra in the wavelength region of interest.

7.2 Preliminary Tests

In the list of program stars, the effective temperature range covered by these stars is 4000-6000 K. The set of models selected for the current work lie in the effective temperature range 5500-6000 K for which molecules play a less important role.

In order to set up a grid of models, we selected the following ranges and steps for the parameters: the gravity is from 1.5 to 4.5 with a step of 0.5; the chemical abundance is chosen from -0.50 to +0.50 with a step of 0.25; and temperature from 5500 to 6000 with a step of 100 K. These criteria resulted in a set of 170 models in the temperature range 5500-6000 K. Of these models, the new convective models at Teff 5500 and 6000, at metallicities of 0.00, 0.5, -0.5, and at the prescribed gravity values are among the existing models. They have been extracted interactively using

the READMOD code. The models with metallicities 0.25 and -0.25 have been computed by scaling models with metallicity 0.00 using the ATLAS8 code. For these models, the opacity distribution functions at -0.25 and 0.25 metallicities have been interpolated between the known nearest ODF's. A complete list of models computed is given in the Tab. 7.1.

All other models are also computed with ATLAS code by scaling the known models at different Teff, gravities, and chemical abundance. Since this procedure takes a long CPU time, the models have been computed in batch mode. It is worth pointing out that the computation time required to compute each model from ATLAS with 15 iterations is about one hour of CPU. Our choice of 15 iterations is to compare the existing models with the ones derived from ATLAS.

In Tab. 7.2, we present an example of command file together with the input model with parameters 5600/4.5/0.0, to which a unit 5 is assigned. ATLAS code scales this input model to new parameters, 5700/4.5/0.0. The output file is written on the unit 7 and the format of this is presented in Tab. 7.3.

As a preliminary step, we performed the following tests on the models and on the derived synthetic spectra. We have compared the synthetic spectra obtained with variation of depth points from 64 to 40: we did not find any difference in the resulting spectral energy distributions. But, for the sake of homogeneity with Kurucz new convective models, we used 64 optical depth points in the following analyses.

As far as the physical processes are concerned, we took into account all the 15 physical processes listed in subsection 7.1. In each case, the chemical abundance for hydrogen and helium is the solar one. Turbulence pressure

has been set to 0.0.

Although the mixing length to the scale height ratio can be varied in the computation of the convective flux, we have used the value of 1.00, as adopted by Kurucz in the new convective models.

On comparing the models computed by ATLAS with models extracted directly, we have not found a difference in the distribution of temperature, electron density with respect to mass depth. This allows us to compute the models from the ATLAS under the same conditions prevailing in the existing models.

The models atmosphere in the form of Tab. 7.3, with some minor changes in the control cards, are used as input for computing synthetic spectra with SYNTH code. In Figs. 7.1 (a,b), we report examples of synthetic spectra in the spectral regions of Hβ and Mg-*b* , respectively. In Fig. 7.2 (a,b), we present examples of broadened spectra, in the regions of spectral features of our interest. Regarding the broadening mechanisms, the broadening due to rotation velocity can be calculated with SYNTH code. We have tested the synthetic spectra for two different velocities of 0 and 20 km/s as reported in the catalog for late-type stars. No evidence of differences can be seen in Fig. 7.3, where the case of Mg-*b* is ilustrated. Most of late-type stars have 0 rotational velocity. We adopt this value for the synthetic spectra.

In order to compare synthetic spectra with the observational ones, one should take into account the contribution of line broadening due to instrumental profile. We computed this profile from the spectrum of the standard source taken at the ESO observatory by our collaborators. Broadening effects due to instrumental profile are measured by fitting the best gaussian

profile with BANDFIT code in one of the sharp features of the standard lamp source.

With the SYNTH code, there is a possibility of getting synthetic spectra at high resolution. We started with the computational resolution ($\Delta\lambda/\lambda$) of 250,000 to extract the synthetic spectra in the range of selected features. The amount of time necessary to get synthetic spectra was about two hours of CPU. To save the computing time and to retain all the atomic features, we made several attempts by varying the resolving power, we arrive at the conclusion that ($\Delta\lambda/\lambda$) of 75,000 would be sufficient. As an example, in Fig. 7.4 we have shown comparison of synthetic spectra obtained in the Mg-*b* region at resolution of 75,000 with 250,000: it is evident from this figure that there is no much difference in the strength of the spectral features. All the synthetic spectra have been computed with this resolution.

The wavelength range have been selected to cover the selected features of H_β and Mg b.

For one of the stars, HD 190248, for which raw data have been reduced and calibrated, we compared the observed spectrum with the synthetic one. The fundamental atmospheric parameters, 5600/4.3/0.30, for this star are taken from Strobel's catalog. The observed spectrum has been normalized to continuum using NORMA code. Since it was very difficult to find regions without lines to chose the continuum, the normalization to the synthetic spectrum may suffer some uncertainty. For example, the comparison between the synthetic spectrum computed with the parameters nearest to those reported in the catalog, say 5600/4.5/0/0.25, and the observed one for Hβ and Mg-*b* is shown in Figs. 7.5 (a,b).

The work done so far permit us to have a first look at the dependency of

Mg-*b* on metallicity. In Figs. 7.6 (a-f), the relationship between equivalent width and metallicity at different temperatures is presented. There is a strong relation between these parameters, in the sense that the equivalent width increases with increasing metallicity. To see the effect of temperature, all these plots are merged together (see Fig. 7.7). There is also indication of temperature dependence compared to gravity effect. This suggests us to take into account determinations of these parameters as accurate as possible for comparison of synthetic spectra with the observed ones. We must also remind that deeper insight will be gained when molecular blancketing will be included in the computation of medels.

7.3 Conclusion and Future Works

Our future work includes the refinement of models taking into account the convergence criteria (more than 15 iterations may be necessary), and inclusion of molecules which are vital for the program stars. We have planned to use Gustaffson models (in the format of ATLAS) for the lowest temperatures: such models have been widely used for investigating the characteristics of late-type stars. Furthermore we intend to include the most recent determinations of oscillator strength values for the atoms and molecules involved in the spectral regions of interest. Other spectral features will be studied for better interpretation in terms of physical parameters of the available observations.

We will compare synthetic spectra with the complete set of our own observations at intermediate resolution for establishing the fiducial reference points. Consequently, the complete grid will allow us to generate composite stellar populations for interpretating extensive observational data for

stellar clusters and galaxies.

The calibration of the Mg b feature and of other suitable indices against metallicity will allow us to disentangle metallicity from age effects in population synthesis models. Eventually, this will allow us to derive the age of stellar systems by an independent method not biased by the interconnection between age and metallicity.

Tab. 7.1: Parameters at which models have been computed for each of the metallicity values: [M/H] = -0.05, -0.25, 0.0, 0.25 and 0.50.

log g	1.5	2.5	3.0	3.5	4.0	4.5
Teff						
5500	x	x	x	x	x	x
5600	x	x	x	x	x	x
5700	x	x	x	x	x	x
5800	x	x	x	x	x	x
5900	x	x	x	x	x	x
6000	x	x	x	x	x	x

Tab. 7.2: Input format of model atmosphere.

```
$ SET DEF DATA:[GULATI.MOD]
$ ASSIGN C5645P00.DAT FOR005
$ ASSIGN C5745P00.DAT FOR007
$ ASSIGN DATA:[IACE.GULATI]BDFBP00.DAT FOR009
$ RUN DATA:[CASTELLI.ATLAS8]ATLAS8
$ EXIT
```

```
FREQUENCIES 122 41 122 BIG
ITERATIONS 15
PRINT 0 0 0 0 0 0 0 0 0 0 0 0 0 0 0 2
PUNCH 0 0 0 0 0 0 0 0 0 0 0 0 0 0 0 1
 TEFF   5600.  GRAVITY 4.500 LTE
TITLE SCALE TEFF FROM 5600 TO 5700
OPACITY IFOP 1 1 1 1 1 1 1 1 1 1 1 1 1 1 0 0 0 0 0
CONVECTION ON 1.00 TURBULENCE OFF 0.00 0.00 0.00 0.00
ABUNDANCE SCALE   1.000 ABUNDANCE CHANGE 1 0.900 2 0.100
READ DECK6 64 RHOX,T,P,XNE,ABROSS,ACCRAD,VTURB
2.72840098E-03   3243.6 8.628E+01 4.856E+09 7.568E-04 9.273E-02 0.000E+00
3.56233795E-03   3819.8 1.126E+02 1.836E+10 7.568E-04 6.332E-02 0.000E+00
4.48552845E-03   3855.1 1.418E+02 2.297E+10 9.140E-04 5.694E-02 0.000E+00
5.51342173E-03   3883.5 1.743E+02 2.796E+10 1.082E-03 5.310E-02 0.000E+00
6.67612348E-03   3908.4 2.111E+02 3.351E+10 1.267E-03 5.476E-02 0.000E+00
8.00316688E-03   3931.6 2.531E+02 3.975E+10 1.474E-03 5.530E-02 0.000E+00
9.52839479E-03   3954.3 3.013E+02 4.684E+10 1.706E-03 5.639E-02 0.000E+00
1.12887733E-02   3977.2 3.570E+02 5.497E+10 1.971E-03 5.795E-02 0.000E+00
1.33258495E-02   4001.1 4.214E+02 6.436E+10 2.272E-03 5.871E-02 0.000E+00
1.56861618E-02   4025.5 4.960E+02 7.519E+10 2.617E-03 5.919E-02 0.000E+00
1.84203739E-02   4050.5 5.825E+02 8.769E+10 3.010E-03 5.959E-02 0.000E+00
2.15925854E-02   4075.9 6.828E+02 1.021E+11 3.460E-03 5.996E-02 0.000E+00
2.52733398E-02   4102.6 7.992E+02 1.189E+11 3.977E-03 5.962E-02 0.000E+00
2.95491815E-02   4128.6 9.344E+02 1.381E+11 4.566E-03 5.957E-02 0.000E+00
3.45134251E-02   4154.4 1.091E+03 1.603E+11 5.237E-03 5.989E-02 0.000E+00
4.02821563E-02   4179.9 1.274E+03 1.859E+11 6.003E-03 6.056E-02 0.000E+00
4.69904728E-02   4205.3 1.486E+03 2.153E+11 6.876E-03 6.159E-02 0.000E+00
5.48004918E-02   4230.5 1.733E+03 2.492E+11 7.872E-03 6.299E-02 0.000E+00
6.39144778E-02   4255.6 2.021E+03 2.885E+11 9.012E-03 6.481E-02 0.000E+00
7.45442584E-02   4280.7 2.357E+03 3.337E+11 1.031E-02 6.704E-02 0.000E+00
8.69314075E-02   4305.6 2.749E+03 3.859E+11 1.180E-02 6.974E-02 0.000E+00
1.01362810E-01   4330.6 3.205E+03 4.462E+11 1.350E-02 7.295E-02 0.000E+00
1.18185394E-01   4355.6 3.737E+03 5.157E+11 1.543E-02 7.676E-02 0.000E+00
1.37787610E-01   4381.0 4.357E+03 5.960E+11 1.764E-02 8.083E-02 0.000E+00
1.60628885E-01   4406.7 5.080E+03 6.887E+11 2.016E-02 8.523E-02 0.000E+00
1.87283099E-01   4432.2 5.922E+03 7.957E+11 2.303E-02 9.027E-02 0.000E+00
2.18355715E-01   4457.9 6.905E+03 9.191E+11 2.630E-02 9.607E-02 0.000E+00
2.54640251E-01   4483.9 8.053E+03 1.062E+12 3.005E-02 1.032E-01 0.000E+00
2.97082365E-01   4511.2 9.395E+03 1.228E+12 3.440E-02 1.120E-01 0.000E+00
3.46599936E-01   4538.8 1.096E+04 1.420E+12 3.938E-02 1.219E-01 0.000E+00
4.04272318E-01   4567.6 1.278E+04 1.643E+12 4.508E-02 1.333E-01 0.000E+00
4.71360028E-01   4597.7 1.491E+04 1.902E+12 5.160E-02 1.463E-01 0.000E+00
5.49450636E-01   4629.7 1.738E+04 2.204E+12 5.908E-02 1.610E-01 0.000E+00
6.40289545E-01   4664.5 2.025E+04 2.557E+12 6.768E-02 1.776E-01 0.000E+00
7.46033728E-01   4702.5 2.359E+04 2.973E+12 7.757E-02 1.966E-01 0.000E+00
8.68908644E-01   4745.0 2.748E+04 3.464E+12 8.895E-02 2.181E-01 0.000E+00
1.01214409E+00   4793.1 3.201E+04 4.051E+12 1.022E-01 2.427E-01 0.000E+00
1.17894447E+00   4848.3 3.728E+04 4.758E+12 1.174E-01 2.703E-01 0.000E+00
1.37232912E+00   4911.8 4.340E+04 5.609E+12 1.349E-01 3.014E-01 0.000E+00
1.59579062E+00   4985.1 5.046E+04 6.640E+12 1.549E-01 3.363E-01 0.000E+00
1.85366726E+00   5070.2 5.862E+04 7.899E+12 1.775E-01 3.750E-01 0.000E+00
2.15223360E+00   5169.2 6.806E+04 9.463E+12 2.034E-01 4.186E-01 0.000E+00
2.49710894E+00   5285.7 7.896E+04 1.147E+13 2.337E-01 4.698E-01 0.000E+00
2.89179444E+00   5422.3 9.145E+04 1.417E+13 2.713E-01 5.348E-01 0.000E+00
3.33196235E+00   5582.0 1.054E+05 1.809E+13 3.233E-01 6.276E-01 0.000E+00
3.80531502E+00   5768.6 1.203E+05 2.437E+13 4.050E-01 7.785E-01 0.000E+00
4.28210974E+00   5984.7 1.354E+05 3.523E+13 5.418E-01 1.036E+00 0.000E+00
4.73634577E+00   6227.5 1.498E+05 5.449E+13 7.672E-01 1.457E+00 0.000E+00
5.14632654E+00   6504.6 1.627E+05 8.982E+13 1.144E+00 2.162E+00 0.000E+00
5.49922276E+00   6855.1 1.739E+05 1.642E+14 1.851E+00 3.389E+00 0.000E+00
5.77578306E+00   7226.5 1.826E+05 2.980E+14 3.121E+00 5.117E+00 0.000E+00
6.00429964E+00   7542.6 1.899E+05 4.777E+14 4.766E+00 6.236E+00 0.000E+00
6.21161985E+00   7827.2 1.964E+05 7.108E+14 6.862E+00 6.803E+00 0.000E+00
6.40726185E+00   8080.3 2.026E+05 9.921E+14 9.327E+00 6.875E+00 0.000E+00
6.60245732E+00   8312.9 2.088E+05 1.327E+15 1.223E+01 6.740E+00 0.000E+00
6.80180788E+00   8530.7 2.151E+05 1.720E+15 1.592E+01 6.594E+00 0.000E+00
7.00859308E+00   8734.5 2.216E+05 2.172E+15 2.025E+01 6.368E+00 0.000E+00
7.22698450E+00   8930.6 2.285E+05 2.695E+15 2.539E+01 6.171E+00 0.000E+00
7.46113873E+00   9120.2 2.359E+05 3.295E+15 3.141E+01 5.923E+00 0.000E+00
7.71474886E+00   9305.7 2.439E+05 3.987E+15 3.848E+01 5.701E+00 0.000E+00
7.99127483E+00   9489.9 2.527E+05 4.786E+15 4.676E+01 5.431E+00 0.000E+00
8.29582500E+00   9669.3 2.623E+05 5.691E+15 5.620E+01 5.208E+00 0.000E+00
8.63381577E+00   9856.2 2.730E+05 6.774E+15 6.758E+01 4.934E+00 0.000E+00
9.00953388E+00  10030.5 2.849E+05 7.947E+15 7.985E+01 5.008E+00 0.000E+00
PRADK 1.3150E+00
SCALE 64 -5.825 0.125 5700 4.5
BEGIN                    ITERATION  15 COMPLETED
END
```

Tab. 7.3: Output format of model atmosphere.

```
TEFF   5700.  GRAVITY 4.500 LTE
TITLE SCALE TEFF FROM 5600 TO 5700
 CONVECTION ON   1.00 TURBULENCE OFF  0.00  0.00  0.00  0.00
ABUNDANCE SCALE   1.000 ABUNDANCE CHANGE 1 0.900 2 0.100
READ DECK6 64 RHOX,T,P,XNE,ABROSS,ACCRAD,VTURB
2.66409875E-03   3321.1 8.425E+01 5.986E+09 7.784E-04 1.012E-01 0.000E+00
3.47661041E-03   3880.4 1.099E+02 1.890E+10 7.784E-04 6.996E-02 0.000E+00
4.36925516E-03   3915.8 1.382E+02 2.358E+10 9.370E-04 6.364E-02 0.000E+00
5.35574742E-03   3945.8 1.694E+02 2.867E+10 1.107E-03 6.165E-02 0.000E+00
6.49297796E-03   3972.3 2.053E+02 3.443E+10 1.298E-03 6.133E-02 0.000E+00
7.77641498E-03   3996.7 2.459E+02 4.084E+10 1.507E-03 6.146E-02 0.000E+00
9.27496795E-03   4020.6 2.933E+02 4.826E+10 1.747E-03 6.171E-02 0.000E+00
1.09974658E-02   4044.1 3.478E+02 5.670E+10 2.017E-03 6.218E-02 0.000E+00
1.29948026E-02   4067.7 4.110E+02 6.642E+10 2.325E-03 6.274E-02 0.000E+00
1.53044211E-02   4091.7 4.840E+02 7.758E+10 2.674E-03 6.330E-02 0.000E+00
1.79845858E-02   4116.2 5.687E+02 9.046E+10 3.073E-03 6.386E-02 0.000E+00
2.10935343E-02   4141.5 6.671E+02 1.053E+11 3.529E-03 6.424E-02 0.000E+00
2.47050971E-02   4167.8 7.813E+02 1.226E+11 4.053E-03 6.426E-02 0.000E+00
2.88984068E-02   4193.7 9.139E+02 1.424E+11 4.649E-03 6.457E-02 0.000E+00
3.37772928E-02   4219.7 1.068E+03 1.654E+11 5.330E-03 6.519E-02 0.000E+00
3.94612290E-02   4245.6 1.248E+03 1.918E+11 6.108E-03 6.613E-02 0.000E+00
4.61004600E-02   4271.7 1.458E+03 2.225E+11 6.999E-03 6.742E-02 0.000E+00
5.38181998E-02   4297.7 1.702E+03 2.579E+11 8.016E-03 6.908E-02 0.000E+00
6.28045350E-02   4323.6 1.986E+03 2.987E+11 9.176E-03 7.115E-02 0.000E+00
7.32672364E-02   4349.6 2.317E+03 3.459E+11 1.050E-02 7.369E-02 0.000E+00
8.54482427E-02   4375.7 2.702E+03 4.003E+11 1.201E-02 7.656E-02 0.000E+00
9.96372625E-02   4402.0 3.151E+03 4.631E+11 1.373E-02 7.962E-02 0.000E+00
1.16168857E-01   4428.1 3.674E+03 5.356E+11 1.569E-02 8.313E-02 0.000E+00
1.35452166E-01   4454.2 4.283E+03 6.193E+11 1.793E-02 8.718E-02 0.000E+00
1.57940909E-01   4480.2 4.994E+03 7.160E+11 2.048E-02 9.182E-02 0.000E+00
1.84274539E-01   4506.3 5.827E+03 8.280E+11 2.340E-02 9.718E-02 0.000E+00
2.15098441E-01   4532.5 6.802E+03 9.577E+11 2.673E-02 1.034E-01 0.000E+00
2.51072228E-01   4559.5 7.940E+03 1.108E+12 3.058E-02 1.114E-01 0.000E+00
2.93006480E-01   4587.2 9.266E+03 1.282E+12 3.500E-02 1.209E-01 0.000E+00
3.41770262E-01   4615.4 1.081E+04 1.483E+12 4.004E-02 1.316E-01 0.000E+00
3.98529470E-01   4644.6 1.260E+04 1.716E+12 4.581E-02 1.439E-01 0.000E+00
4.64570045E-01   4675.3 1.469E+04 1.986E+12 5.239E-02 1.577E-01 0.000E+00
5.41442156E-01   4707.9 1.712E+04 2.300E+12 5.994E-02 1.734E-01 0.000E+00
6.30954564E-01   4743.3 1.995E+04 2.669E+12 6.860E-02 1.913E-01 0.000E+00
7.35506833E-01   4782.1 2.326E+04 3.103E+12 7.857E-02 2.116E-01 0.000E+00
8.57492745E-01   4825.7 2.712E+04 3.617E+12 9.004E-02 2.345E-01 0.000E+00
9.99498665E-01   4874.6 3.161E+04 4.227E+12 1.032E-01 2.603E-01 0.000E+00
1.16453826E+00   4930.3 3.683E+04 4.958E+12 1.183E-01 2.894E-01 0.000E+00
1.35564566E+00   4994.2 4.287E+04 5.834E+12 1.356E-01 3.221E-01 0.000E+00
1.57660234E+00   5067.8 4.986E+04 6.898E+12 1.552E-01 3.588E-01 0.000E+00
1.83228731E+00   5153.5 5.794E+04 8.205E+12 1.777E-01 4.000E-01 0.000E+00
2.12825584E+00   5253.3 6.730E+04 9.852E+12 2.038E-01 4.476E-01 0.000E+00
2.46903324E+00   5371.2 7.808E+04 1.202E+13 2.354E-01 5.060E-01 0.000E+00
2.85425162E+00   5509.6 9.026E+04 1.503E+13 2.768E-01 5.847E-01 0.000E+00
3.27652645E+00   5671.6 1.036E+05 1.955E+13 3.370E-01 7.018E-01 0.000E+00
3.72122073E+00   5861.6 1.177E+05 2.700E+13 4.340E-01 8.970E-01 0.000E+00
4.15540600E+00   6080.6 1.314E+05 3.991E+13 5.932E-01 1.219E+00 0.000E+00
4.56353855E+00   6327.2 1.443E+05 6.267E+13 8.524E-01 1.738E+00 0.000E+00
4.93009329E+00   6611.3 1.559E+05 1.045E+14 1.282E+00 2.592E+00 0.000E+00
5.24096775E+00   6974.9 1.657E+05 1.932E+14 2.123E+00 4.156E+00 0.000E+00
5.48121929E+00   7345.3 1.733E+05 3.450E+14 3.563E+00 6.144E+00 0.000E+00
5.68272781E+00   7656.1 1.797E+05 5.421E+14 5.370E+00 7.318E+00 0.000E+00
5.86725616E+00   7938.7 1.855E+05 7.939E+14 7.662E+00 7.873E+00 0.000E+00
6.04234743E+00   8188.0 1.911E+05 1.096E+15 1.031E+01 7.854E+00 0.000E+00
6.21868181E+00   8419.1 1.966E+05 1.452E+15 1.357E+01 7.702E+00 0.000E+00
6.39908314E+00   8634.0 2.023E+05 1.865E+15 1.756E+01 7.467E+00 0.000E+00
6.58658123E+00   8836.2 2.083E+05 2.337E+15 2.225E+01 7.188E+00 0.000E+00
6.78579092E+00   9030.3 2.146E+05 2.878E+15 2.776E+01 6.943E+00 0.000E+00
6.99948025E+00   9219.3 2.213E+05 3.501E+15 3.425E+01 6.652E+00 0.000E+00
7.23195171E+00   9402.9 2.287E+05 4.209E+15 4.176E+01 6.385E+00 0.000E+00
7.48693514E+00   9588.6 2.367E+05 5.039E+15 5.067E+01 6.083E+00 0.000E+00
7.76781940E+00   9766.7 2.456E+05 5.961E+15 6.065E+01 5.805E+00 0.000E+00
8.08103943E+00   9955.5 2.555E+05 7.079E+15 7.283E+01 5.521E+00 0.000E+00
8.42887783E+00  10129.8 2.665E+05 8.275E+15 8.588E+01 5.567E+00 0.000E+00
PRADK 1.4116E+00
BEGIN                    ITERATION  15 COMPLETED
```

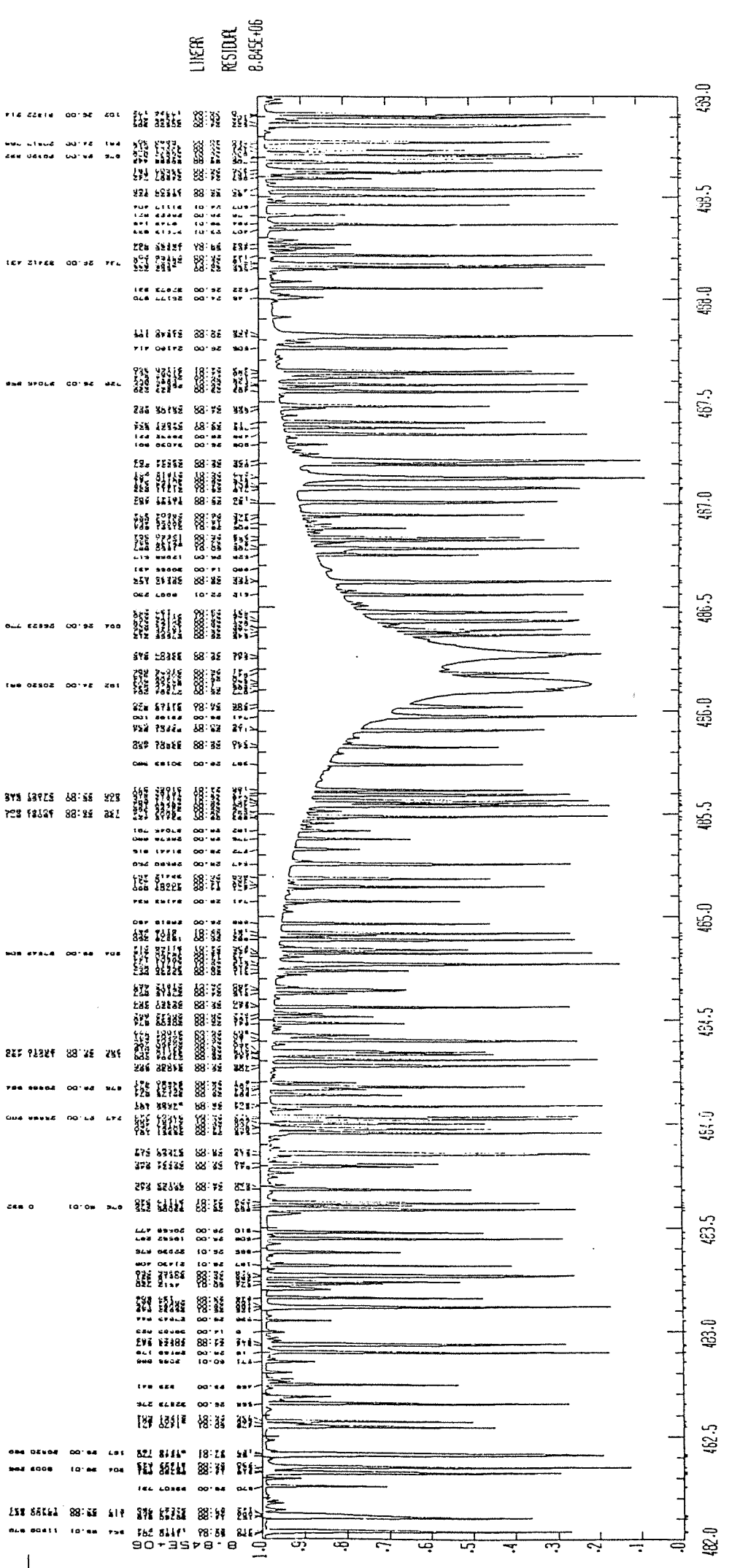

Fig. 7.1a: Synthetic spectrum of Hβ for parameters 5800/3.5/0.0.

Fig. 7.1b: Synthetic spectrum of Mg-*b* for parameters 5800/4.5/0.0.

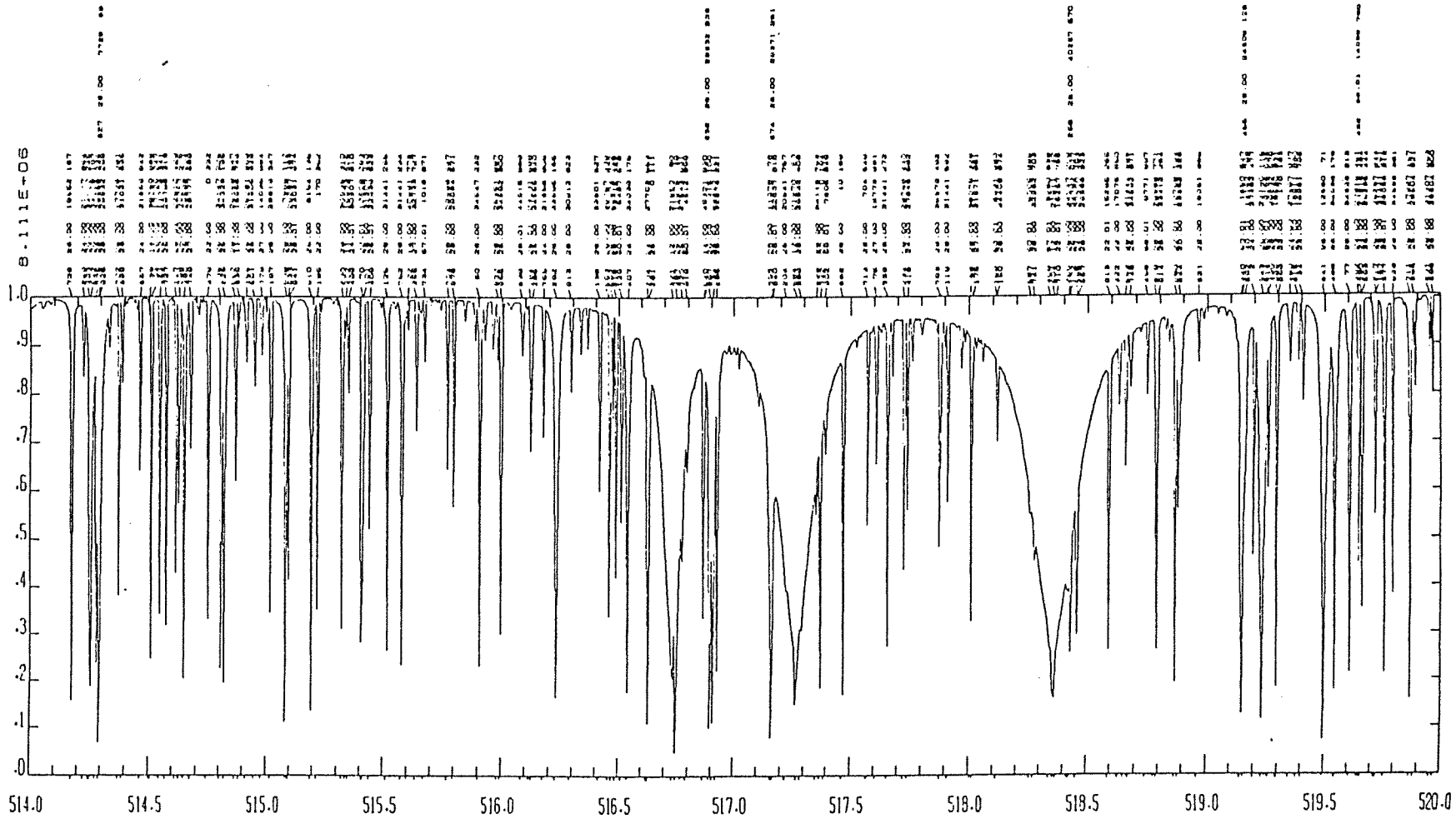

Fig. 7.2a: Synthetic spectrum broadened due to instrumental profile of Hβ for parameters 5800/3.5/0.0.

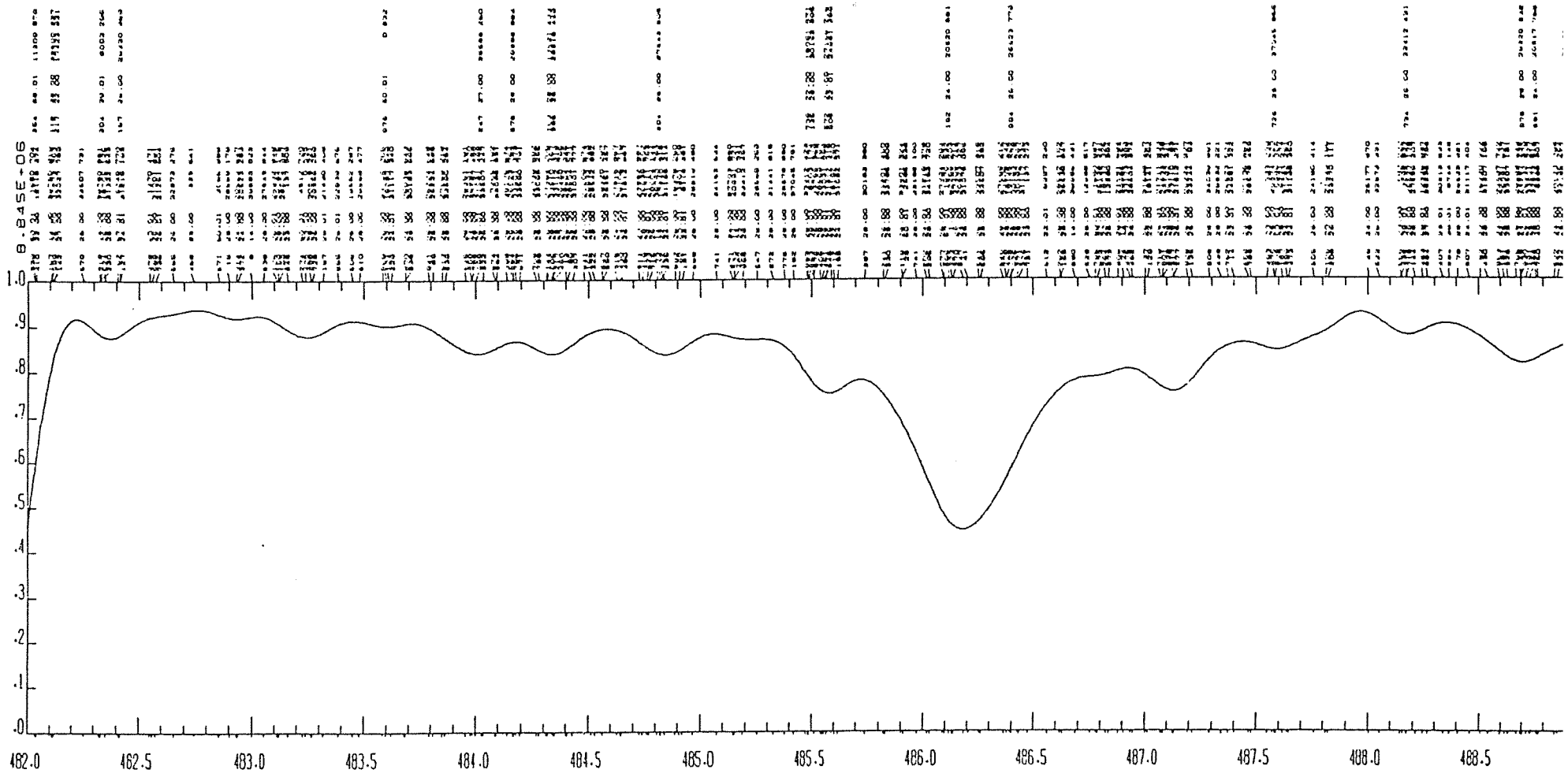

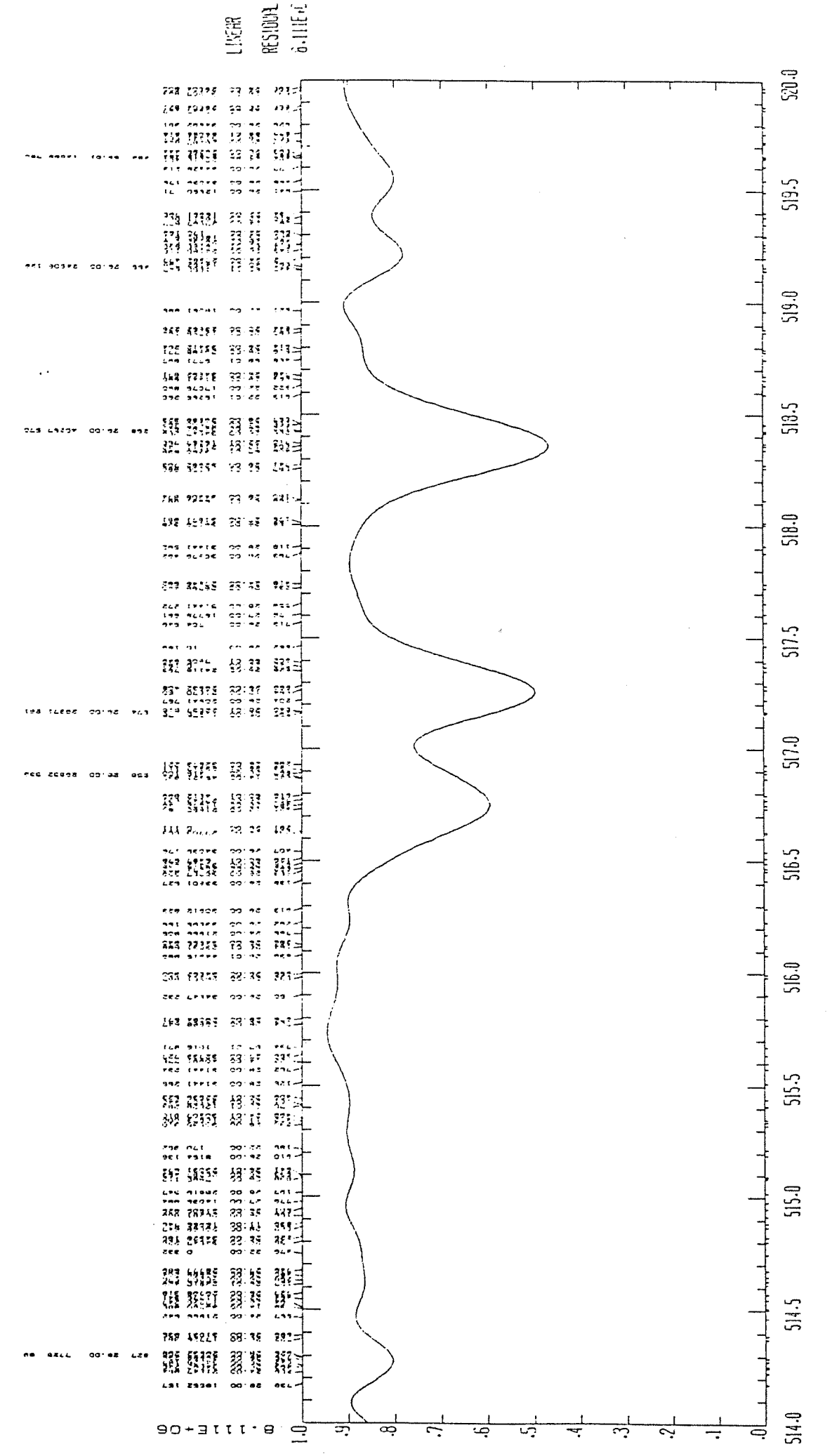

Fig. 7.2b: Same as Fig. 7.2a of Mg-*b* for parameters 5800/4.5/0.0.

Fig. 7.3: Comparison of synthetic spectra at different rotational velocities for prameters 6000/4.0/0.0 (thick line refers to rotation velocity of 20.0 km/s and thin line to 0.0 km/s)

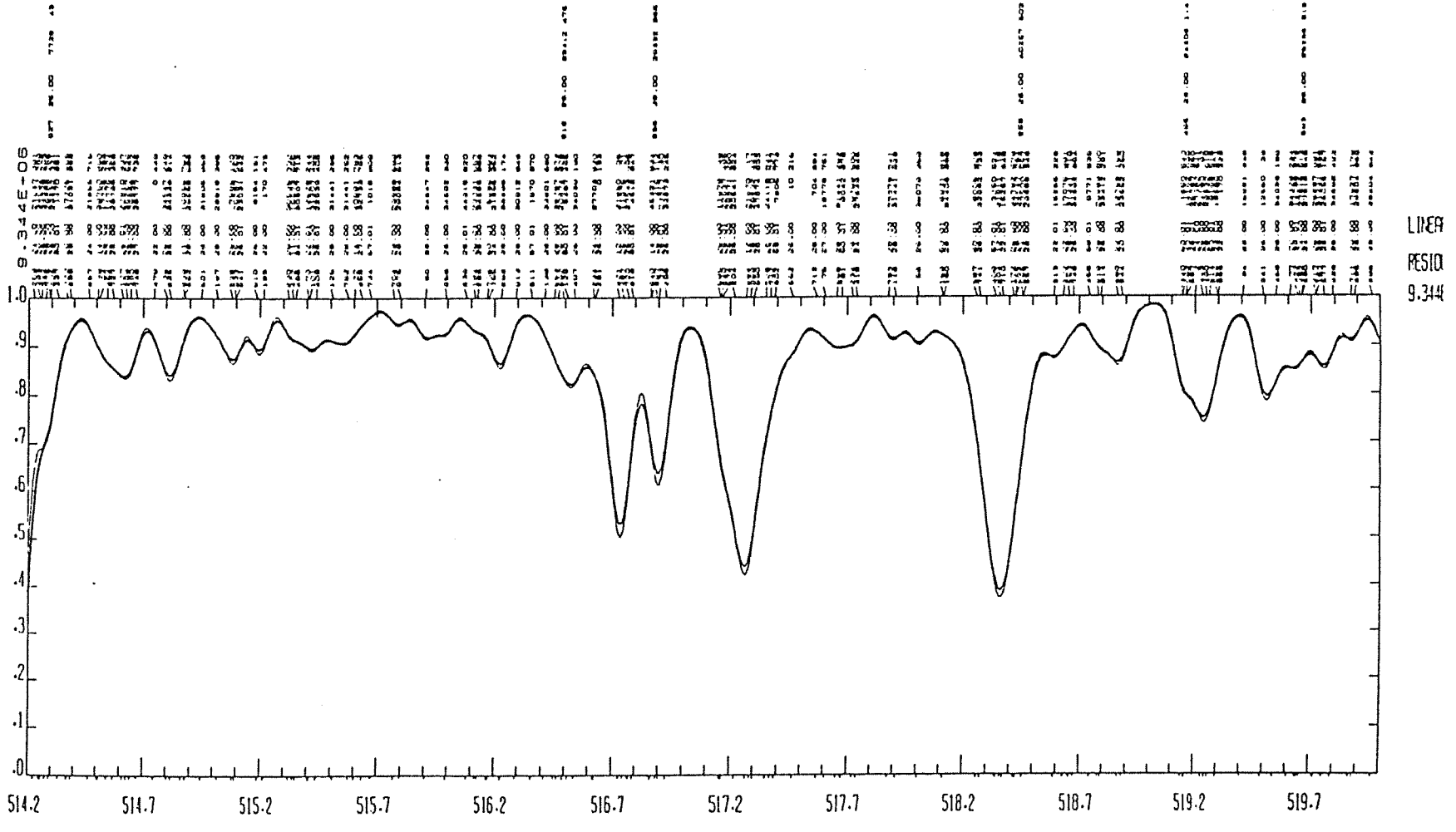

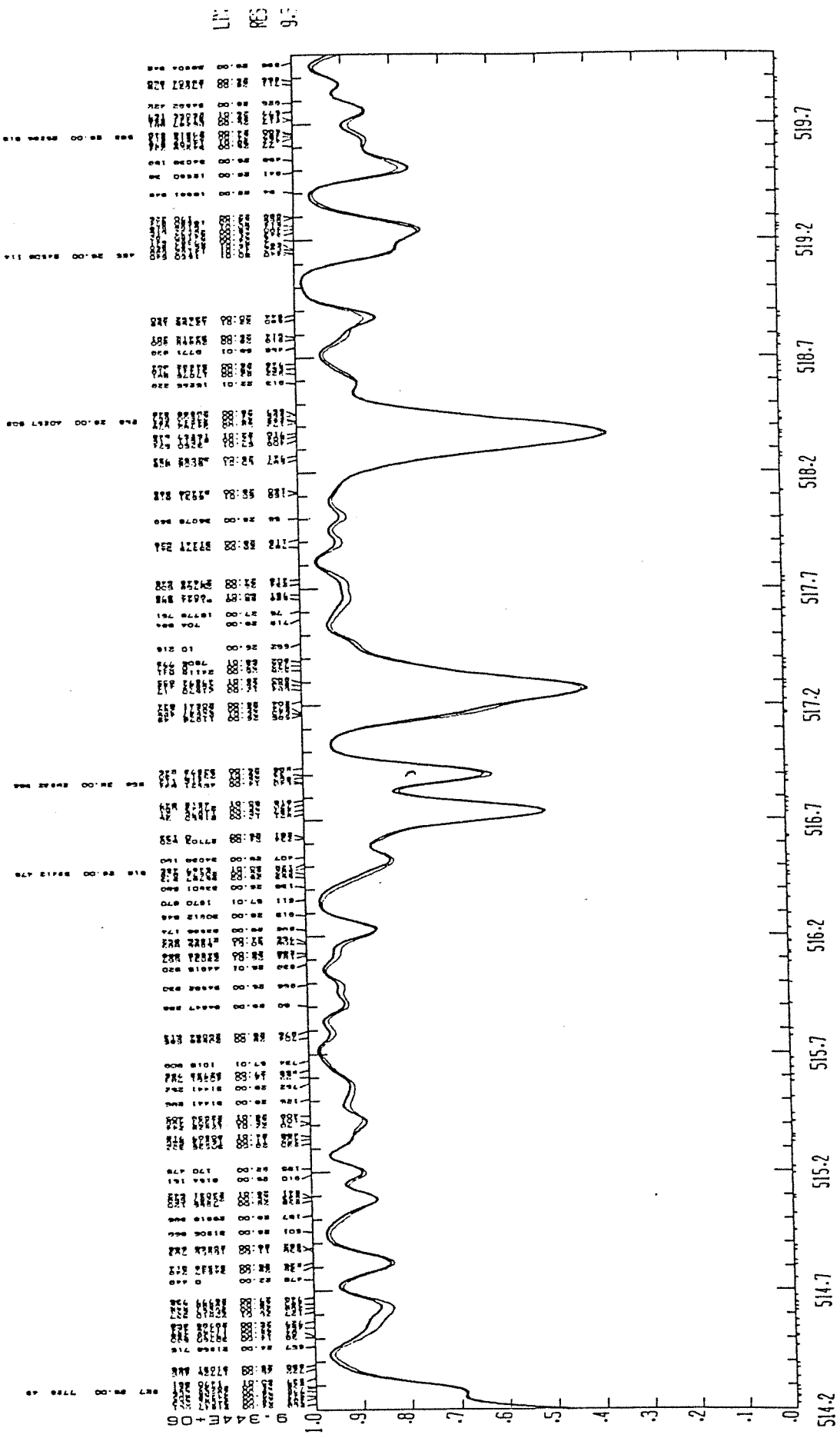

Fig. 7.4: Comparison of synthetic spectra at different resolutions for prameters 6000/4.0/0.0 of Mg-*b* (thick line refers to resolution of 250,000 and thin line to 75,000).

Fig. 7.5a: Comparison of synthetic spectra with observed star (HD 190248) in the Hβ region. (thick line refers to synthetic spectrum (5600/4.5/0/25), and thin line to stellar spectrum (5600/4.3/0.30)).

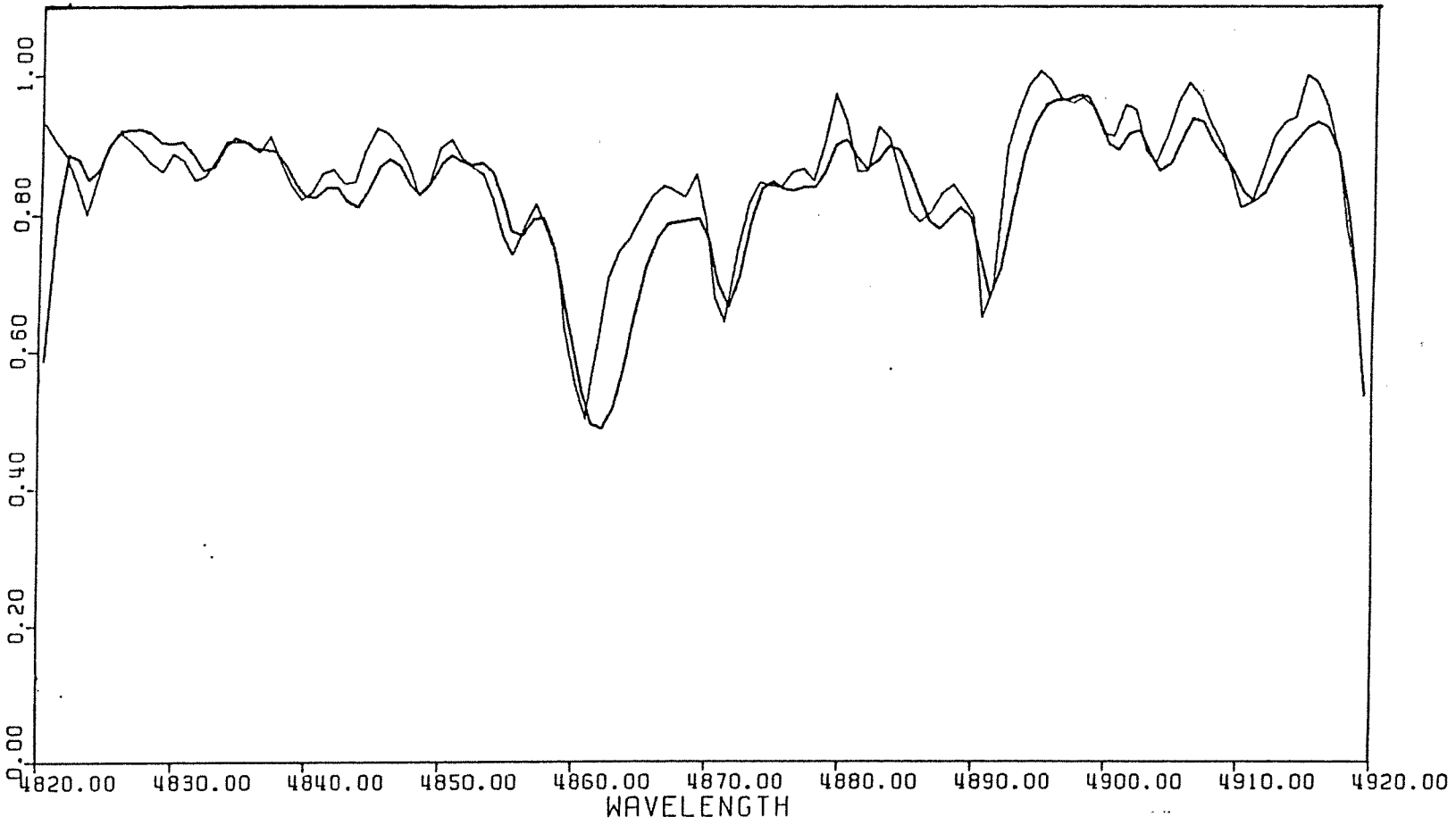

Fig. 7.6: Comparison of synthetic spectra at different metallicities in the Mg-*b* region for prameters 5800/4.0 (thick line refers to metallicity of 0.50 thin line to -0.50).

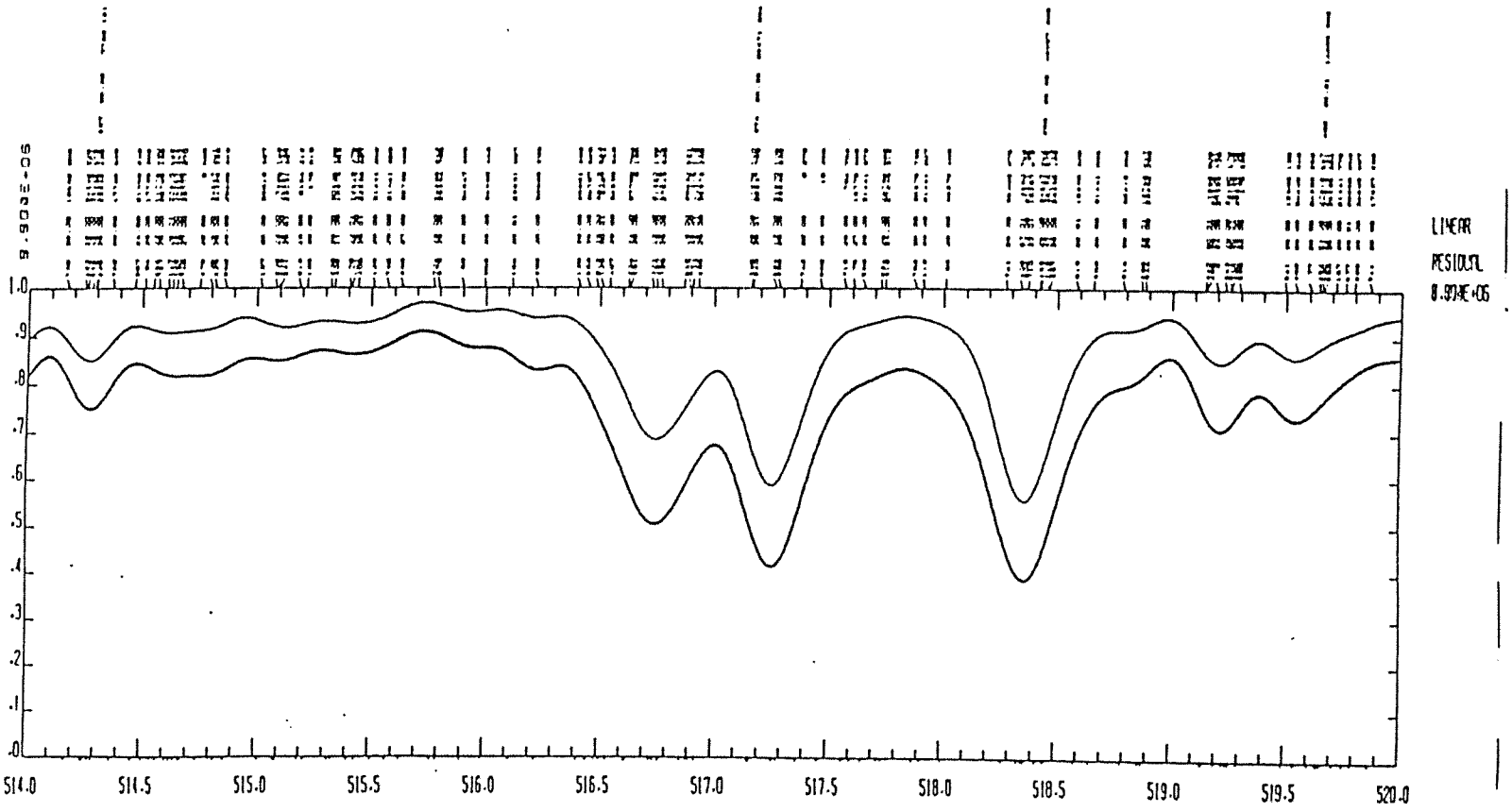

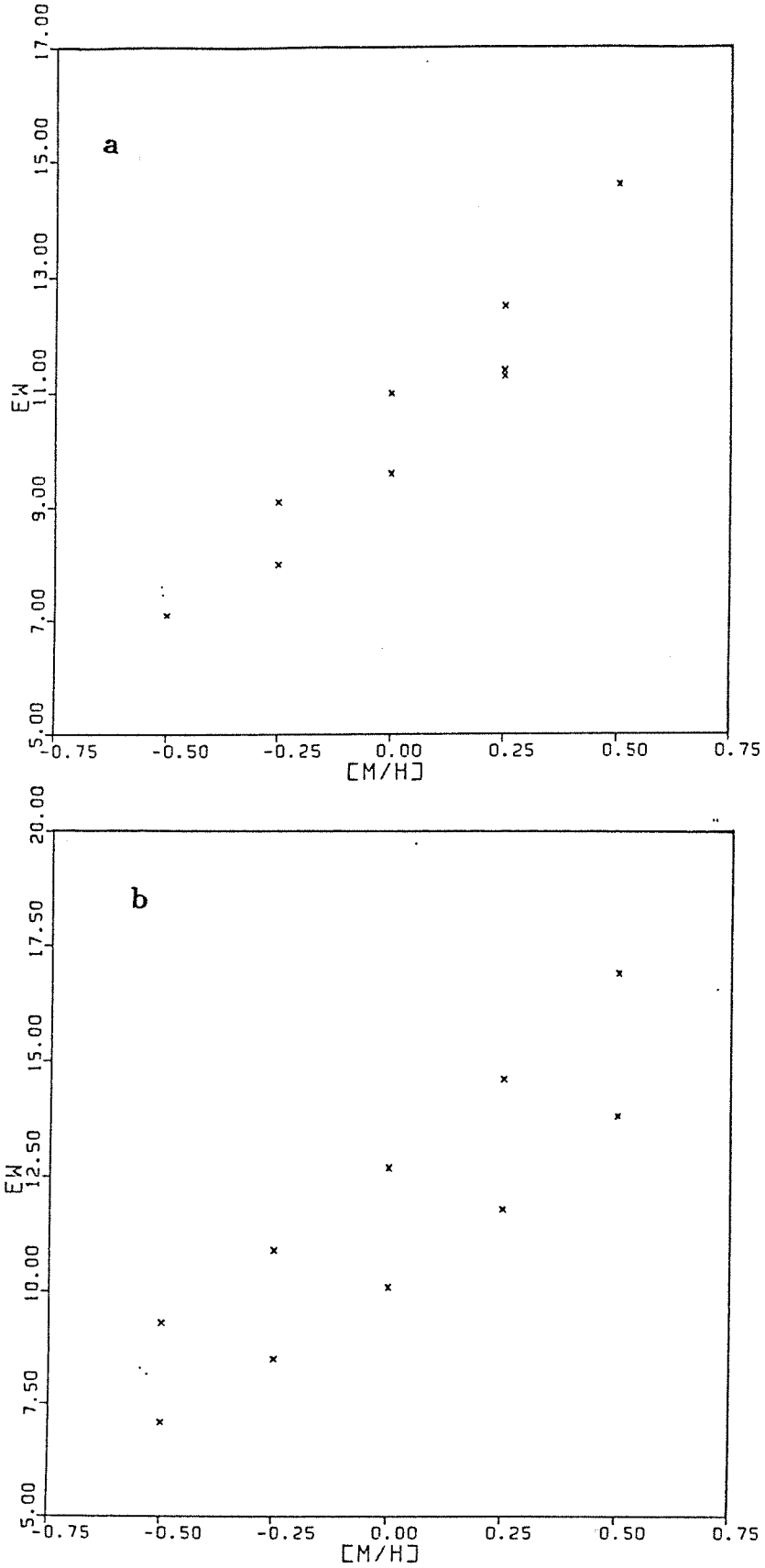

Fig. 7.7a-f: Correlation between synthetic equivalent width (EW) and metallicity at temperatures : a) 5500 K ; b) 5600 K ; c) 5700 K ; d) 5800 K; e) 5900 K; and f) 6000 K.

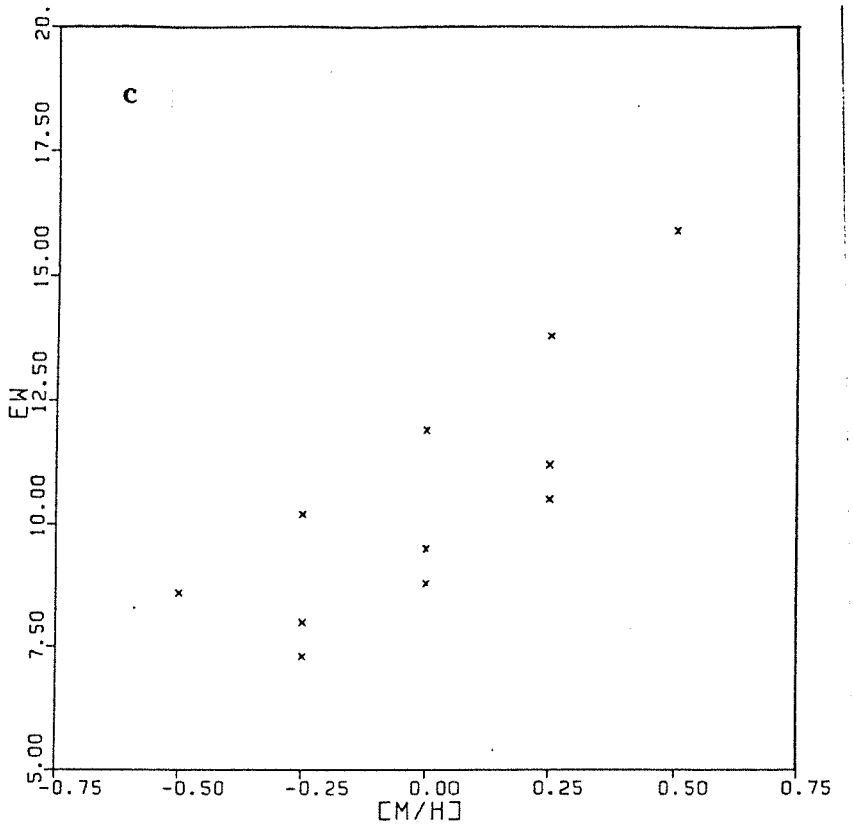
c
EW
20.
17.50
15.00
12.50
10.00
7.50
5.00
-0.75
-0.50
-0.25
0.00
0.25
0.50
0.75
[M/H]

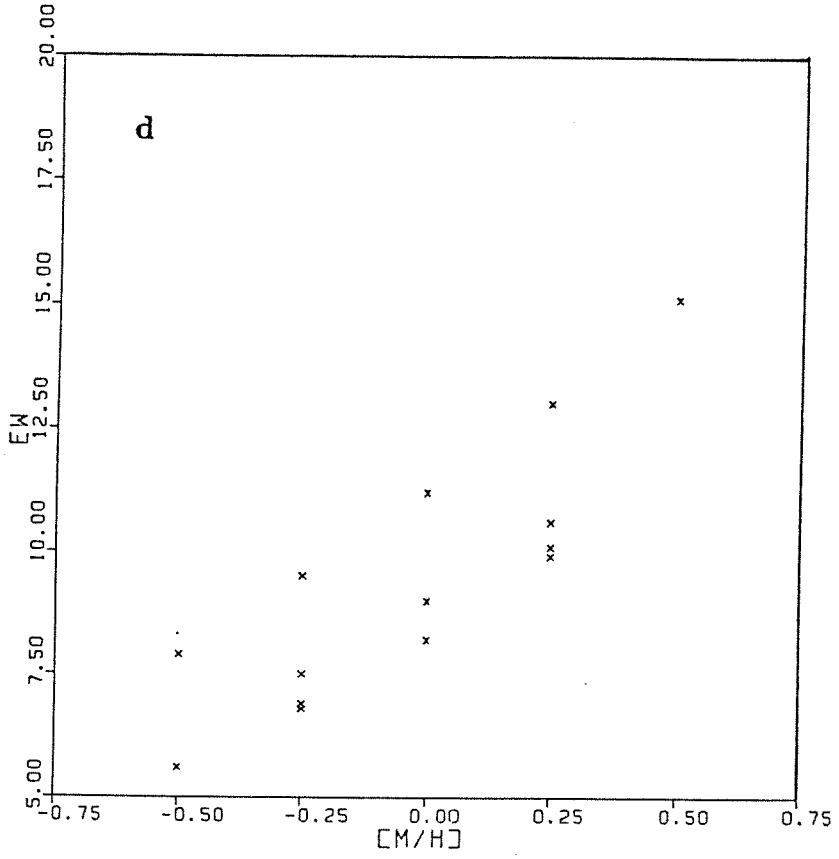
d
EW
20.00
17.50
15.00
12.50
10.00
7.50
5.00
-0.75
-0.50
-0.25
0.00
0.25
0.50
0.75
[M/H]

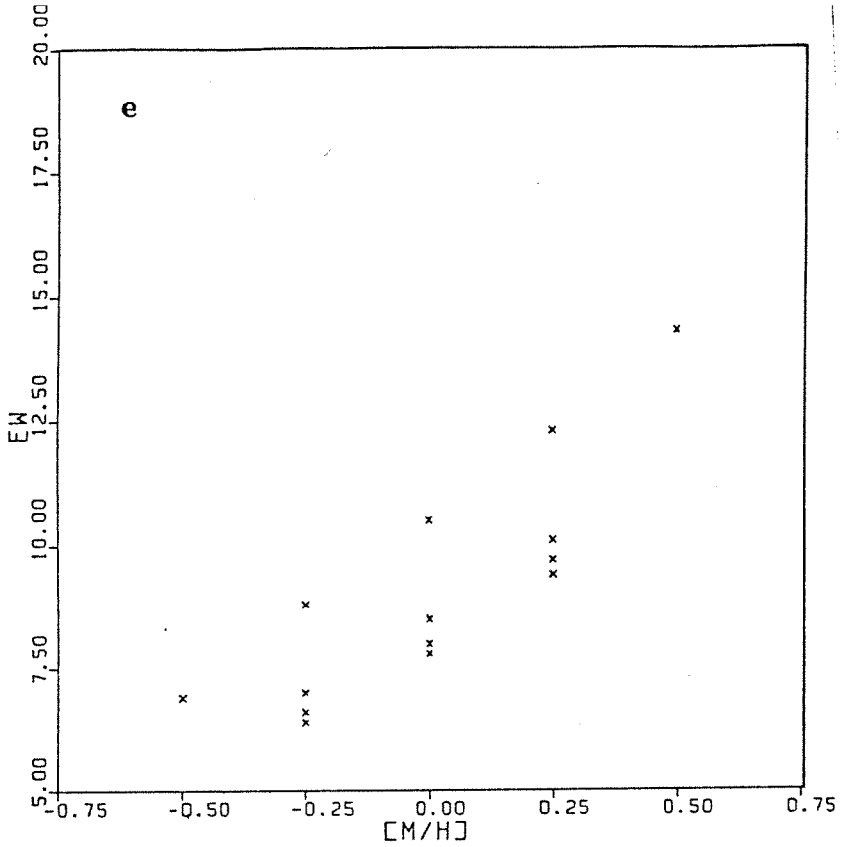
e
EW
20.00
17.50
15.00
12.50
10.00
7.50
5.00
-0.75
-0.50
-0.25
0.00
0.25
0.50
0.75
[M/H]

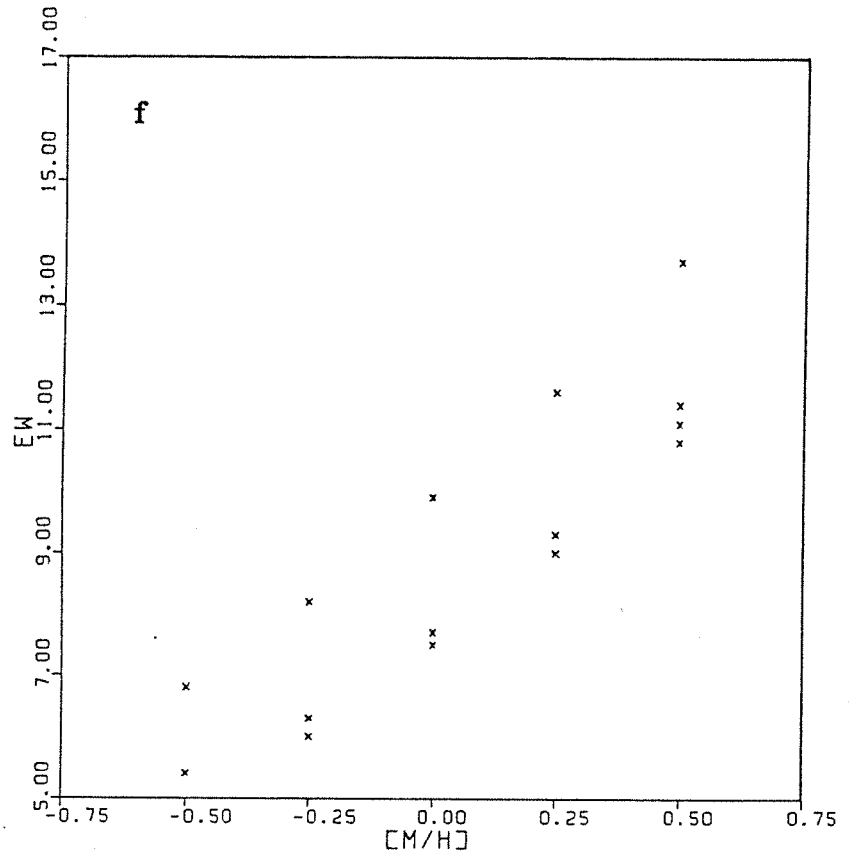
f
EW
17.00
15.00
13.00
11.00
9.00
7.00
5.00
-0.75
-0.50
-0.25
0.00
0.25
0.50
0.75
[M/H]

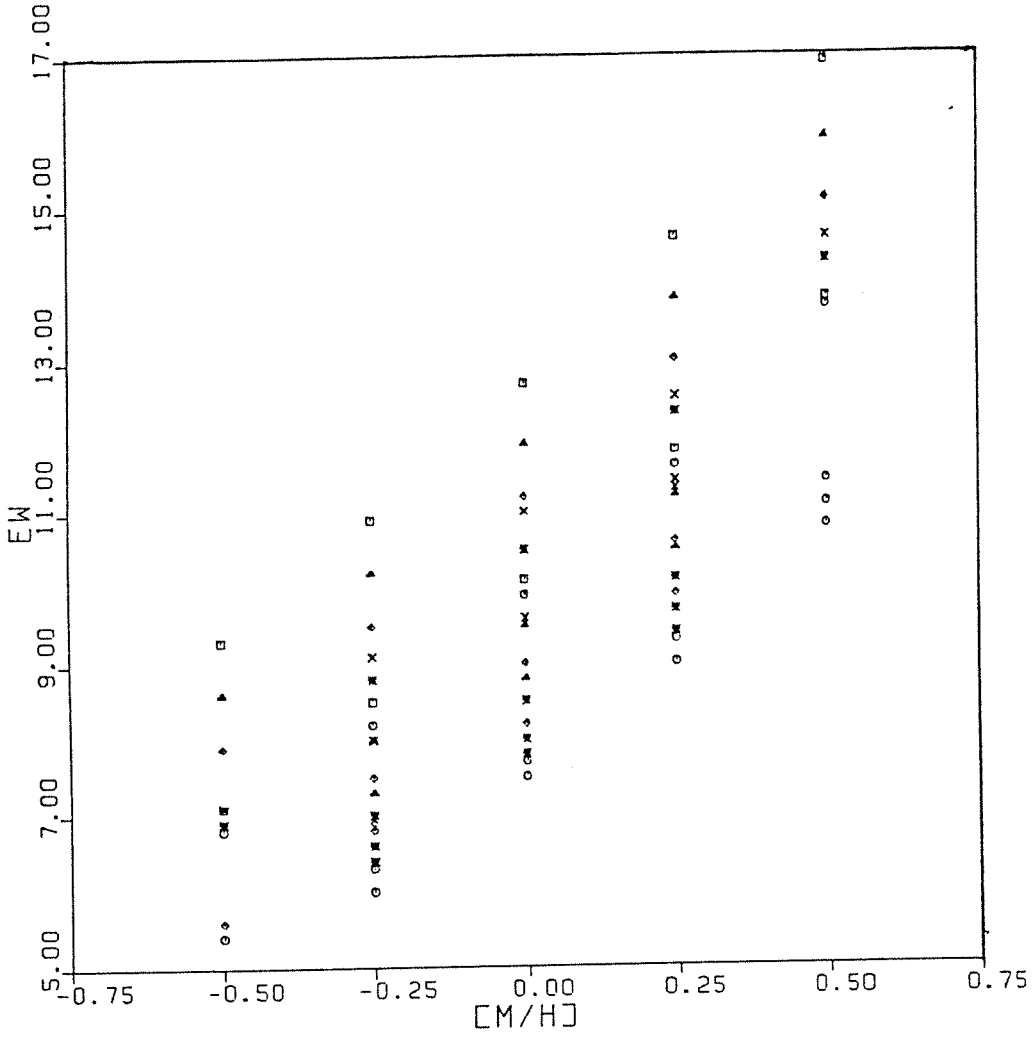

Fig. 7.8: Same as in Fig. 7.7 at six different values of temperatures. (Crosses refer to Teff 5500; Squares to 5600; Triangles to 5700; Diamonds to 5800; Asterisks to 5900; and Octagons to 6000 K)

References

[1] Arimoto, N., Yoshi, Y. : 1986, *Astron. Astrophys.* **164**, 260.

[2] Arp, A. : 1966, *Astrophys. J. Suppl. Ser.* **14**, 43.

[3] Baade, W. : 1944, *Astrophys. J.* **100**, 147.

[4] Barbaro, G., Olivi, F.M. : 1986, in *Erice Workshop, Spectral Evolution of Galaxies*, eds. C.Chiosi and A. Renzini (Dordrecht:Reidel), p. 283.

[5] Baum, W. : 1959, *Pub. Astron. Soc. Pacific* **71**, 106.

[6] Bruzual, A.G. : 1983, *Astrophys. J.* **273**, 105.

[7] Buonanno, R., Corsi, C.E., Fusi Pecci, F. : 1986, *Astron. Astrophys.* **145**, 97.

[8] Buzzoni, A., Fusi Pecci, F.,Buonanno, R., Corsi, C.E. : 1983, *Astron. Astrophys.* **128**, 94.

[9] Buzzoni A. : 1988, in *Erice Workshop, Towards Understanding Galaxies at Large redshifts*, eds. R.G. Kron and A. Renzini (Dordrecht:Kluwer), p.61.

[10] Buzzoni, A. : 1989, *Astrophys. J. Suppl. Ser.* in press

[11] Castelli, F. : 1988, *Pubbl. Osservatorio Astronomico di Trieste*, N. **1164**

[12] Ciardullo, R.B., Demarque, P. : 1977, Trans. Astr. Obs. Yale Univ., **35**, 1.

[13] Carbon, D.F., Gingerich, O.J. : 1969 in *Theory and Observations of Normal Stellar Atmospheres*, ed. O.J. Gingerich (Cambridge, Mass.: The M.I.T. Press), p. 377.

[14] Cohn, G., Frogel, J.A., Persson, S.E. : 1978 *Astrophys. J.* **222**, 165.

[15] Copeland, H., Jensen, J.O., Jogensen, H.E. : 1970, *Astron. Astrophys.* **5**, 12.

[16] Christensen, C.G.: 1978, em Astron. J. **83**, 244.

[17] Crocker, D.A., Rood, R.T., and O'Connell, R.W. : 1988, *Astrophys. J.* **332**,236

[18] D'Antona, F. and Mazzetelli, I. : 1985,*Astrophys. J.* **296**, 502.

[19] Deeming, T.J. : 1960, *Mon. N. Roy. Astron Soc.* **121**, 52.

[20] Dickow, P., Gyldenkerne, K., Hansen, L., Jacobsen, P.U., Johansen, Kjaergaard, P., Olsen, E.H. : 1970,*Astron. Astrophys. Suppl. Ser.* **2**, 1.

[21] de Vaucouleurs, G. : 1959, *Handbuch der Physik.* **53**, 275.

[22] de Vaucouleurs, G., de Vaucouleurs, A. : 1959, *Pub. Astron. Soc. Pacific* **71**, 83.

[23] Eggen, O.J., Lynden-Bell, D., Sandage, A.R. : 1962, *Astrophys. J.* **136**, 748.

[24] Faber, S.M. : 1972, *Astron. Astrophys.* **18**, 361.

[25] Faber, S.M. : 1973, *Astrphys. J.* **179**, 731.

[26] Faber, S.M. : 1977, in *The Evolution of Galaxies and Stellar Populations*, eds. B.M. Tinsley and R.B. Larson (New Haven: Yale Universemy Observatory).

[27] Faber, S.M., Burstein, D., Dressler, A. : 1977, *Astron. J.* **82**, 941.

[28] Faber, S.M., Friel, E.D., Burstein, D., Gaskell, C.M. : 1985, *Astrphys. J. Suppl. Ser.* **57**, 711.

[29] Freeman, K.C. : 1986, in *Stellar Population*, eds. C.A. Norman, A. Renzini, and M.Tosi, Cambridge Univ. Press, Cambridge, p. 227.

[30] Fusi Pecci, F., Renzini, A. : 1976, *Astron. Astrophys.* **46**, 447.

[31] Fusi Pecci, F., Renzini, A., : 1978, in *IAU Symposium No. 80, The HR diagram*, eds. A.G.D. Philip and D.S.Hayes, (Dordrecht:Reidel),p.225.

[32] Gingold, R.A. : 1974, *Astrophys. J.* **193**, 177.

[33] Gingold, R.A. : 1976, *Astrophys. J.* **204**, 116.

[34] Gilmore, G., Reid, N. : 1982, *Mon. Not. R. Astron. Soc.* **236**, 430.

[35] Gottileb, D.J., Bell, R.A. : 1978,*Astron. Astrophys.* **19**, 434.

[36] Gustafsson, B., Bell, R.A. : 1978, *Astron. Astrophys.* **74**, 313.

[37] Gustafsson, B., Kjaergaard, P., Anderson, S. : 1974, *Astron. Astrophys.* **34**, 99.

[38] Gustafsson, B., Bell, R.A., Eriksson, K., Nordlund, A. : 1974, *Astron. Astrophys.* **42**, 407.

[39] Gunn, J.E., Stryker, L.L., Tinsley B. : 1981, *Astrophys. J.* **249**, 48.

[40] Hansen, L., Kjaergaard, P. : 1971, *Astron. Astrophys.* **15**, 123.

[41] Huchra, J.P. : 1977, *Astrophys. J.* **217**, 928.

[42] Iben, I. Jr., Rood, R.T : 1970, *Astrophys. J.* **161**, 587.

[43] Iben, I. Jr., Renzini, A. : 1982 a, *Astrophys. J. Lett.* **259**, L79.

[44] Iben, I. Jr., Renzini, A. : 1982 b, *Astrophys. J. Lett.* **263**, L188.

[45] Jacobi, G.H., Hunter, D.A., Christian, C.A.: 1984, *Astrophys. Suppl. Ser.* **56**, 257.

[46] Johnson, H.L. : 1966, *Ann. Rev. Astron. Ap.* **4**, 193.

[47] Kurucz, R. : 1970, *Smithson. Ap. Obs. Spec.* Rep. No. 309

[48] Kurucz, R., Peytremann, E., Avrett, E.H. : 1974, *Blanketed Model Atmospheres for Early-Type Stars* (Washington, D.C.: Smithsonian Institute Press), p. 189.

[49] Kurucz, R. : 1979, *Astrophys. J. Suppl.* **40**, 1.

[50] Larson, R.B. : 1976, *Comments Astrophys.* **6**, 139.

[51] Malagnini, M.L., Faraggiana, R., Morossi, C : 1983, *Astron. Astrophys.* **128**, 375.

[52] Malagnini, M.L., Faraggiana, R., Morossi, C, Crevallari, L. : 1982, *Astron. Astrophys.* **114**, 170.

[53] McClure, R.D. : 1970, *Astron. J.* **75**, 41.

[54] McClure, R.D., Van den Bergh : 1968, *Astron.J.* **73**, 313.

[55] Mengel, J.G., Sweigart, A.V., Demarque, P., Gross, P.G. : 1979 *Astrophys. J. Suppl.* **40**, 733.

[56] Mihalas, D., Binney, J. : 1981, in *Galactic Astronomy: Structure and Kinematics*, (Second Edition), W.H. Freeman, San Francisco.

[57] Morgan, W.W., Mayall, N.U. : 1957, *Pub. Astron. Soc. Pacific* **69**, 291.

[58] Morgan, W.W. : 1958, *Pub. Astron. Soc. Pacific* **70**, 364.

[59] Morgan, W.W.,: 1959, *Pub. Astron. Soc. Pacific* **71**, 394.

[60] Morgan, W.W., Oterbrock, D.E., : 1969, *Astron. J.* **74**, 55.

[61] Mould, J. : 1978, *Astrophys. J.* **220**, 434.

[62] O'Connell, D.J.K. (ed.) : 1958, in *Stellar Populations* (New York : Interscience).

[63] O'Connell, R.W. : 1980, *Astrophys. J.* **236**, 430.

[64] O'Connell, R.W. : 1986, in *Erice Workshop, Spectral Evolution of Galaxies*, eds. C.Chiosi and A. Renzini (Dordrecht:Reidel) , p. 321.

[65] Paczynski, B. : 1970, *Acta Astron.* **20**, 47.

[66] Paczynski, B. : 1971, *Acta Astron.* **20**, 47.

[67] Peytremann, E. : 1972, *Astron. Astrophys.* **17**, 76.

[68] Peytremann, E. : 1974a, *Astron. Astrophys.* **33**, 203.

[69] Peytremann, E. : 1974b, *Astron. Astrophys. Suppl. Ser.* **18**, 81.

[70] Pickles A.J. : 1985, *Astrophys. J. Suppl Ser.* **59**, 33.

[71] Pickles A.J., Van der Kruit, P.C. : 1988,in *Erice Workshop, Towards Understanding Galaxies at Large redshifts*, eds. R.G. Kron and A. Renzini (Dordrecht:Kluwer), p.29.

[72] Price, M. J. : 1966, *Mon. Not. R. Astron. Soc.* **134**, 135.

[73] Rabin, : 1980, *Ph.D. Thesis*, California Instemue of Techinology.

[74] Reimers, D. : 1975, *Mem. Soc. Roy. Sci. Liége*, 6^{th} Ser., **8**,369.

[75] Renzini, A., Voli, M. : 1981, *Astron. Astrophys.*, **94**, 175.

[76] Renzini, A., Buzzoni, A. : 1983,*Mem. Soc. Astron. It.* **54**, 739.

[77] Renzini, A., Buzzoni, A. : 1986, in *Erice Workshop, Spectral Evolution of Galaxies*, eds. C.Chiosi and A. Renzini (Dordrecht:Reidel) , p.195.

[78] Renzini, A., Fusi Pecci, F. : 1988, *Ann. Rev. Astron. Ap.* **26**, 199.

[79] Roberts, M.S. : 1956, *Astron. J.* **61**, 195.

[80] Rood, R.T. : 1983, *Astrophys. J.* **184**, 815.

[81] Sandage, A. R., Bedke, J. : 1988, *Atlas of Galaxies*, ed. NASA.

[82] Sandage, A. R. : 1961, *The Hubble Atlas of Galaxies*, Carnegie Instemute of Washington, Washington

[83] Sandage, A.R., and Wildey, R. : 1967,*Astrophys. J.* **150**, 469.

[84] Sandage, A. R. : 1986, *Ann. Rev. Astron. Ap.* **24**, 421.

[85] Schönberner, D. : 1979, *Astron. Astrophys.* **94**, 175.

[86] Schönberner, D. : 1981, *Astron. Astrophys.* **103**, 119.

[87] Schwarzschild, M. : 1979, *Astrophys. J.* **232**, 236.

[88] Searle, L. : 1986, in *Stellar Population*, eds. C.A. Norman, A. Renzini, and M.Tosi, Cambridge Univ. Press, Cambridge, p. 3.

[89] Seinkiewicz, R. : 1982, *Acta Astron.* **32**, 275.

[90] Sil'chenko, O.K. : 1983, *Soviet Astr. Lett.* **9**, 145.

[91] Sweigart, A.V., Gross, P.G. : 1976, *Astrophys. J. Suppl. Ser.* **32**, 367.

[92] Sweigart, A.V., Gross, P.G. : 1978, *Astrophys. J. Suppl. Ser.* **36**, 405.

[93] Spinrad, H., Taylor, B.J. : 1969, *Astrophys. J.* **157**, 1279.

[94] Spinrad, H., Taylor, B.J. : 1971, *Astrophys. J. Suppl.* **22**, 445.

[95] Tinsley, B.M. : 1975, *Mem. Soc. Astron. It.* **46**, 3.

[96] Tinsley B., Gunn, J.E. : 1976, *Astrophys. J.* **203**, 52.

[97] Tinsley, B.M. : 1980, *Found. Cosmic Phys.* **5**, 287.

[98] Toomre, A.,Toomre, J. : 1972, *Astrophys. J.* **178**, 623.

[99] VandenBerg, D.A. : 1983, *Astrophys. J. Suppl.* **51**, 29.

[100] VandenBerg, D.A., Hartwick, F.D..A., Alexander, D.R. : 1983, *Astron. Astrophys.* **5**, 12

[101] VandenBerg, D.A. : 1985, *Astrophys. J. Suppl.* **58**, 711.

[102] VandenBerg, D.A., Bell, R.A. : 1985, *Astrophys. J. Suppl.* **58**, 561.

[103] VandenBerg, D.A., Laskarides P.G. : 1987, *Astrophys. J. Suppl.* **64**, 103.

[104] van den Berg, S. : 1976, *Astrphys. J.* **206**, 883.

[105] van den Berg, S. : 1985, *Astron. J.* **72**, 1.

[106] Whipple, F.L. : 1935, *Harvard College Obs. Circ.* **404**, 1.

[107] Whitford, A.E., Rich, R.M. : 1980, *Bull. AAS* **12**, 838.

[108] Whitford, A.E., Rich, R.M. : 1980, *Astrophys. J.* **274**, 723.

[109] Williams, P.M. : 1971, *Mon. Not. R. Astron. Soc.* **155**, 171.

[110] Wood, D.B. : 1966, *Astrophys. J.* **145**, 36.

[111] Wood, P.R., Cahn, J. H. : 1981, *Astrophys. J.* **211**, 499.

[112] Zinn, : 1985, *Astrophys. J.* **236**, 430.

ACKNOWLEDGEMENTS

First of all, I would like to thank my supervisor, Prof. M.L. Malagnini, for introducing me to this field . Her suggestions and continuing encouragement have been indispensable prerequisite for the thesis work.

I am indebted to Prof. M. Hack, who has always generously shared her time and has given me inspirations and valuable suggestions.

My sincere thanks are also to Dr. Morossi for always helping me when I have computational problems and to Dr. Castelli for providing ATLAS and SYNTH programs.

I acknowledge the hospitality and computing facilities offered by Osservatorio Astronomico di Trieste and Dipartimento di Astronomia, dell' Universita di Trieste.